

Modeling and Simulation of Mudflows Impacting Railway Infrastructure Using Smoothed Particle Hydrodynamics

FangFang Gu

A Thesis
In
The Department
of
Building, Civil, and Environmental Engineering

Presented in Partial Fulfillment of the Requirements
for the Degree of
Master of Applied Science (Civil Engineering) at
Concordia University
Montréal, Québec, Canada

December 2020

© FangFang Gu, 2020

CONCORDIA UNIVERSITY
School of Graduate Studies

This is to certify that the thesis prepared

By: FangFang, Gu

Entitled: Modeling and Simulation of Mudflows Impacting Railway Infrastructure Using Smoothed Particle Hydrodynamics

and submitted in partial fulfillment of the requirements for the degree of

Master of Applied Science (Civil Engineering)

complies with the regulations of the University and meets the accepted standards with respect to originality and quality.

Signed by the final Examining Committee:

_____ Chair

Dr. A. M. Hanna

_____ Examiner

Dr. A. M. Hanna

_____ Examiner

Dr. M. Paraschivoiu

_____ Supervisor

Dr. A. M. Zsaki

Approved by: Dr. Michelle Nokken

Chair of Department or Graduate Program Director

Date: December 08, 2020

Dr. Mourad Debbabi

Dean of Faculty

ABSTRACT

Modeling and Simulation of Mudflows Impacting Railway Infrastructure Using Smoothed Particle Hydrodynamics

FangFang Gu

In the Canadian context, it is common that railway tracks transverse a mountainous area prone to natural disaster like mudflows. In the geographical areas where Champlain clays of the Ottawa Valley and St. Lawrence Lowlands in Canada are prone to mudflows, which results in further safety implications when a freight train is passing through this area, further threatening human lives in addition to public properties. Therefore, the investigation of the interaction of flow with trains, the parameters affecting mudflows' destructive force and the train derailment potential is important to determine the amount of potential damage.

The aim of this research was to study the feasibility of modeling mudflows utilizing the smoothed particle hydrodynamics method based on the available data in the literature and model the scenario of mudflows impacting railway cars on top of a railway embankment and quantitatively investigate the interaction of mudflow with trains. The parametric studies were performed including the identification of key factors, such as geometric characteristics of the natural hillslope and the railway embankment, mudflows' properties and freight train loading. To calibrate the simulation tool for reproducing the mudflow flowing on hillslope as in the real-world, a series of flume tests were modeled based on the physical large-scale experiment carried out by Bugnion et al. (2010), paved the way for implementation of the case studies' environment and properties of mudflow in the simulation tool in order to be modeled. The control variable method was introduced in numerical model studies to individually study each parameter and its effect on the impact force exerted by mudflows on railway cars. As a contribution, this study provides the information of critical case resulting train derailment with geometric terrain parameters and mudflows' quantities, which could be used as a reference for guidelines used in railway industry.

ACKNOWLEDGEMENT

Obviously, no research endeavor is ever carried out in solitude. I owe my deep gratitude to a great number of people. First and foremost, I am very grateful for the help and support from my supervisor, Dr. A. M. Zsaki, who provided me this opportunity to join in his group and provided invaluable and indispensable academic support and played a key role in guiding my research. His inspiring guidance and consistent support helped me to become an independent researcher.

Special thanks to my parents, Jun and Sheng, who accompanied me and supported me for always being with me during the highs and lows of these years. This work would not be possible without the endless love and support both in the study and life from my parents.

My gratitude also goes to my friends Shuo and ChungLi, who helped me, encouraged me and accompanied me throughout the whole research process. You tolerated me when I was not myself and made me go forward. You encouraged me whenever I was worried, frustrated or hopeless.

Finally, I would like to acknowledge the financial support from my supervisor, through the GCS FRS funds and from a Concordia SEED Individual research grant held by my supervisor to help me successfully complete the research work.

Table of Contents

List of Figures	viii
List of Tables	xii
Notation	xiv
Chapter One: Introduction	1
1.1 Background	1
1.2 Objective	2
1.3 Methodology	2
Chapter Two: Literature Review	4
2.1 The Fundamental Mechanics of Mudflow	4
2.1.1 Introduction.....	4
2.1.2 Types of sediment-moving phenomena	4
2.1.3 Definition of debris flow.....	6
2.1.4 Classification of debris flow	7
2.1.5 Characteristics of mudflow	8
2.1.6 Mechanics of debris flow	9
2.2 The Smoothed Particle Hydrodynamics (SPH) Method	12
2.2.1 Introduction.....	12
2.2.2 The simulation tool: DualSPHysics	13
2.2.3 Implementation of SPH method for mudflows	14
2.2.4 Analysis of numerical measurement in DualSPHysics.....	19
2.3 Railways	21
2.3.1 Early beginning and the development of the railway	21
2.3.2 The components of a railway system.....	23
2.3.3 The general operation of railways.....	25
2.3.4 Railway embankments	26
2.3.5 The derailment of trains	29
Chapter Three: Key Parameters of the Model	32
3.1 Introduction	32

3.2 Parameters for Railway Embankments	32
3.2.1 Railway embankment slope ratio.....	32
3.2.2 Railway embankment height.....	33
3.3 Parameters for Freight Trains	36
3.3.1 Loading from rolling stock	36
3.3.2 Track gauge.....	37
3.3.3 The sleepers or cross ties	37
3.4 Parameters Related to Mudflow	42
3.4.1 Impact force of mudflow.....	42
3.4.2 The viscosity of mudflow	47
3.5 Parameters Influencing Impact Force	48
Chapter Four: Model Calibration and Verification	51
4.1 Introduction	51
4.2 Variables Considered in the Calibration Test	51
4.2.1 Artificial viscosity coefficient.....	51
4.2.2 Initial particle distance	51
4.3 Calibration Test	52
4.4 Calibration Test Results	58
4.4.1 Tests with changes in artificial viscosity	58
4.4.2 Tests with changes in the value of d_p	62
4.4.3 Tests with different combination set values.....	67
Chapter Five: Parametric Model Studies and Interpretation of Result of Mudflows Impacting Trains	75
5.1 Introduction	75
5.2 Considerations in Model Implementation	75
5.2.1 The hillslope terrain	76
5.2.2 The railway embankment.....	76
5.2.3 The buffer plane	77
5.2.4 Mudflow material properties.....	77
5.3 Model Parameters and Model Set-up	77

5.3.1 Parameters describing terrain geometry.....	78
5.3.2 Parameters describing mudflow.....	79
5.3.3 Modelling experiments of a mudflow impacting trains	80
5.4 Results and Discussions	81
5.4.1 The effect of buffer distance D and railway embankment height H_2 (Set I)	82
5.4.2 The effect of hillslope steepness α (Set II).....	89
5.4.3 The effect of railway embankment slope ratio $H:V$ (Set III).....	92
5.4.4 The effect of mudflow volume V (Set IV)	96
5.4.5 The effect of surface roughness n (Set V).....	102
5.4.6 Discussion and summary	103
Chapter Six: Conclusion and Recommendations.....	106
6.1 Introduction.....	106
6.2 Conclusion.....	106
6.3 Recommendations	108
References	110

List of Figures

Figure 2. 1. Mechanical resemblances and differences for subaerial mass movements (Takahashi 2006).....	6
Figure 2. 2. Equivalent friction coefficients in debris flow, landslide/debris avalanche and pyroclastic flow (data from Chigira (2001), Iverson (1997), Hsu (1975) and Kaneko and Kamata (1992)).....	7
Figure 2. 3. Mudflows (Leidenfrost 2012).....	9
Figure 2. 4. The numerical computation of fluid particle velocity (DualSPHysics 2018).....	20
Figure 2. 5. The numerical computation of fluid particle pressure (DualSPHysics 2018).....	20
Figure 2. 6. The numerical computation of interactive force of fluid particles and boundary particles (DualSPHysics 2018).....	21
Figure 2. 7. Horse-drawn Trains (Henninig 2006).....	22
Figure 2. 8. The locomotive in the Age of Steam (Bentley 2014).....	22
Figure 2. 9. High-speed railway (People.cn 2015).....	23
Figure 2. 10. Railway track structure (Li et al. 2016).....	24
Figure 2. 11. Ballasted Track (AGICO GROUP 2020).....	25
Figure 2. 12. Railway infrastructure (Li et al. 2016).....	26
Figure 2. 13. Railway track-bed formation (Sujay 2017).....	27
Figure 2. 14. The new fill embankment construction (Li et al. 2016).....	28
Figure 2. 15. The side-hill construction (Li et al. 2016).....	29
Figure 2. 16. Wheel-rail action at the commencement of derailment (Nadal 1896).....	30
Figure 3. 1. Railway track (Ciotlaus et al. 2016).....	34
Figure 3. 2. The simple layout of a rails upon an embankment (Sujay 2017).....	38
Figure 3. 3. Timber sleepers (LooiNL 2007).....	39
Figure 3. 4. Steel railway sleepers (AGICO GROUP 2020).....	40
Figure 3. 5. Mono block concrete sleepers (AGICO GROUP 2020).....	40
Figure 3. 6. Twin-Block concrete sleepers (Remennikov and Kaewunruen 2006).....	41
Figure 3. 7. Twin-block concrete sleepers (AGICO GROUP 2020).....	41
Figure 3. 8. Standard particle size of debris flow (He et al. 2016).....	44

Figure 3. 9. Distribution of sensitive clay and associated landslides in Ottawa Valley (Fransham et al. 1977).....	45
Figure 3. 10. Classification of sensitive clay slopes (Fransham and Gadd 1977).....	46
Figure 3. 11. Bingham Model (Widjaja et al. 2014)	48
Figure 3. 12. Layout of terrain condition in model	50
Figure 4. 1. The slope in large-scale field test (Bugnion et al. 2010)	52
Figure 4. 2. Pressure plates used in the field test to measure impact pressure (left side) and (right side) debris flow impacting the pressure plates (Bugnion et al. 2010)	53
Figure 4. 3. a) The slope modeled in DualSPHysics.....	55
Figure 4. 3. b) The slope modeled in DualSPHysics with a pressure sensor at 30m downslope position and a barrier at the end of the channel (continued)	56
Figure 4. 4. a) Diagram of velocity versus artificial viscosity for the first series simulations.....	59
Figure 4. 4. b) Diagram of impact coefficient C versus artificial viscosity for the first series simulations (continued).....	60
Figure 4. 5. a) The fluid behaviour when $dp=0.125m$ with artificial viscosity=5	61
Figure 4. 5. b) The fluid behaviour when $dp=0.125m$ with artificial viscosity=10	61
Figure 4. 5. c) The fluid behavior when $dp=0.125m$ with artificial viscosity=15 (continued).....	62
Figure 4. 6. a) Diagram of velocity versus dp for Test A	63
Figure 4. 6. b) Diagram of impact coefficient C versus dp for Test A (continued).....	64
Figure 4. 7. a) The visualization snapshot with $dp=0.125m$ (the instant that the mudflow hits the pressure plate)	64
Figure 4. 7. b) The visualization snapshot with $dp=0.1m$ (the instant that the mudflow hits the pressure plate) (continued).....	65
Figure 4. 7. c) The visualization snapshot with $dp=0.075m$ (the instant that the mudflow hits the pressure plate) (continued).....	65
Figure 4. 7. d) The visualization snapshot with $dp=0.05m$ (the instant that the mudflow hits the pressure plate) (continued).....	66
Figure 4. 7. e) The visualization snapshot with $dp=0.025m$ (the instant that the mudflow hits the pressure plate) (continued).....	66
Figure 4. 8. a) Test B series with $dp=0.1m$, artificial viscosity=15	70
Figure 4. 8. b) Test C series with $dp=0.075m$, artificial viscosity=7.5	70
Figure 4. 8. c) Test D series with $dp=0.05m$, artificial viscosity=5 (continued)	71

Figure 4. 8. d) Test E series with $d_p=0.025\text{m}$, artificial viscosity=2.5 (continued).....	71
Figure 5. 1. The sketch of the terrain environment in the model	76
Figure 5. 2. The components of model created in DualSPHysics.....	77
Figure 5. 3. The slope terrain and railway embankment of Subtest 1	83
Figure 5. 4. Diagram of the impact force exerted on the railway car for Set I tests (note: the critical value of train derailment $Q=1293.6\text{kN}$)	83
Figure 5. 5. a) Snapshot of mudflow motion at time=0s for a model with $D=1\text{m}$ and $H_2=1\text{m}$	84
Figure 5. 5. b) Snapshot of mudflow motion at time=30s for a model with $D=1\text{m}$ and $H_2=1\text{m}$..	84
Figure 5. 5. c) Snapshot of mudflow motion at time=87s for a model with $D=1\text{m}$ and $H_2=1\text{m}$ (continued)	85
Figure 5. 5. d) Snapshot of mudflow motion at time=95s for a model with $D=1\text{m}$ and $H_2=1\text{m}$ (continued)	85
Figure 5. 6. a) Snapshot of mudflow motion at time=0s for a model with $D=1\text{m}$ and $H_2=3\text{m}$	86
Figure 5. 6. b) Snapshot of mudflow motion at time=30s for a model with $D=1\text{m}$ and $H_2=3\text{m}$..	86
Figure 5. 6. c) Snapshot of mudflow motion at time=87s for a model with $D=1\text{m}$ and $H_2=3\text{m}$ (continued)	87
Figure 5. 6. d) Snapshot of mudflow motion at time=100s for a model with $D=1\text{m}$ and $H_2=3\text{m}$ (continued)	87
Figure 5. 6. e) Snapshot of mudflow motion at time=110s for a model with $D=1\text{m}$ and $H_2=3\text{m}$ (continued)	88
Figure 5. 7. a) Diagram of the impact force exerted on the railway car with hillslope inclination equal to 10 degrees	90
Figure 5. 7. b) Diagram of the impact force exerted on the railway car with hillslope inclination equal to 20 degrees	90
Figure 5. 7. c) Diagram of the impact force exerted on the railway car with hillslope inclination equal to 30 degrees (continued)	91
Figure 5. 8. The relationship between the maximum impact force and the hillslope inclination (note: the horizontal dashed line is $Q=1293.6\text{ kN}$)	92
Figure 5. 9. a) Comparison diagram of the impact force exerted on a railway car with hillslope inclination equal to 10 degrees.....	94
Figure 5. 9. b) Comparison diagram of the impact force exerted on a railway car with hillslope inclination equal to 20 degrees.....	94
Figure 5. 9. c) Comparison diagram of the impact force exerted on a railway car with hillslope inclination equal to 30 degrees (continued)	95

Figure 5. 10. a) Diagram of the impact force exerted on the railway car with mudflow volume $V=50\text{m}^3$ 98

Figure 5. 10. b) Diagram of the impact force exerted on the railway car with mudflow volume $V=75\text{m}^3$ 98

Figure 5. 10. c) Diagram of the impact force exerted on the railway car with mudflow volume $V=100\text{m}^3$ (continued)..... 99

Figure 5. 11. The relationship between the maximum impact force and the volume of mudflow (note: the horizontal dashed line is the critical value of train derailment $Q=1293.6\text{ kN}$) 100

Figure 5. 12. The impact force obtained of Test 17 (note: the horizontal dashed line is the critical value of train derailment $Q=1293.6\text{ kN}$) 101

Figure 5. 13. The relationship between the impact force and the terrain roughness (note: the horizontal dashed line is the critical value of train derailment $Q=1293.6\text{ kN}$) 103

List of Tables

Table 2. 1. The details of hardware used.....	14
Table 3. 1. Desirability of soil type for new slopes (Li et al. 2016).....	33
Table 3. 2. Typical minimum slope ratios of horizontal to vertical (assuming the material is compacted to a high relative density) (Li et al. 2016).....	33
Table 3. 3. Parameters for rail superstructure and load conditions (Ciotlaus et al. 2016)	34
Table 3. 4. Soil properties of the layers comprising an embankment (Ciotlaus et al. 2016)	34
Table 3. 5. Safety factor (FS) for different embankments heights and soil types using Bishop’s method (Ciotlaus et al. 2016)	35
Table 3. 6. Typical HAL freight trains around the world (Li et al. 2016)	37
Table 3. 7. Railway gauge values (Selig and Waters 1994).....	37
Table 3. 8. A worldwide survey of sleepers in railway networks (International Federation for Structural Concrete 2006)	42
Table 3. 9. A summary of calculation methods based on various empirical parameters for a typical debris flow.....	43
Table 3. 10. Grain size distribution of mud-rock flow, mudflow and water-rock flow (Zhang 1993)	47
Table 4. 1. Empirical coefficients in hydrodynamic models.....	54
Table 4. 2. Input data for the first series of calibration tests	59
Table 4. 3. Values for the Test A series in the second step of calibration tests with changes in d_p	63
Table 4. 4. Values for the Test B series under the condition of $d_p=0.1\text{m}$ and artificial viscosity from 1 to 20.....	68
Table 4. 5. Values for the Test C series under the condition of $d_p=0.075\text{m}$ and artificial viscosity from 1 to 20.....	68
Table 4. 6. Values for the Test D series under the condition of $d_p=0.05\text{m}$ and artificial viscosity from 1 to 20.....	68
Table 4. 7. Values for the Test E series under the condition of $d_p=0.025\text{m}$ and artificial viscosity from 1 to 20.....	68
Table 4. 8. Results of the models simulated with different combinations of artificial viscosity and d_p	69
Table 4. 9. Models simulated with different combinations of artificial viscosity and d_p	72

Table 4. 10. Values for the Test F series under the condition of $d_p=0.05\text{m}$ and artificial viscosity from 5 to 7.5	73
Table 4. 11. Results from the Test F series under the condition of $d_p=0.05\text{m}$ and artificial viscosity from 5 to 7.5	74
Table 5. 1. The values of parameters in the numerical investigation.....	80
Table 5. 2. Input data of Set I for the investigation of the effect of buffer distance and railway embankment height	82
Table 5. 3. Input data of Set II for the investigation of the effect of hillslope steepness	89
Table 5. 4. Input data of Set III for the investigation of the effect of railway embankment slope ratio.....	93
Table 5. 5. Input data of Set IV for the investigation of the effect of mudflow volume	97
Table 5. 6. Input data of Test 17 for the investigation of the critical mudflow volume	101
Table 5. 7. Input data of Set V for the investigation of the effect of surface roughness.....	102

Notation

d_p	=	Flow particle diameter (m)
h	=	Depth of flow (m)
σ	=	Particle density (kg/m^3)
ρ	=	Interstitial fluid density (kg/m^3)
g	=	Gravity acceleration (m/s^2)
μ	=	Viscosity of a viscous fluid (poise/Pa·s)
C	=	Coarse particle concentration by volume
e	=	Restitution coefficient of particles
ϕ	=	Friction coefficient between particles
u	=	Velocity of flow (m/s)
z	=	Height of flow (m)
T_c	=	Inertial particle shear stress (Pa)
T_t	=	Turbulent mixing stress (Pa)
ρ_m	=	Density of interstitial fluid (kg/m^3)
L	=	Length of flow (m)
T_{sq}	=	Quasi-static Coulomb friction stress (Pa)
T_{fq}	=	Viscous shear stress due to the deformation of the fluid (Pa)
N_{Bag}	=	Bagnold number
N_{mud}	=	Index determining flow's type
N_{Rey}	=	Reynolds number
U	=	Mean cross-sectional velocity (m/s)
C_3	=	Threshold value of solids concentration
N_{Sav}	=	Savage number
N	=	Total number of particles
$W(x,h)$	=	Kernel function
h	=	Smoothing length

k	=	Particle k
r_k	=	Particle position
v_k	=	Particle volume (m ³)
v_k	=	Particle velocity (m/s)
m_k	=	Particle mass (kg)
r	=	Distance between any two given particles (m)
P_k	=	Pressure of fluid particle k (Pa)
ρ_k	=	Density of particle k (kg/m ³)
c_{ab}	=	Mean speed of sound (m/s)
μ_{ab}	=	Coefficient $\mu_{ab} = hv_{ab} \cdot r_{ab} / (r_{ab}^2 + \eta^2)$
η^2	=	Value of $\eta^2 = 0.01h^2$
ν_0	=	Kinematic viscosity of fluid (m ² /s)
$\vec{\tau}$	=	SPS stress tensor
ρ_0	=	Reference water density (1000 kg/m ³)
c_0	=	Speed of sound at the reference density (m/s)
γ	=	Equals 7 in DualSPHysics
Ψ_{ab}	=	Density diffusion
δ_Φ	=	Coefficient equals to 1 in DualSPHysics
F	=	Force of particles (kN)
Q	=	Transverse wheel-rail force (impact force by mudflows) (kN)
P	=	Vertical wheel-rail force (kN)
T	=	Tangential friction
N	=	Force of the wheel-rail contact (kN)
μ'	=	Friction coefficient of the wheel-rail contact
α'	=	Flange angle (°)
k	=	Empirical factor
P	=	Fluid pressure (Pa)
C	=	Impact empirical coefficient

F_r	=	Froude number
τ	=	Shear stress (Pa)
τ_y	=	Yield stress (Pa)
n	=	Coefficient representing terrain roughness
R	=	Hydraulic radius in Manning's Equation (m)
θ	=	Channel slope in Manning's Equation ($^\circ$)
b	=	Width of flow (m)
H_1	=	Natural hillslope height (m)
H_2	=	Railway embankment height (m)
D	=	Buffer distance (m)
α	=	Natural hillslope inclination ($^\circ$)
β	=	Railway embankment slope inclination ($^\circ$)
V	=	Volume of mudflow (m^3)
dp	=	Initial particle distance (m)

Chapter One: Introduction

1.1 Background

At the beginning of the third decade of the 21st century, there is an increasing demand of carrying more goods and heavier loads over our railway lines. This, coupled with a decrease in construction of new railway lines, taxes the existing railway lines, which were built decades ago using design standards that could not anticipate the volume and weight of freight trains currently in service. To meet the new demands, the better utilization of existing lines by carrying more loads is an important issue to be considered, especially in mountainous area which has large risk of occurring mudflows, posing detrimental effect to railway cars. In certain parts of the country, for instance, in the St. Lawrence Lowlands or the Ottawa Valley, railways were constructed on soils that are prone to destructive mudflows. However, such soils are not localized only to Canada, but can be found in SiChuan province in China, where the mountainous areas and abundant precipitation lead to mudflows. Since both geographic areas are home to millions of people with advanced infrastructure, it is inevitable that railway tracks traverse these areas. These tracks built near slopes formed by mudflow-prone soils are in danger of inundation and damage. This, in a severe case might result in the inhabitants' life of the area being threatened or the property and vegetation damage. Certain soils, like the Leda or Champlain Sea clays of Canada or the Chengdu clays of the southwest region in China lose most of their strength when are disturbed by abundant precipitation, generating mudflows. When a mudflow hits a railway line, the consequences and damage can range from temporary interruption of service to the total destruction of railway infrastructure. Particularly, if railcars are located on a railway embankment when a mudflow occurs, the possibility of serious derailment greatly increases. The occurrence of any of the above dangerous situations can have a severe loss of human life and individual or even public property. Therefore, proper consideration has to be given to such potential mountainous environment and the risk of train derailment problem, it is necessary to avoid it, if possible, or reduce the impact of these situations. The factors of environmental condition under which are prone to mudflows and has the potential of train derailment have to be investigated, furthermore, on basis of that, the corresponding mitigation countermeasures should be prepared to reduce losses when or if a mudflow occurs. Additionally, not only the terrain environmental condition, the mudflows' property like volume released is also essential to be considered, as the quantity of mudflow generated could be great volume in the reality, it could very well be that no protective measures would result in preventing a railway car from being tipped over when the quantity of mudflow exceeds a certain volume. However, the damage in such incidents would have been reduced or would not have occurred if there could be a way to divert or reduce the discharge of mudflow to be less than this certain volume, that is, the critical mudflow volume, which is also necessary to investigate.

With the rapid development of computer technology, numerical methods have been widely adopted, it is possible to examine the interaction of fluid flow with solid objects by using a simulation tool instead of measurements on site or in the laboratory. Due to the free surface, most conventional methods used in fluid mechanics incur a great cost due to tracking the surface and updating the mesh at every time step. However, particle-based computational fluid dynamics methods, such as Smoothed Particle Hydrodynamics (SPH), can resolve the free surface with ease.

1.2 Objective

In the study area, the St. Lawrence Lowlands or the Ottawa Valley, natural slope consisting of Champlain Sea clays close to rail lines has large potential of triggering mudflows which could cause the train derailment. It could potentially threaten railway car safety, not only public property but also human life. Therefore, the investigation of the interaction of potential flow with trains, the parameters affecting mudflows' destructive force, and the train derailment potential is important to be performed. Based on the mesh-free numerical methods, this research is devised to investigate the influence of natural slope geometric parameter, embankment geometric factor and mudflow material properties on the impact force exerted by mudflows on trains. Within the proposed model, a railway car is assumed to be on top of an embankment and the interaction of mudflow with rail vehicles is quantitatively examined and analyzed. The case of train derailment serves as a criterion to quantify the effect. And finally, the most critical case can be obtained for given combination parameters, which could be regarded as a reference in practice. Here, the detailed objectives of this research can be summarized as follows:

- To study the feasibility of modeling mudflows utilizing the smoothed particle hydrodynamics method based on the available data in the literature.
- To develop a numerical 3D model of mudflows impacting trains in the simulation tool to perform parametric model studies.
- To quantitatively analyze the interaction of flow with trains and what parameters affect the flow and its destructive force.
- To investigate the most critical (worst) case and geometric parameters and suggest corresponding mitigation measures.

To simplify simulation and calculation, 3D models assuming a cube-shaped object with a certain weight as a railway car in all cases, which generates vertical wheel-rail force. Accordingly, the interactive force between mudflow and railway cars could be compared to that force and observe the potential of the train derailment. Moreover, any other environmental changes, such as temperature and wind, are not considered as well.

1.3 Methodology

The methodology is a critical step in determining the success of a research. In this numerical investigation, the methodology opted to achieve the abovementioned objectives was to determine the fundamental mechanics of mudflow, the principles of the smoothed particle hydrodynamics (SPH) method and the general operation of railways by studying previous research. Then, the key model parameters that describe a model of mudflows impacting trains (mudflow material properties, slope profiles, embankment geometries, loading due to trains, etc.) were gathered based on a literature review. Accordingly, adopting the properties of mudflow and slope profile in the simulation tool, and calibrating the program based on a physical large-scale field experiment performed and reported by literature to reproduce a real-world mudflow process. Finally, the scenarios of mudflows impacting railway cars under different cases were simulated with the aid of

the simulation tool to perform parametric model studies. The influence of each principal parameter was investigated separately using a *Control Variable* method. A comprehensive parametric study of the primary parameters was conducted among five sets of models, including:

- 1) Set I : Buffer distance and railway embankment height being variable
- 2) Set II : Natural hillslope inclination being variable
- 3) Set III: Railway embankment slope ratio (H:V) being variable
- 4) Set IV: Mudflow volume being variable
- 5) Set V : Terrain roughness being variable

On basis of that, the results obtained by the parametric study were analyzed, along with the graphical representations to better investigate the most critical case of train derailment under these conditions.

Chapter Two: Literature Review

2.1 The Fundamental Mechanics of Mudflow

2.1.1 Introduction

Currently, more and more attention is being paid to natural disasters, such as floods, hurricanes, tornadoes, volcanic eruptions and earthquakes. Any of the abovementioned natural disasters could cause various sediment moving phenomena, especially in mountainous areas or lowlands near river. Although the whole society and technology have already developed and reached to an unprecedented level, the problems of the natural disasters still cannot be ignored. Various sediment moving phenomena play a very important role within these disasters, which are extremely destructive to human lives and property.

2.1.2 Types of sediment-moving phenomena

Generally, natural sediment motion or transportation on a slope is divided into two types: one moves in a mass and motivated by gravity and the another one is driven by fluid dynamic forces and moves as an individual particle motion (Takahashi 2014). Natural sediments, are all particulate substances from clay particle size to huge boulders. While, the first type, sediment motions or transportations in a mass motivated by gravity have four representatives (Takahashi 2014):

1. Landslides and landslips (cliff failures)
2. Debris avalanches
3. Pyroclastic flows
4. Debris flows and immature debris flows

Among these geophysical sediment moving phenomena, in 1996 the World Landslide Inventory Commission defined landslides and landslips as the gravitational mass down slope motions of rock, debris or earth (Takahashi 2014). The second type, individual particle motions which is motivated by fluid dynamic forces include bed load, suspended load and wash load in river flows, blown sand in the deserts or at the seacoasts.

According to Takahashi (2014), the essential mechanisms of the four geophysical massive sediment motions mentioned above are outlined as follows:

1. In the case of landslides and landslips, the block moves on a slip surface, and the deformation inside the block is small. Therefore, it is essentially a rigid body movement phenomenon. The distance of motion is short. When it reaches an almost horizontal area, the maximum distance can be almost twice the height of the scar.
2. Debris avalanches are mainly caused by a very large landslides of a few million cubic meters or more. The rapid demolition of a sliding block occurs early in the initial slipping stage and it can reach much further distance than a landslide or landslip. A slipping rigid body will decelerate and finally stop when the kinetic friction force becomes larger than the gravitational driving force. The friction force is the product of the load acting vertically to the slip surface and the kinetic friction coefficient. As the kinetic friction coefficient has a nearly constant value, if the mass does not change, the friction force acting on the rigid

body becomes larger as the slope angle becomes flatter; on the contrary, the driving force which becomes smaller with a decreasing slope gradient. Hence, with a decreasing slope gradient, the motion of rigid body will stop.

3. A natural disaster event of a pyroclastic flow has occurred at the Unzen volcano in Japan in 1990. According to relevant reports from that time, the pyroclastic flow at Unzen was produced by the collapse of the lava dome and during the process of falling down, a huge rock block was crushed into fine material and it flowed down to a distant flat area. This is one type of pyroclastic flow. Although there are several types based on the classification by the material composition, processes of occurrence and magnitude. The mechanics of flow in any type are all controlled by the gas ejection from the material itself. The volcanic gas ejected from the material can form an upward gas flow which is fast enough to sustain the particle's weight, and then the gas flow produces a fluidized layer within the flow. Because the inter-particle friction force in the fluidized layer is minimal, thus large mobility is attained.
4. As mentioned before, debris flows are a combination of moving water and a great volume of sediment in various ratios. Therefore, numerous particles dispersed in water or slurry move within the debris flow. As it can flow even on a gentle slope, the buoyancy acting on each particle must have some effects on the large mobility. However, buoyancy is not strong enough to sustain the entire weight of heavy particles by itself, hence, some other mechanisms to sustain particles and to keep the distances between particles wide enough to make the motion of particles easier.

With the attention of people on natural sediment motion or transportation, more and more classifications of sediment motions have been proposed. Among them, one proposed by Varnes (1978) is the most popular. The schematic illustration of various moving patterns is demonstrated on a plane whose orthogonal two axes are the types of motion (falling, tilting and toppling, sliding, lateral spreading, and flow) and the material types before the initiation of motion (bedrock, coarse rock debris, rock debris, sand, and fine particles), respectively. Later, Furuya (1980) modified Varnes' diagram slightly for including surface landslips and improve some defects of Varnes' diagram. Ohyagi (1985) split the Varnes' plane into multi-layered planes related to the velocities of motion and changed it from one plane (Varnes' diagram) to a three-dimensional one by adding the vertical axis to represent velocity. More and more classifications are proposed, among them, Pierson and Costa (1987) focused on velocity and solids concentration; Coussot and Meunier (1996) had more interest in velocity, solids concentration and material cohesion. These classifications are all empirical and qualitative, although easy to understand, but not enough. The physical mechanisms of motion and transition process from rigid body to flow is still not considered.

Takahashi (2001) classified the subaerial mass flows consisting of granular materials (particle sizes may vary from powder to rigid body like mountain blocks) focusing on the essential mechanism to control the phenomena. The classification (Takahashi 2006) is shown in Figure 2.1. Subaerial massive sediment motions, closely related to sediment hazards, are basically divided into falls, flows and slips. Based on the specific aspects, the phenomena are presented by eight blocks as following Figure 2.1 The upper five blocks represent the phenomena in which particles are dispersed in the flowing body, and the lower three represent the phenomena in which the moving bodies are mostly the blocks of soil and rocks.

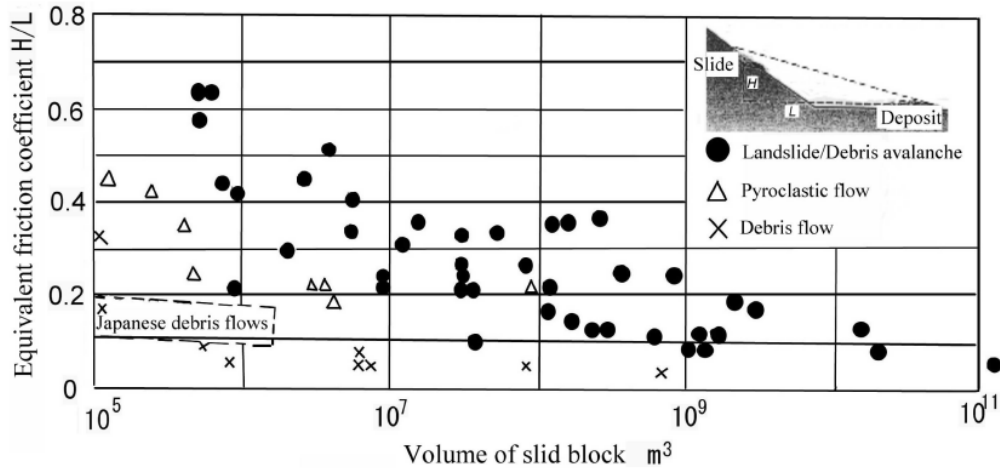


Figure 2.2. Equivalent friction coefficients in debris flow, landslide/debris avalanche and pyroclastic flow (data from Chigira (2001), Iverson (1997), Hsu (1975) and Kaneko and Kamata (1992))

It is evident from Figure 2.2 that debris flows have a lower friction, thus debris flows have a much higher mobility than any other pyroclastic flow and landslide, suggesting debris flows have a larger water content than any other mass movements which makes a large mobility.

2.1.4 Classification of debris flow

The definition of debris flows mentioned before does not take into consideration the concentrations of sediment in flow, material's sizes, distributions, the properties of interstitial fluid, and the hydraulic conditions of flow (such as velocity, depth and channel slope gradient). The behaviors and the destructive powers of debris flows differ depending on these factors. Thus, there are various types of debris flows based on these different essential factors, and the ways to classify debris flow are also different. Among these different methods of classifications, the classifications by material involved are often used. According to Zhang (1993), the debris flow can be classified into three common types:

1. Mud-rock flow
2. Mudflow
3. Water-rock flow

Besides that, classifications based on other points are also possible. For example, the classification based on causes and processes of occurrence is described by Takahashi (2014), the causes of debris flow generation are:

1. Rainfall
2. Earthquake
3. Melting of ice and snow
4. Volcanic eruption

5. Destruction of lake

In Japan, based on appearance, the debris flow can be identified three types, as follows (Takahashi 2014):

1. Stony-type debris flows
2. Turbulent-muddy-type debris flows (much turbulent from the forefront to the rear end)
3. Viscous debris flows (the concentration of coarse particles in slurry is more than 50% by volume)

Different from Japan, in China, debris flows are classified into two types depend on whether the interstitial fluid is slurry or water (Takahashi 2014):

1. Mud-stone flows
2. Water-stone flows

It is worth mentioning that the mud-stone flow was further classified (Kan 1996) based on the apparent density of the flowing material:

1. Fluid debris flows (1.3–1.8 t/m³)
2. Quasi-viscous debris flows (1.8–2.0 t/m³)
3. Viscous debris flows (2.0–2.3 t/m³)
4. Highly viscous debris flows (>2.3 t/m³)

2.1.5 Characteristics of mudflow

Based on the information presented in the former two sections, a debris flow is a moving mass composed of loose mud, water, sand, soil, rock, and air, moving down a slope under the influence of gravity. Regarding the size of the grains involved, the debris flow can be classified into three common types: mud-rock flow, mudflow, and water-rock flow (Zhang 1993). Among these three fluid types, mudflow, growing in volume with the addition of water and grains smaller than sand, is a mixture of water and soil solids in various ratios. While in the other two fluid types, more than half of the solids are larger than sand grains. Thus, a mudflow is the sandy but more watery counterparts of debris flow.

According to above, debris flow and mudflow are a combination of moving water and a great volume of sediment in various ratios that travel down a slope. Within a debris flow, different sediments involved generate different fluid types with various characteristics, and different ratios between water and sediment represent different consistency, which is like that of pancake batter. Both are similar to flash floods and can occur suddenly without adequate time for warning people, which will pose a large risk to human lives and property. Therefore, it is important and necessary to investigate the detrimental effect of debris flow. With recent developments in coupling the fluid flow model with rigid body dynamic, it is possible to examine the interaction of flow with solid objects. The fundamental mechanics of debris flow paves the way to implement mudflow using numerical methods, which is presented in the following sections.



Figure 2. 3. Mudflows (Leidenfrost 2012)

2.1.6 Mechanics of debris flow

As mentioned before, debris flows are composed of highly concentrated coarse particles and water or slurry. From the perspective of mechanics, the stresses within the debris flow will be generated due to: a) the collision of coarse particles; b) the turbulence of fluid body composed of particles and slurry; c) the friction between particles; d) the deformation of interstitial fluid or of the apparent viscous fluid consisting of the mixture of particles and slurry; e) and the effect between solid particles and fluid resulting from their relative motion.

Assuming that, the characteristics of flow are depended on the shearing rate d_u/d_z , the representative particle diameter d_p , the depth of flow h , the particle density σ , the interstitial fluid density ρ , acceleration due to gravity g , the viscosity of a viscous fluid comprised of particles and slurry or water μ , the coarse particle concentration by volume C , the restitution coefficient of particles e , and the friction coefficient between particles $\tan \phi$, where u is the velocity of flow at height z measured vertically from the bed surface. The stresses within this flow are the shearing stress and pressure, and these stresses have the dimension $[ML^{-1}T^{-2}]$, in which $[L]$ is the length, $[T]$ the time, and $[M]$ is the mass.

The collision stresses will be generated by the exchange of momentum on the occasion of particle collision. Therefore, they should depend on the collision frequency, the particle mass and the restitution coefficient. Because the collision frequency is the encounter frequency of particles which is embedded in the vertically adjacent two layers, it is assumed to be a function of the shear rate and the particle concentration. Based on these considerations, assumptions and the dimensional analysis. The shear stress due to particle collision T_c would be written as:

$$T_c = f(C, e)\sigma d_p^2 \left(\frac{d_u}{d_z}\right)^2 \quad (2.1)$$

where $f(C, e)$ represents a function of C and e , and this function is thought to become large with increasing C and e .

By the application of principles of fluid mechanics, the macro turbulent mixing stress of fluid body T_t is written as:

$$T_t = \rho_m l^2 \left(\frac{d_u}{d_z} \right)^2 \quad (2.2)$$

where ρ_m is the apparent density of interstitial fluid or entire mixture. The length L takes an important role within this expression; when the particles within flow are large, the particle concentration is also large and then it would have the scale of distance between particles, and as Iverson (1997) assumed, it would be estimated as $L \sim d_p$. But, as in the case of the turbulent-muddy-type debris flow, when the entire mixture body is violently turbulent, it would be estimated as $L \sim h$ (large-scale mixing case). In this case, the interstitial fluid, ρ_m is equal to the density of interstitial fluid ρ or the density of the entire mixture body.

At height z , the quasi-static Coulomb friction stress T_{sq} , which is caused by enduring particles contacts, is affected by the total weight of all particles existing above the height z , and it is written as:

$$T_{sq} = C(\sigma - \rho_m)g(h - z)\tan\varphi \quad (2.3)$$

For a Newtonian fluid, the shearing stress T_{fq} due to the deformation of fluid is:

$$T_{fq} = \mu \left(\frac{d_u}{d_z} \right) \quad (2.4)$$

Concerning the effect between particles and fluid resulting from the relative motion, the solid-fluid interaction stresses, Iverson (1997) noticed the permeability of the inter-particle void space, which are related to the buffering effect to the direct inter-particle action. Owing to the dispersion of particles in viscous fluid is the result of this buffering effect, herein, these stresses are not considered.

The ratio of inertial particle stress T_c and viscous shear stress due to the deformation of fluid T_{fq} that is given by:

$$N_{Bag} = \frac{f(C, e)\sigma d_p^2 \left(\frac{d_u}{d_z} \right)}{\mu} \quad (2.5)$$

Where the value of this ratio is called the Bagnold number, representing the relative predominance of the respective stresses. In inertial debris flows the Bagnold number is large.

The ratio of turbulent mixing stress T_t and inertial particles stress T_c does not have such an important meaning when $L \sim d_p$, but, when L is assessed by h (large-scale mixing case), like the turbulent-muddy-type debris flow, the ratio is given by:

$$N_{mud} = \frac{1}{f(C, e)} \left(\frac{\rho_m}{\sigma} \right) \left(\frac{h}{d_p} \right)^2 \quad (2.6)$$

meaning that the relative depth defined by (h/d_p) , can be the index to determine whether the debris flow is the inertial stony-type or the turbulent-muddy-type. When L is replaced by h , the ratio of T_t and T_{fq} is given by:

$$N_{Rey} = \frac{\rho_m h^2}{\mu} \left(\frac{d_u}{d_z} \right) \frac{hU}{\left(\frac{\mu}{\rho_m} \right)} \quad (2.7)$$

where the Rey represents the Reynolds number, which is the index to classify whether the flow is turbulent or laminar and U is the mean cross-sectional velocity.

The ratio of T_c and T_{sq} indicates the relative importance between the particle collision shear stress and quasi-static Coulomb friction stress. To transmit the quasi-static Coulomb friction stress, particles must always be in contact even though their relative position continuously changes. This condition requires that the solids concentration should be larger than a threshold value C_3 (Takahashi 2014). Bagnold (1966) indicates that this condition is fulfilled when C is larger than 0.51 for natural beach sand, but it would depend on the size of particles. As for widely distributed material sizes, the threshold concentration would be larger because small particles will be stored in the void between large particles. Under such a densely concentrated condition, other stresses, except for T_{sq} , become small and the motion would be a quasi-static one. Iverson (1997) gave the ratio of T_c and T_{sq} as follows:

$$N_{sav} = \frac{\sigma d_p \left(\frac{d_u}{d_z} \right)^2}{N(\sigma - \rho) g \tan \phi} \quad (2.8)$$

where N is the total number of particles above the height z and N_{sav} is the Savage number. Iverson (1997) claims if N_{sav} (Savage number) is less than 0.1, the particle collision stress T_c is much smaller than the Coulomb friction stress T_{sq} . Since in most debris flow, the Savage number N_{sav} is less than 0.1, so most debris flows are those in which Coulomb friction stresses play predominant role.

Meanwhile, if the denominator in equation (2.8) multiplied by d_p , this term becomes equal to the Coulomb friction stress operating on the plane at height z . But, multiplying the numerator by d_p does not result in the particle collision shear stress. Furthermore, it is necessary to multiply by $f(C, e)$ to represent the collision shear stress T_c and the coefficient $f(C, e)$ can be large (Campbell 1990). More importantly, to generate the Coulomb friction stress T_{sq} , solids concentration should be larger than the threshold. Therefore, the quasi-static debris flow in which Coulomb friction stress predominate can only occur when its solids concentration is more than the threshold value of about 0.5 (Takahashi 2014).

Therefore, a conclusion can be drawn from the above discussion that there are two kinds of debris flows from mechanical aspects in a wider sense: one is the quasi-static debris flow in which Coulomb friction stress dominates and the other is the dynamic debris flow which are divided into

three kinds, as stated previously. From aspect of mechanics of three types flows: 1) The stony type generated when the grain collision stress dominates; 2) Debris flow becomes the turbulent-muddy type as the turbulent mixing stress dominates; 3) When the viscous stress dominates, it becomes viscous type that the concentration of coarse particles in slurry is more than 50% by volume.

In the real life, the possibility of generation of debris flow is large, especially in inclement weather and mountainous area which could pose a serious threat to human life and public infrastructures. Therefore, it is necessary to predict and simulate the debris flow in advance, and then make the corresponding measures to minimize losses as possible as we can.

2.2 The Smoothed Particle Hydrodynamics (SPH) Method

2.2.1 Introduction

In general, there are three approaches to study the multiphase flow: experiments, theoretical analysis and numerical methods (Wang et al. 2016). With the rapid development of computer technology, numerical methods have been widely adopted. The Finite Difference Method (FDM), Finite Volumes Method (FVM) and Finite Elements Method (FEM) are some of the most commonly used methods (Chung 2002). However, the modeling of debris flow poses serious numerical problems, particularly with regard to the significant distortions of the numerical grid, as it is usually applied in both Eulerian and Lagrangian mesh-based approaches. Among these commonly used numerical methods in modeling physical phenomena, the development of FEM is based on Lagrangian approach, whereas other widely used methods like FVM and FDM originate from Eulerian one. For all these three methods, grid generation is required as the computational frame to provide spatial discretization for the governing equations. Although these numerical methods have been applied successfully, the drawbacks still exist, in terms of grid generation, there could be many possibilities: structured grids, unstructured grids and adaptive meshes (Minatti and Pasculli 2011). Furthermore, when simulating some multiphase flow with large distortions, moving material interfaces, deformable boundaries and free surfaces, these methods can encounter some difficulties. The Eulerian methods (FVM and FDM) are inefficient in treating moving material interfaces, deformable boundaries, free surfaces, etc. In addition, the numerical solutions of fluid flows problems modelled by the Navier-Stokes equations, involving incompressibility and convective terms. In order to avoid the latter one (convective terms), the Lagrangian approach is commonly selected instead of the Eulerian one.

However, within mesh-based Lagrangian methods, like FEM, they cannot resolve well the problems with large mesh element distortion, unless the problem is re-meshed as the simulation proceeds. What's more, a frequent update of the grid is required in order to decrease the excessive mesh distortion due to large deformations, which could consume too much time. Moreover, meshing methods may encounter the problems like mesh distortion, deformity, overlay and twisting which may occur when tracking the interface. Unfortunately, at presents, these drawbacks are hardly avoided owing to they are inherent with grid-based methods.

Therefore, it is clear that the methods that avoid the numerical instability due to the convective terms, lower the grid generation time and that are capable of easily taking free surfaces into account, are very desirable to model free surface flows. Due to the complicated and enormous amount of grid generation and re-generation, in alternative, various mesh-less type techniques have been proposed by different authors over the past decades. Among these mesh-less approaches, Smoothed

Particle Hydrodynamics (SPH) method receives more and more attention owing to its purely mesh-free Lagrangian nature which is suitable for computing highly transitory free surface flows of complex fluids in complex geometries. Different from mesh-based methods, instead of grid generation, the computational domain of SPH is filled with a series of particles to represent the fluid and interact with solid objects. In other words, particles are the computational frame used in SPH method. Each of these particles has a set of physical properties. For fluid dynamics, for example, these properties could be velocity, density, pressure. For the fluid particles, the motion changes and their physical properties follow the governing equation.

2.2.2 The simulation tool: DualSPHysics

As the preceding brief description of SPH method, in the study of fluid mechanics, Smoothed Particle Hydrodynamics (SPH) is a numerical method increasingly used within the field of Computational Fluid Dynamics (CFD) to simulate complex free-surface flows. As a Lagrangian meshless method, SPH does not require enormous computational mesh while particles represent the flow and interact with structures.

SPHysics is an open-source numerical model based on SPH method appeared in the domain of fluid simulation, which developed by researchers from the Johns Hopkins University (US), the University of Vigo (Spain), the University of Manchester (UK) and the University of Rome, La Sapienza, written initially in FORTRAN. However, due to its high computational cost, SPHysics is rarely applied to real engineering problems, hardware acceleration and parallel computing are required to make it more useful and practical. But in the reality, supercomputers are expensive to buy and maintain, thus, the appearance of Graphics Processing Units (GPUs) perfectly solve this problem which becomes a cheap alternative to accelerate numerical models. What's more, GPUs are designed to treat large data flows and to render pixels at a several tens of frames per second. From a computational point of view, they are highly efficient thanks to their multi-threading capability. Thus, comparing running on a single Central Processing Units conventionally, the novel computing architectures GPUs perform much faster. As consequence, after a combination of CPU-GPU code, the code named DualSPHysics has been developed by starting from the SPH formulation implemented in the FORTRAN SPHysics code. DualSPHysics is implemented in C++ and CUDA, the real engineering problems with software can be run on either CPUs or GPUs. GPUs calculations of DualSPHysics model, as one of its biggest advantages, this makes the time of calculation lowered significantly which can be efficiently applied over large domains and make up the shortcoming of SPHysics. Consequently, DualSPHysics not only possesses the accuracy and stability performed by the former SPHysics code, also with the performance enhancement available from GPUs and CUDA. Within the recent years, the DualSPHysics model has already been increasingly performed in hydrodynamic cases by various researchers, like a dam break impacting with an obstacle, which be validated accurate and efficient when dealing with a gravity-dominated flow problem. Therefore, this research focus on implementing SPH formulations for hydrodynamic modeling by running DualSPHysics code on GPUs.

The following simulations performed in this thesis were carried out using an NVIDIA Tesla-P6 GPU, the details of hardware used were presented below:

Device	Compute capability	Memory size	CUDA cores
Tesla P6	6.1	16 GB	2,048 (16 Multiprocessors, 128 CUDA Cores/MP)

Table 2. 1. The details of hardware used

The SPH simulations in DualSPHysics code could be either two-dimensional or three-dimensional. Although 3D simulations have a high computational cost in terms of computing time resulting from the need for many particles, the three-dimensional effects are important in the case of the impact of the flowing material on structures and buildings (Pastor et al. 2014). Since the three-dimensional nature of the real-world phenomenon constitutes the main feature of the problem of the interaction between fluids and solid structures (Gómez-Gesteira and Dalrymple 2004). The resulting velocity, pressure and forces exerted by the fluid on solid objects maybe not fully correct in the two-dimensional model due to the limited information in the dimension of width (Y-axis). For more reliable results, it is essential to model mudflows over realistically complex three-dimensional (3D) conditions to reproduce realistic mudflow events in the real-world. Moreover, the proposed 3D model in DualSPHysics can import data with the format of scientific visualization tools, like Paraview, into a high-quality 3D rendering software where solutions for many visual effects are also provided. For this reason, the interpretation of viscous, uniform and continuous characteristics of mudflows is fairly limited in two-dimensional (2D) models. 3D models are the basis of models describing all existing fluid and solid phases and their interactions (Pastor et al. 2014).

Therefore, the 3D version of the model was chosen in DualSPHysics to reproduce the three-dimensional phenomenon of mudflows impacting railway cars. In the following sections, the implementation of the SPH model for mudflows was firstly presented, followed by model calibration and numerical simulation of mudflows impacting railway cars in 3D conditions.

2.2.3 Implementation of SPH method for mudflows

On basis of the particles in SPH numerical method, the most important step in SPH is using kernel and particle approximations to find out approximate numerical solutions. The core SPH formulations implemented by DualSPHysics are presented by following:

2.2.3.1 Kernel function

SPH is a pure Lagrangian meshless method, points substituting meshes to represent particles. When SPH is used for the simulation of fluid dynamics, the discretized Navier-Stokes equations are locally integrated at the location of each of these particles, in accordance with the physical properties of surrounding particles. The surrounding neighbor particles are determined by a function on a basis of distance either in two-dimension or in three dimensions, the associated characteristic length or smoothing length often defined as h . At each timestep, new values of the physical quantities will be calculated for each particle, and the position of particles will then be updated according to the new physical quantities.

It is necessary for the conservation laws of continuum fluid dynamics transfer from their partial differential form into a function suitable in the particle-based simulation. This transformation could be achieved by using integral equations based on interpolation functions which is typically referred as the kernel function (W). This kernel function has many different forms but the most commonly

used is the cubic and the quintic. But in all forms, it always represents a function $F(r)$ defined in r' by the integral approximation:

$$F(r) = \int F(r')W(r - r', h)dr' \quad (2.9)$$

The smoothing kernel must fulfill certain properties (Monaghan 1992; Liu 2003), such as compact support, positivity inside a defined zone of interaction. Then, the function F can be approximated in a discrete, non-continuous form on a basis of the set of particles, forming an interpolation at a single particle through a summation over all the particles within its region of compact support which defined by the smoothing length h :

$$F(r_a) \approx \sum_b F(r_b)W(r_a - r_b, h) \Delta v_b \quad (2.10)$$

Where r_k and v_k are the particle position and particle volume respectively, the subscript a denotes an individual particle where being interpolated, b is the neighboring particle, v_b is the volume of a neighboring particle b . When the neighboring particle b with a mass m and a density ρ , then the equation (2.10) can be represented:

$$F(r_a) \approx \sum_b \frac{F(r_b)m_b}{\rho_b} W(r_a - r_b, h) \quad (2.11)$$

2.2.3.2 Smoothing kernel

As mentioned earlier, compact support is defined by the smoothing length h , while within the smoothing kernel, kernel is expressed as a function of the non-dimensional distance between particles given by $q = r/h$, where r is the distance between any two given particles a and b and the smoothing length h which determines the size of the area around particle a in which neighboring particles b are considered. The performance of an SPH model depends heavily on the choice of the smoothing kernel. Thus, the choice of the smoothing kernel will largely affect the performance of an SPH model. Within DualSPHysics, there are two common kernel definitions applied:

- Cubic Spline (Monaghan and Lattanzio 1985):

$$W(r, h) = \alpha_D \begin{cases} 1 - \frac{3}{2}q^2 + \frac{3}{4}q^3 & 0 \leq q \leq 1 \\ \frac{1}{4}(2 - q)^3 & 1 \leq q \leq 2 \\ 0 & q \geq 2 \end{cases} \quad (2.12)$$

Where α_D is equal to $10/7\pi h^2$ in 2D and $1/\pi h^3$ in 3D.

- Quintic (Wendland 1995):

$$W(r, h) = \alpha_D \left(1 - \frac{q}{2}\right)^4 (2q + 1) \quad 0 \leq q \leq 2 \quad (2.13)$$

Where α_D is equal to $7/4\pi h^2$ in 2D and $21/16\pi h^3$ in 3D. And commonly, the Wendland kernel definition is default in DualSPHysics.

2.2.3.3 Momentum equation

In SPH method, the momentum conservation equation in a continuum is applied to update the value of the acceleration of a particle which is given by:

$$\frac{dv}{dt} = -\frac{1}{\rho} \nabla P + g + \Gamma \quad (2.14)$$

Where Γ presents the dissipative terms of the equation and g is the gravity acceleration. The three methods are used in DualSPHysics to define the dissipative term:

- Artificial viscosity (Monaghan 1992) which is a common method within fluid simulation by using SPH due to its simplicity, then Eq. (2.14) can be rewritten:

$$\frac{dv_a}{dt} = - \sum_b m_b \left(\frac{P_b + P_a}{\rho_b \cdot \rho_a} + \Pi ab \right) \nabla_a W_{ab} + g \quad (2.15)$$

Where P_k and ρ_k presents the pressure and density corresponding to particle k respectively and the viscosity term Πab is given by:

$$\Pi ab = \begin{cases} \frac{-\alpha c_{ab} \mu_{ab}}{\rho_{ab}} & v_{ab} \cdot r_{ab} < 0 \\ 0 & v_{ab} \cdot r_{ab} > 0 \end{cases} \quad (2.16)$$

Where $v_{ab} = v_a - v_b$ and $r_{ab} = r_a - r_b$ with v_k and r_k being the velocity and particle position respectively. $\mu_{ab} = h v_{ab} \cdot r_{ab} / (r_{ab}^2 + \eta^2)$, $c_{ab} = 0.5(c_a + c_b)$ meaning speed of sound and $\eta^2 = 0.01 h^2$. α is a coefficient that needs to be tuned to achieve the proper dissipation of the fluid and 0.01 has been validated to have the best results in studying wave propagation and wave loadings exerted onto coastal structures (Altomare et al. 2015).

- Laminar viscosity (Lo and Shao 2002). In SPH, the momentum equation of laminar viscosity is:

$$\frac{dv_a}{dt} = - \sum_b m_b \left(\frac{P_b + P_a}{\rho_b \cdot \rho_a} \right) \nabla_a W_{ab} + g + (v_0 \nabla^2 v)_a \quad (2.17)$$

Where the v_0 is kinematic viscosity of fluid (typically 10^{-6} m²/s for water), laminar viscous stresses $(v_0 \nabla^2 v)_a$ in this momentum equation can be expressed as:

$$(v_0 \nabla^2 v)_a = \sum_b m_b \left(\frac{4 v_0 r_{ab} \cdot \nabla_a W_{ab}}{(\rho_a + \rho_b)(r_{ab}^2 + \eta^2)} \right) v_{ab} \quad (2.18)$$

- Sub-Particle Scale (Gotoh et al., 2001) :

The method of the Sub-Particle Scale (SPS) was first described by Gotoh et al. (2001) to represent the effects of turbulence in their Moving Particle Semi-implicit (MPS) model. The momentum conservation equation is defined as:

$$\frac{dv}{dt} = -\frac{1}{\rho} \nabla P + g + v_0 \nabla^2 V + \frac{1}{\rho} \nabla \cdot \tau \quad (2.19)$$

Where the laminar term is applied as Eq. (2.18) and τ means the SPS stress tensor. The description of SPS used in SPH by the means of Favre-averaging (Dalrymple and Rogers 2006):

$$\left(\frac{1}{\rho} \nabla \tau\right)_a = \sum_b m_b \left(\frac{\tau_{ij}}{\rho_b^2} + \frac{\tau_{ij}}{\rho_a^2}\right) \nabla_a W_{ab} \quad (2.20)$$

Thus, Eq. (2.19) can be represented:

$$\begin{aligned} \frac{dV}{dt} = & -\frac{1}{\rho} \nabla P + g + \sum_b m_b \left(\frac{4v_0 r_{ab} \cdot \nabla_a W_{ab}}{(\rho_a + \rho_b)(r_{ab}^2 + \eta^2)}\right) v_{ab} \\ & + \sum_b m_b \left(\frac{\tau_{ij}}{\rho_b^2} + \frac{\tau_{ij}}{\rho_a^2}\right) \nabla_a W_{ab} \end{aligned} \quad (2.21)$$

Normally, the combination of laminar viscosity and Sub-Particle Scale (SPS) is used to describe the dissipative term in DualSPHysics.

2.2.3.4 Weakly compressible approach using Equation of state

Commonly, following the work of Monaghan (1994), the fluid in the SPH formalism defined in DualSPHysics is treated as weakly compressible and the equation of state is used to determine fluid pressure based on particle density. The relationship between pressure and density follows the expression (Monaghan et al. 1999; Batchelor 1974):

$$P = b \left[\left(\frac{\rho}{\rho_0}\right)^\gamma - 1 \right] \quad (2.22)$$

Where $\gamma = 7$, $\rho_0 = 1000 \text{ kg/m}^3$ as the reference density and $b = c_0^2 \rho_0 / \gamma$, where $c_0 = c \rho_0$ which is the speed of sound at the reference density. Thus, this data will be set for the current simulations.

2.2.3.5 Density diffusion term

During the simulation of a weakly-compressible SPH, the mass of each particle remains constant and only their associated density fluctuates. These fluctuations are computed by using the continuity equation, in SPH form:

$$\frac{d\rho_a}{dt} = \sum_b m_b v_{ab} \cdot \nabla_a W_{ab} \quad (2.23)$$

Which can be used to calculate the density of a particle. It is possible to apply a density diffusion term to reduce density fluctuation. The equation of state describes a very stiff density field, and together with the natural disordering of the particles, high-frequency low amplitude oscillations are found to populate the density scalar field. DualSPHysics uses a diffusive term in the continuity equation written as:

$$\frac{d\rho_a}{dt} = \sum_b m_b v_{ab} \cdot \nabla_a W_{ab} + \delta_\Phi h c_0 \sum_b \Psi_{ab} \cdot \nabla_a W_{ab} \frac{m_b}{\rho_b} \quad (2.24)$$

With

$$\Psi_{ab} = 2(\rho_b - \rho_a) \frac{x_{ab}}{\|x_{ab}\|^2} \quad (2.25)$$

Which represents the density diffusion formulation proposed by Molteni and Colagrossi (2009), with a coefficient of 0.1 (δ_Φ) is recommended for most application in DualSPHysics which will be set in the current simulation. This equation represents exactly a diffusive term in the bulk domain and the changes of behavior close to open boundaries such as free surface.

2.2.3.6 Time integration scheme

A choice of numerical integration schemes is included in DualSPHysics, if the momentum, density and position equations are given by:

$$\frac{dv_a}{dt} = F_a \quad (2.26)$$

$$\frac{d\rho_a}{dt} = D_a \quad (2.27)$$

$$\frac{dr_a}{dt} = v_a \quad (2.28)$$

These three equations could be integrated in time by using a computationally simple Verlet based scheme or a more numerically stable but computationally intensive two-stage Symplectic method.

- Verlet method (Verlet 1967)

Comparing some other integration techniques, this algorithm has a low computational overhead primarily as it does not require multiple (i.e. predictor and corrector) calculations for each step which leads to an instability issue, hence, the Symplectic scheme should be used instead.

- Symplectic method (Leimkuhler 1996)

The Symplectic scheme is an explicit second-order scheme with time accuracy of $O(\Delta t^2)$ and involves a predictor and corrector stage. Firstly, for the predictor stage, the density and acceleration are estimated at the middle of the time step:

$$\rho_a^{n+\frac{1}{2}} = \rho_a^n + \frac{\Delta t}{2} D_a^n \quad (2.29)$$

$$r_a^{n+\frac{1}{2}} = r_a^n + \frac{\Delta t}{2} v_a^n \quad (2.30)$$

where the superscript n presents the time step. Then, for the corrector stage, the updated value of velocity can be calculated by using $dv_a^{n+\frac{1}{2}}/dt$:

$$v_a^{n+1} = v_a^{n+\frac{1}{2}} + \frac{\Delta t}{2} F_a^{n+\frac{1}{2}} \quad (2.31)$$

From which the corrected value of positions of the particles can be estimated:

$$r_a^{n+1} = r_a^{n+\frac{1}{2}} + \frac{\Delta t}{2} v_a^{n+1} \quad (2.32)$$

And then using the updated values of velocity and positions, the corrected density values can be written as:

$$D_a^{n+1} = \frac{d\rho_a^{n+1}}{dt} \quad (2.33)$$

2.2.3.7 Shifting algorithm

There is one important stability issue in SPH called anisotropic particle spacing which especially occurs in violent flows. The thing is that it is impossible for the particles to maintain a uniform distribution, which can result in an introduction of noise in velocity and pressure and the creation of voids in the particle distribution. In order to deal with this problem of anisotropic particle spacing, Xu et al. (2009) proposed a particle shifting algorithm to prevent the instabilities which applied in DualSPHysics to mitigate this problem. The function of this algorithm is to move ("shift") particles towards areas with lower particles concentration, allowing the domain to maintain a uniform particle distribution and eliminating any voids that may occur due to the noise.

2.2.3.8 Boundary conditions

In DualSPHysics, the boundary is described by a set of particles that are considered as a separate set to the fluid particles and the Dynamic Boundary Condition (DBC) is the default method provided by DualSPHysics, which regarding boundary particles satisfying the same equations as fluid particles, but they do not move according to the forces exerted on them and fixed in position. In this simulation, the Dynamic Boundary Condition (DBC) are applied.

2.2.4 Analysis of numerical measurement in DualSPHysics

During the simulations performed, besides the visualization of the simulation could be achieved by visualization application like ParaView, a further numerical calculation is needed to compare experimental and numerical values. The numerical calculation can be implemented by the MeasureTool code and ComputeForces code in DualSPHysics to calculate the flow velocity during the process of flows, the corresponding pressure, and the interactive forces exerted by the flow on objects.

2.2.4.1 Computed velocity

The computation of fluid velocity in DualSPHysics can be achieved by MeasureTool code, which is implemented by means of an SPH interpolation of the values of the neighboring particles around a given position, for example, giving a certain location of a particle within model (the center point of the circle as shown in Figure 2.4), the numerical velocity is computed by using velocity values of neighboring fluid particles:

$$v_a = \frac{\sum_b v_b W_{ab}}{\sum_b W_{ab}} \quad (2.34)$$

Where the subscript a, b indicates individual particles, particle b is a neighbouring particle of particle a , v_a is the velocity of particle a , v_b is the velocity of neighbouring fluid particles.

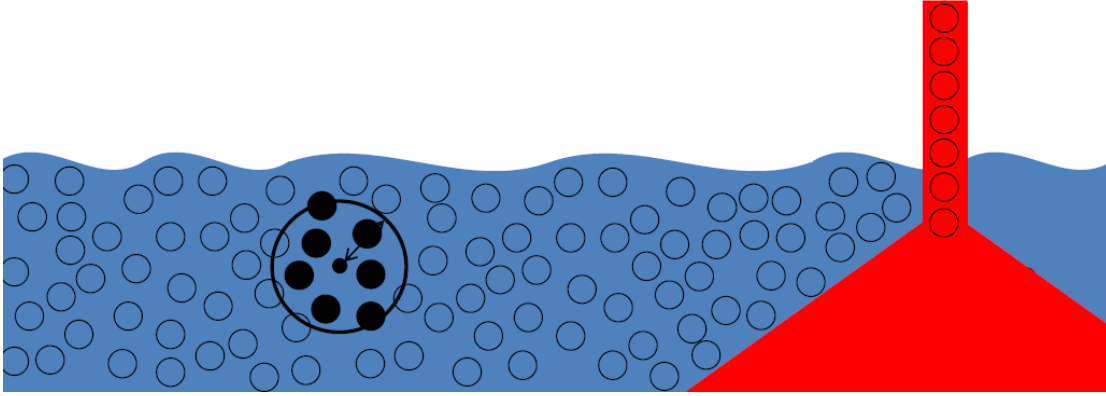


Figure 2. 4. The numerical computation of fluid particle velocity (DualSPHysics 2018)

2.2.4.2 Computed pressure

Similar to the computation of velocity, for a given location in model (the center point of the circle shown in Figure 2.5, which is also the position that the flow interacts with boundary), numerical pressure could be computed utilizing pressure values of neighboring fluid particles:

$$P_a = \frac{\sum_b P_b W_{ab}}{\sum_b W_{ab}} \quad (2.35)$$

Where the subscript a, b indicates individual particles, particle b is a neighbouring particle of particle a , P_a is the pressure of particle a , P_b is the pressure of neighbouring fluid particles.

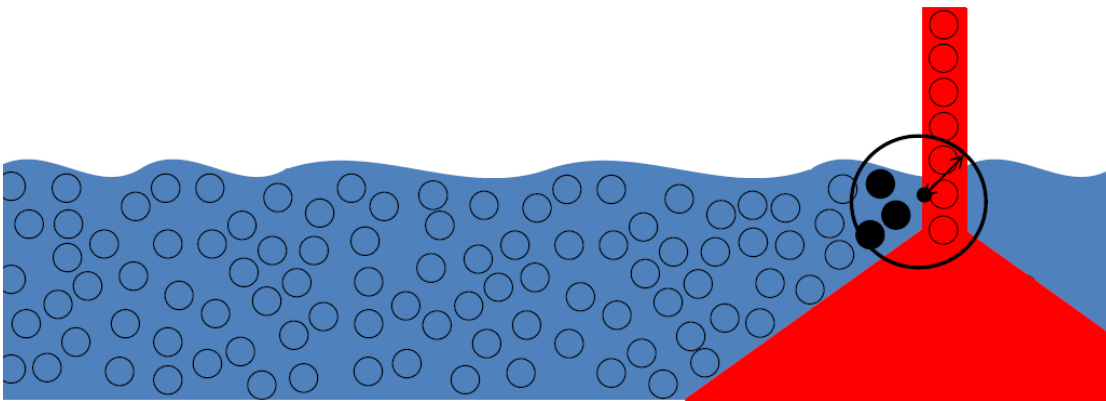


Figure 2. 5. The numerical computation of fluid particle pressure (DualSPHysics 2018)

2.2.4.3 Computed forces

Generally, the ComputeForces code within DualSPHysics is employed to compute the force exerted by the fluid onto a boundary object. The value of force is calculated as the summation of the acceleration values (solving the momentum equation) multiplied by the mass of each boundary particle. Firstly, a range of boundary particles are selected (the grey circles shown in Figure 2.6), then DualSPHysics computes numerical acceleration of those boundary particles (the yellow circle) by solving the particle interactions with fluid neighboring particles (the black circles):

$$\frac{dv_a}{dt} = - \sum_b m_b \left(\frac{P_b}{\rho_b^2} + \frac{P_a}{\rho_a^2} + \Pi_{ab} \right) \nabla_a W_{ab} + g \quad (2.36)$$

Then, summing the acceleration values of selected boundary particles obtaining the corresponding force.

$$F = m \Sigma \left(\frac{dv_a}{dt} \right) \quad (2.37)$$

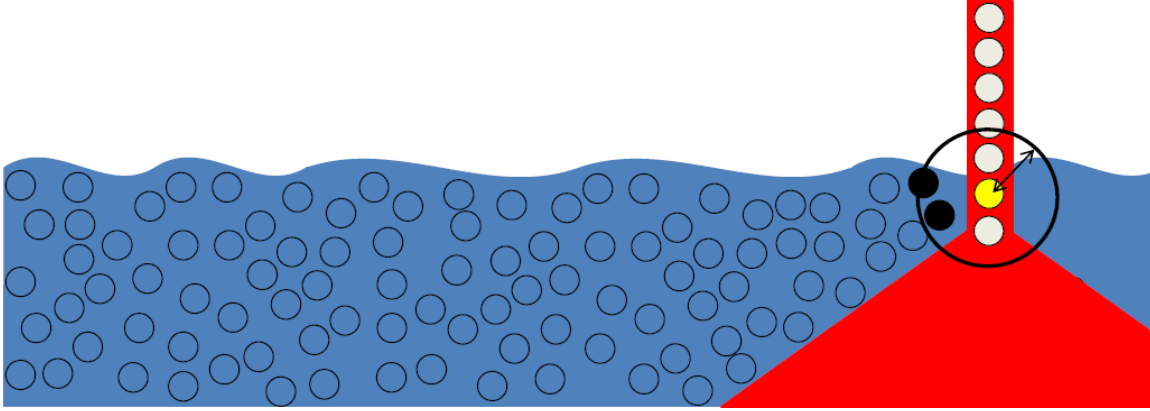


Figure 2. 6. The numerical computation of interactive force of fluid particles and boundary particles (DualSPHysics 2018)

2.3 Railways

2.3.1 Early beginning and the development of the railway

In medieval times people mostly travelled by foot or horseback and any form of wheeled land transportation was mainly for moving goods. The first appearance of railways was in the Seventeenth and Eighteenth Century, which were mainly horse-drawn trains of wagons in collieries and quarries (Bonnett 1996). These ‘hauling ways’ initially had a surface of stone slabs or timber baulks, with the loads carried inevitably grew heavier, it is be soon proved unsatisfactory with the demand imposed on them. Soon after, as the Industrial Revolution progressed, the idea was developed further by adding cast iron or wrought iron plates to reduce wear on the wooden baulks. Then, by the Age of Steam, the locomotives came on the historical stage, in the early nineteenth century, wrought iron rails and later steel rails were developed which were strong enough to support these heavy axle loads without assistance from longitudinal timbers.

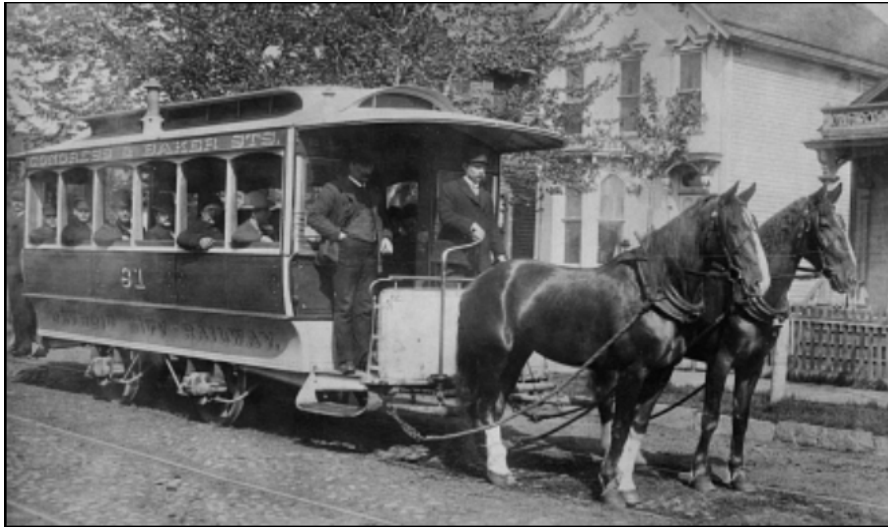


Figure 2. 7. Horse-drawn Trains (Henning 2006)



Figure 2. 8. The locomotive in the Age of Steam (Bentley 2014)

Essentially, the track itself, together with its supports, has the basic function of safely transmitting the loads and forces imposed by passing trains to the ground beneath. Various other civil engineering skills were also involved in the construction of early railways, which include the building of bridges, tunnels and gravity retaining walls as well as extensive earthworks and drainage (Bonnett 1996).

With the development of industrialization, manufacturing techniques and society in general, more and more different kinds of railways came into existence. For instance, electric power railway systems, diesel power railway systems and high-speed railways gradually appeared in people's life.



Figure 2. 9. High-speed railway (People.cn 2015)

2.3.2 The components of a railway system

Generally, no matter what kind of railway it is, the whole railway system is composed of three main parts: stations, rolling stock and track.

2.3.2.1 Station

Stations on a railway system vary enormously in terms of their complexity, suitability and effectiveness. In planning any station, there are many objectives that cannot be ignored, for instance attractiveness in appearance, safe evacuation in emergency, safe accumulation and dispersal of crowds, reliable operation of train service and cost effectiveness of investment, for example.

A cause in one aspect or another among these, will have a direct influence on the general comfort of the passengers. For example, if trains are infrequent, if lighting is poor, or if the surface is maintained inadequately and there is no adequate shelter in bad weather for passengers, can all have a direct adverse effect. Therefore, a successful station is the product of well-designed infrastructure, appropriate information and signing systems for the purpose, and a clear well published management philosophy.

2.3.2.2 Rolling stock (rail vehicles)

Generally, rolling stock in the rail transport industry means vehicles that run on hard wheels on hard rails (Bonnett 1996). The wheels of a rolling stock are supported and guided by the rails. In all cases, not only the load hauled, but also rolling stock transmits vertical, horizontal and longitudinal forces to the track and its supports. Railway rolling stock running on the hard wheels usually include both powered and unpowered (in medieval times) vehicles (Bonnett 1996). For example, these are locomotives, railroad cars, coaches and wagons. In order to simplify the analysis, modeling and simulation in this thesis, the consideration is then restricted to specific case of trains whose power is provided by a separate locomotive.

2.3.2.3 Track

The basic components of the track are steel rails, track bed and subgrade. The steel rails, installed on crossties (sleepers) are set in ballast, on which the rolling stock that fitted with metal wheels moves. Currently, the rolling stock with hard steel flanged wheels of most railways running on two rails is set at around 1432 mm standard gauge (Bonnett 1996), supported in some way to spread loads to the ground below.

The track bed is comprised of ballast and any sub-ballast layers, which are aimed to support the track, to drain water from the bottom of the sleepers and to distribute the track load to such a degree that the subgrade can resist it without excessive deformation. The subgrade is the natural soil stratum, or embankment soil, upon which the trackbed is constructed after trimming off organic topsoil and made ground (Bonnett 1996).

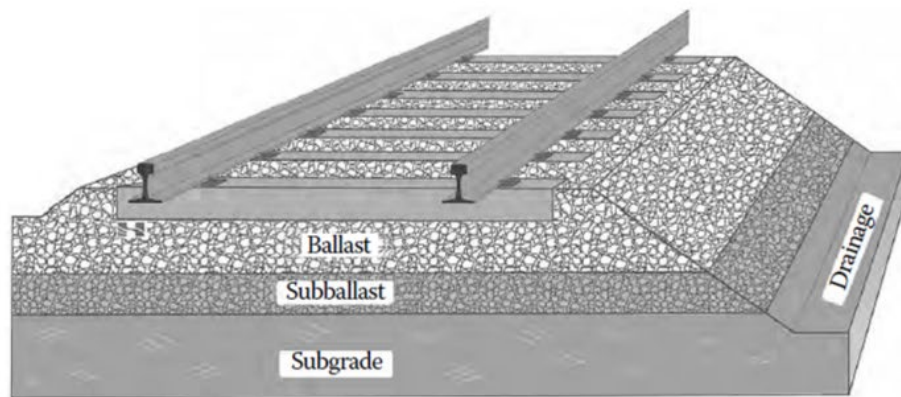


Figure 2. 10. Railway track structure (Li et al. 2016)

2.3.2.4 Ballasted track and its features

As can be seen from the Figure 2.10, ballast is a granular material placed as the top substructure layer and it is the layer that is in direct contact with the ties (sleepers). Ballasted track forms the trackbed (the ballast and any sub-ballast layers) on which railroad ties (sleepers) are laid. Ballast is set between, below, and around the ties (sleepers), as shown below in Figure 2.11. It is used to bear the load from the railroad ties, to facilitate drainage of water, also to keep vegetation out that might be influenced by the track structure. This also serves to hold the track in place when the trains roll by. Good quality track ballast is typically made of crushed stone.



Figure 2. 11. Ballasted Track (AGICO GROUP 2020)

Ballast has many functions that are required for well-supported track. The most important functions are listed as following (Li et al. 2016):

- Supports the rail–fastener–tie track panel by providing adequate vertical, lateral, and longitudinal resistance.
- Transmits and reduces wheel or rail forces.
- Facilitates surfacing and lining operations.
- Provides drainage.
- Provides resilience and damping of dynamic wheel or rail forces.

Ballasted track is not sealed like highway pavement but is designed as an open structure to provide rapid drainage and facilitate maintenance. However, good quality track ballast needs regular maintenance. Ballast-related track maintenance methods include surfacing and lining, stone-blowing, track renewal and superstructure replacement, ballast undercutting to restore drainage and resilience, polluted ballast removal which include crib excavation with backhoe loader or vacuum, and ballast compaction often by a dynamic track stabilizer (Li et al. 2016). Owing to every maintenance of the track ballast requires a lot of manpower and financial resources, the maintenance is required when one of the following problems occurs: excessive vertical or lateral track deformation, excessive ballast degradation (ballast fouling), or drainage is no longer effective (Li et al. 2016).

2.3.3 The general operation of railways

For the satisfactory operation and maintenance of a railway, certain basic resources are required, which can be grouped into human resources, fixed assets and mobile machinery (Bonnett 1996). Inadequacy in any of these will mean that good operation cannot be maintained, irrespective of the performance on the other areas.

As in any large organization, careful selection and adequate training of personnel at all levels is essential and required. The railway system is no exception to this rule.

Fixed assets can also be regarded as fixed infrastructures of the whole railway system. There are four main parts within the railway system: tracks, structure, power and communication. Each of them has many components as shown in Figure 2.12.

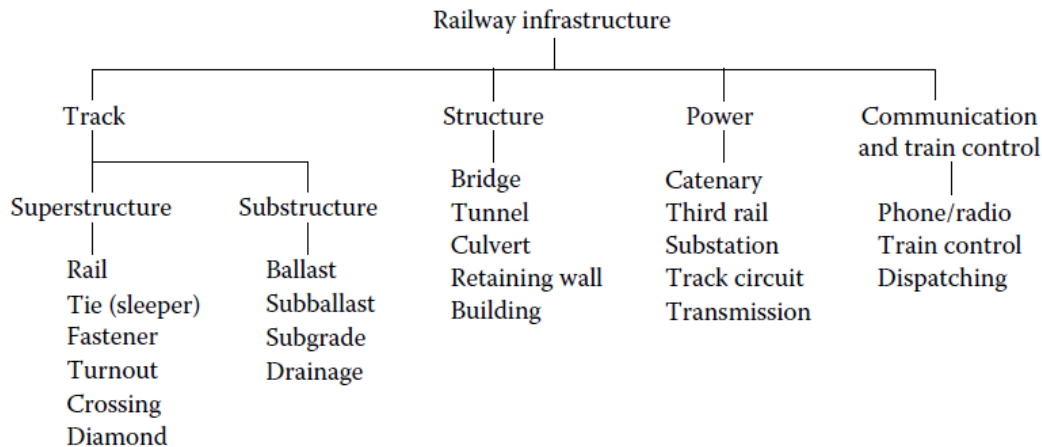


Figure 2. 12. Railway infrastructure (Li et al. 2016)

Mobile machinery is another name for the rolling stock. The most important task, also the only task of the rolling stock is safely carrying passengers or goods to the destination, which is the goal of the construction of the whole railway system in the first place. Not only the good operation of both of the rolling stock and the fixed infrastructures, any railway relies upon proper maintenance of both its rolling stock and its infrastructures to ensure that efficient and reliable operation of the whole railway system is sustained. Both operational and maintenance considerations need to be fully considered at the planning stage. Most importantly, all assets should be checked and monitored yearly, with an aim to keep the standard of satisfaction of railway system.

Above all, fixed assets and mobile machinery that are necessary to operate and maintain a railway system satisfactorily, but it is vital also to keep in mind that in all areas, adequate human resources are often the key to success or failure.

2.3.4 Railway embankments

2.3.4.1 The basic concept of and the material used in railway embankments

As previously discussed, the naturally occurring soil stratum is known as subgrade, upon which the track bed is constructed, which is comprised of ballast and any sub-ballast layers. When the naturally occurring soil stratum is prepared to receive the ballast and track, it is called formation. When it is made after cutting the ground, it is called cutting. The embankment is a formation be raised on bank of earth (Sujay 2017). A railway line is normally constructed onto an embankment.

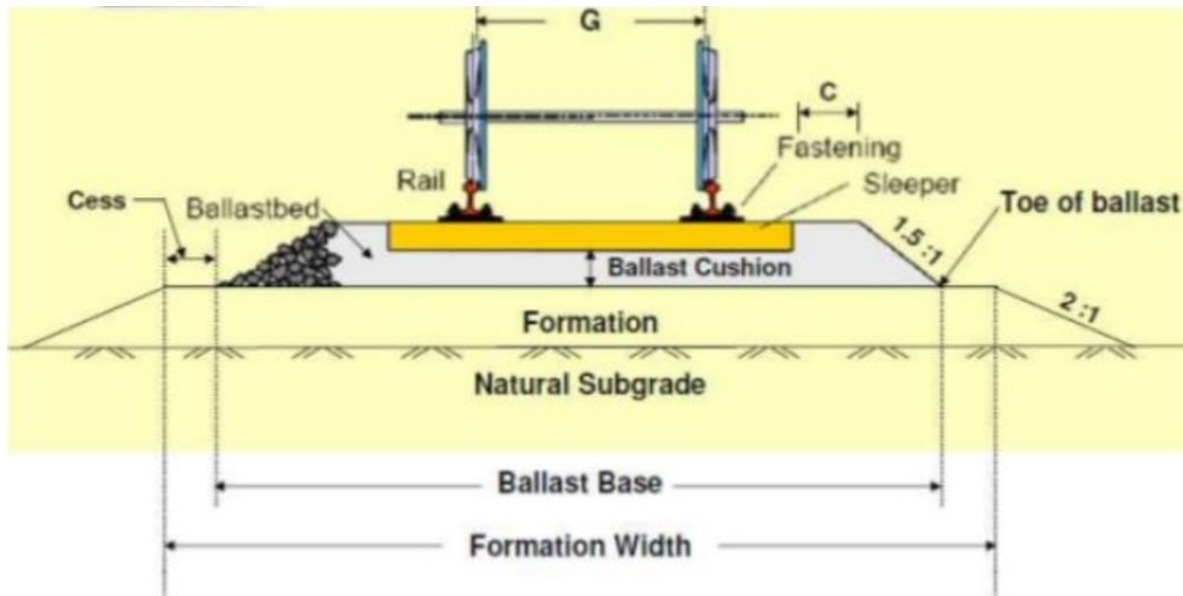


Figure 2. 13. Railway track-bed formation (Sujay 2017)

Embankments are often constructed using material obtained from a nearby cut. Ideally, embankments need to be constructed using non-aerated and waterproof, compacted (or entirely non-porous) material to provide adequate support to the formation and a long-term stable and level surface. Proper design of an embankment and excavation cuts require consideration of the type of soil and rock material that are encountered in situ or are being placed, as well as the geometric configuration of the slope (height and width). For convenience, the majority of fill embankments use locally available material, which can vary from fine-grained soil to hard, competent rock (Li et al. 2016).

2.3.4.2 Stresses developed in railway embankments

The railway is subjected to heavy, dynamic and complex stresses, originating from the weight of the moving trains, from the shocks in the joint areas, irregularities and other causes related to deviations from admitted tolerances. Also, the axle loads increase with the traffic speed (Ciotlaus et al. 2016). These stresses are transmitted through the railway-sleeper system to the ballast bed towards the embankment, where stresses and strains occur due to these forces and the earth's own weight. Thus, railway embankments are subjected to stresses coming from traffic, self-weight and accidental stresses affected by the vibrations caused by railway traffic and earthquakes (not often).

2.3.4.3 The design of railway embankments

Prior the construction of a new railway embankment specific information must be gathered about the proposed site. The information used for design includes the proposed height of the embankment, if the locally available material is sufficient for the embankment construction, foundation conditions of the existing ground upon which the embankment will be constructed and the lithology where the cut slope will be excavated (Li et al. 2016). Therefore, the field investigation should not only include observations of local geologic conditions, also include observation of the condition of existing slopes in the area, which are usually carried out by experienced engineers or geologists.

The design of new slopes must consider not only the embankment fill, but also the foundation condition under the proposed embankment.

The foundation of a new slope is the existing ground on which the fill is constructed (Li et al. 2016). As for relatively thick and compressible soil layer, if it is not considered in design properly, the situation can lead to continual long-term consolidation of the completed embankment fill and even more, shear failure of the foundation soil. Therefore, stiffening and strengthening the foundation soil must take into consideration prior to the embankment construction to minimize long-term settlement of the track. Thus, it is desired to have a more compacted density of a fill material, which provides higher strength and lower settlement of an embankments. Accordingly, when constructing a fill embankment, it is important that the fill material be placed in layers and compacted near to the maximum density and close to the optimum moisture content. Figure 2.14 below provides some common suggestions for a new embankment construction.

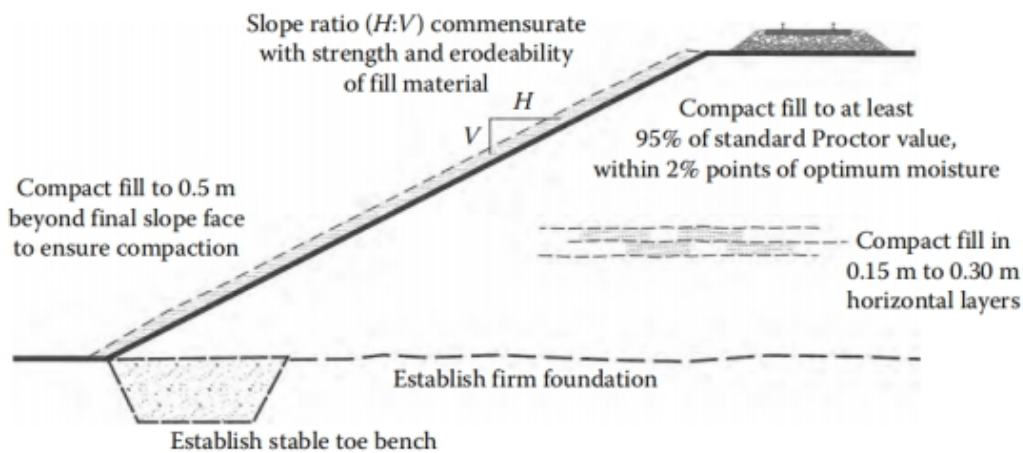


Figure 2. 14. The new fill embankment construction (Li et al. 2016)

Sometimes, there could be a natural embankment that exists at a construction site, but a new fill slope still needs to be built adjacent this existing embankment to expand it. For this case, the interface between the old and new slopes must be well connected to prevent any slippage between the existing and new material.

Owing to the long-term consideration, for the hillside construction, when new fill is added adjacent to an existing embankment that has failed, the proper connection between new fill and existing fill could also apply to post-failure reconstruction. Figure 2.15 below shows general recommendations for one hillside construction of an existing embankment.

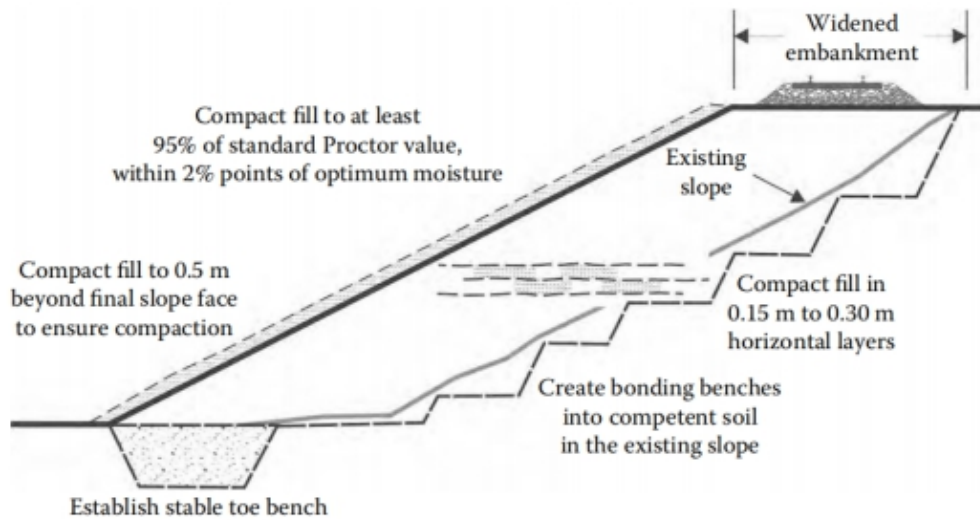


Figure 2. 15. The side-hill construction (Li et al. 2016)

In addition, according to Figures 2.14 and 2.15, it is worth noting when constructing new slopes, whether it is a full embankment or a side-hill fill, a toe bench is constructed into the existing ground at the toe of the slope, as shown in above two figures. The toe bench provides stability at the critical zone at the bottom of the slope where shallow surficial movement tends to originate (Li et al. 2016). Therefore, the construction of a toe bench ensures that the potential zone of movement (failure plane) goes through, or around, the toe bench, thus decreasing the risk of instability and increasing safety.

2.3.5 The derailment of trains

As stated previously, it is quite possible that railway tracks traverse the areas that prone to mudflows like the Ottawa Valley, which perhaps could lead to train derailment. In the simulations performed in the thesis, the focus is on examining the interactive force between mudflows and stationary railway vehicles, anticipating the effect of mudflow posed on trains and their derailment potential. Hence, in order to take measures to prevent this, it is important to understand the circumstances under which a train can derail. In 1896, a French engineer, Nadal first put forward an equation to calculate the critical derailment coefficient Q/P , which according to the relationship of normal force N and tangential friction T with transverse wheel-rail force Q and vertical wheel-rail force P as presented in Figure 2.16. He regarded the following equation as the basis of start of derailment:

$$\frac{Q}{P} = \frac{\tan\alpha' - \mu'}{1 + \mu'\tan\alpha'} \quad (2.38)$$

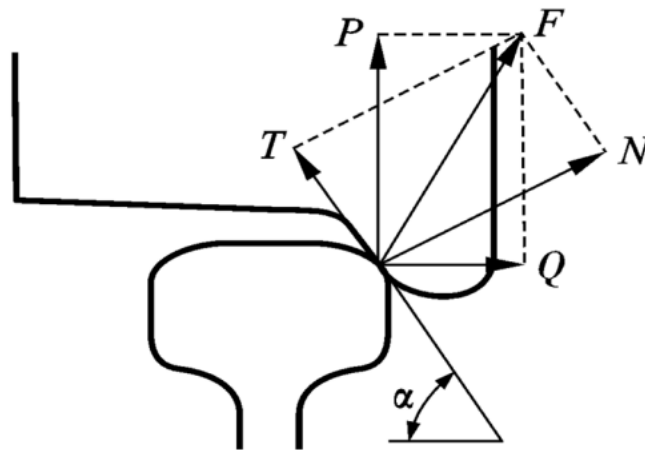


Figure 2. 16. Wheel-rail action at the commencement of derailment (Nadal 1896)

Where μ' is the dynamic friction coefficient of the wheel-rail contact and α' is the flange angle. Depending upon Nadal's equation, various calculation methods of the value of the critical derailment coefficient were carried out by scientists. For instance, in North America, scientists measure the vertical and transverse anti-reaction force of wheelset by using track loading vehicle exert on normal vertical force and gradually increase the transverse force on truck and the critical derailment coefficient is measured by tests on the wheel lift of the single wheelset. While, in Japan the critical derailment coefficient $Q/P=0.95$ is obtained using a standard wheel flange angle $\alpha = 60^\circ$ and friction coefficient $\mu = 0.3$ (Xiang and Zeng 2005). Actually, specification standards of the critical derailment coefficient for derailment prevention are different in various countries (Xiang and Zeng 2005) :

- In Japan, $Q/P=0.8$ and the continuous action time within 0.015s
- In Western Europe, $Q/P<0.8$
- In North America, $Q/P<1.0$
- In China, $Q/P=1.0$ (allowable limit) and 1.2 (danger limit)

Besides the critical derailment coefficient, when train derailment occurs, the wheel lift value also needs to be regarded. At the effect of the action of transverse force Q and the moment, the wheel load at the wheel-rail contact point decreases. The reduction of wheel load $\Delta P = P_0 - P_d$ (P_d is the measured wheel load value) over the static wheel load P_0 represents the wheel load reduction rate $\Delta P/P_0$. According to the physical concept, a larger value of the wheel load reduction rate $\Delta P/P_0$ indicates a higher possibility of train derailment. Similar to the critical derailment coefficient, specification standards of the wheel load reduction rate for derailment prevention is also different in various countries (Xiang and Zeng 2005) :

- In Japan, $\Delta P/P_0=0.6$ (static), 0.8 (dynamic)
- In North America, $\Delta P/P_0 <0.9$
- In China, $\Delta P/P_0= 0.6$ (allowable limit), 0.65 (danger limit)

Since the Ottawa Valley study area is in North America, in the research, assuming the train derailment occurs when the critical derailment coefficient $Q/P \geq 1.0$, where Q is transverse force

and P is vertical wheel-rail force (static train vertical load). Hence, it is important to determine the transverse force also called impact force exerted by mudflows on railway cars, and also it is necessary to pay more attention on the parameters which could affect the impact force generated by mudflows.

In this chapter, the fundamental mechanics of mudflow, the principles of the simulation tool, the general operation of railways and the criteria of the train derailment were stated studying previous research. On basis of that, key model parameters of the specific case, for example, slope geometry parameter, embankment geometry parameter and mudflow properties will be discussed and analyzed in following chapters.

Chapter Three: Key Parameters of the Model

3.1 Introduction

Mudflows triggered by heavy rainfall on natural or man-made hillslope are a common geomorphic phenomenon in many parts of the world, especially in mountainous areas. For instance, in Canada, the Ottawa Valley and St. Lawrence Lowlands are prone to rain-induced mudflows, and it is quite possible that railway tracks traverse these areas that are prone to mudflows. In order to avoid the danger posed by mudflows on railway infrastructure, the investigation of a derailment potential of railway cars when hit by a mudflow is recommended. As discussed before, a particle-based computational fluid dynamics method, Smoothed Particle Hydrodynamics (SPH) can resolve with ease the free surface flows that often characterize mudflows. Thus, by using SPH with appropriate models, it can be used to represent scenarios of a mudflow hitting a railway infrastructure. With recent developments of coupling a fluid flow model with rigid body dynamics, it is possible to examine the interaction of flow with solid object (railway infrastructure/cars). Furthermore, perhaps providing mitigative measures to ensure the safety of trains in such circumstances.

Hence, within the proposed model, the objective of this thesis is to quantitatively examine the interaction of mudflows with rail vehicles. Moreover, observe the derailment potential of rail vehicles hit by a mudflow. As a result, the outcome is hoped to provide insights into the safety of such embankments when exposed to mudflows, perhaps which will lead to the revision of current guidelines used by the railway industry. Therefore, it is important to identify key parameters of a system in order to create a reasonable model representing physical reality.

In this chapter, accompanied by model development used in simulations, the proposed parametric studies will be discussed. The key parameters of the slope and embankment geometries, fluid properties and train loadings will be considered respectively as follows.

3.2 Parameters for Railway Embankments

As mentioned in the previous chapter, a railway line is normally constructed on an embankment, and railway vehicle loads are transferred from rails to the rail-sleeper system and then to the embankment through a ballasted bed. Thus, the stability of railway embankments is the key factor to assure the safety of the whole railway civil infrastructure and vehicles. Parameters for a railway embankment include embankment slope ratio and embankment height.

3.2.1 Railway embankment slope ratio

Regarding the construction of a railway embankment, for convenience, the majority of fill used in embankments is from locally sourced materials, which can vary from fine-grained soil to hard, competent rock (Li et al. 2016). However, at times it is hard to find a proper type of soil or rock in situ to satisfy the standard criteria of construction. Understandably, for designing stable slopes, the material properties of embankment fills must be taken into account. Because of that, the strength and erodibility of the soil and rock will decide the slope ratios that are one key element for stability of embankments. Thus, some typical soil types used in construction of embankments are presented

in Table 3.1. Furthermore, based on the strength and erodibility of the different soil types, the values of slope ratio, horizontal to vertical (H:V), are also variable, as shown in Table 3.2 below:

Material type	Erosion resistance	Embankment strength
Rock fill	Excellent	Excellent
Gravel, well to poorly graded	Excellent - Good	Good
Sand, well to poorly graded	Good - Fair	Good
Clays of low plasticity, sand clays	Good	Good
Clays of high plasticity	Poor	Fair
Silts	Poor	Fair
Organic clay and silt	Poor	Poor

Table 3. 1. Desirability of soil type for new slopes (Li et al. 2016)

Material type	Typical minimum slope ratio (H:V)
Rock fill	1.5:1
Sand and gravel	1.8:1
Sand	2:1
Fine-grained clay and silt	3:1 to 2.5:1

Table 3. 2. Typical minimum slope ratios of horizontal to vertical (assuming the material is compacted to a high relative density) (Li et al. 2016)

Based on Table 3.2, it is evident that the typical minimum slope ratio (H:V) ranges from 1.5:1 to 3:1, depending on soil type. Also, it is important to note that the materials should be compacted to a high relative density, as greater compacted density of fill materials provides higher strength and lower settlement of an embankment. Additionally, AREMA's Manual for Railway Engineering recommends a typical embankment slope ratio of 2H:1V (AREMA 2010).

3.2.2 Railway embankment height

As stated previously, in an existing railway system in certain parts of country like the Ottawa Valley and St. Lawrence Lowlands in Canada, it is inevitable that railway tracks traverse areas prone to mudflows. In addition to these geographic areas, the construction of embankments in mountainous areas will be under the danger of mudflows or debris flows/avalanches as well. When embankments are constructed too low, the mudflow will easily threaten rail vehicles; when the embankments are too high, it is hard to assure the overall stability of slope and the cost of construction is not optimal. For this reason, the height of embankments is another one of key elements to ensure the stability of a slope and the safety of the railway vehicles on it. Similarly, like slope ratios, based on the strength and erodibility of the different soil and rock types, different heights of embankments are required to ensure the stability of slopes of railway embankments.

Ciotlaus et al. (2016) carried out research based on the limit equilibrium method to determine the safety factor (FS) of embankments. In this research, the analysis was made with Bishop's method, which considers the effects of forces acting upon the slices comprising a slope. The method is based on dividing the slope into slices and considering equilibrium of every strip, incorporating horizontal interslice forces (Ciotlaus et al. 2016). Embankments comprised of three types of soils (rock fill, gravel with sand and dust clay) were studied. Displacements with respect to slope ratio and height were considered with special attention to the case of appropriate soils to be used for fills.

According to their research, calculations were performed with pre-stressed concrete sleepers (model T17), and the rail model had the following values:

Parameter	Value
Winkler or ballast coefficient C [daN/cm^3]	5.00
Sleeper spacing [cm]	60.00
Crushed stone ballast thickness [cm]	30.00
Rail inertial momentum I_x [cm^4]	3055.00
Sleeper inertial momentum [cm^4]	15035.00
Rail elastic modulus [daN/cm^2]	2.10×10^6
Concrete elastic modulus [daN/cm^2]	3.35×10^5
Sleeper width b [cm]	27.50
Dynamic coefficient φ	2.00
Speed V [km/h]	200.00
Equivalent beam length L [cm]	130.00
Weight per axle G [kN]	250.00
Pressure distributed at sleeper base P [kN/m^2]	53.00

Table 3. 3. Parameters for rail superstructure and load conditions (Ciotlaus et al. 2016)

In addition, the different layers comprised of three types of soils within an embankment were characterized by them as in Table 3.4:

Layer	Soil type	Bulk density γ (g/cm^3)	Internal friction angle φ ($^\circ$)
Sub layer	Sand	1.7	20
Embankment	1. Dust clay	1.9	18
	2. Gravel with sand insertions	1.8	33
	3. Rock fill	1.7	35

Table 3. 4. Soil properties of the layers comprising an embankment (Ciotlaus et al. 2016)

For the simulation in the research conducted by Ciotlaus et al. (2016), different heights of embankments were considered, ranging from 4m to 12m (values of 4, 6, 8, 10, and 12m). Within these cases, the railway infrastructure stability was simulated with each soil type and each embankment height for a certain railway track configuration (Figure 3.1), resulting in a safety factor (FS). The slope ratio of the embankment (H:V) was 1.5:1 and pressure $P=53\text{kPa}$ (Table 3.3) was transmitted from rail through the rail-sleepers system and distributed by the ballast.

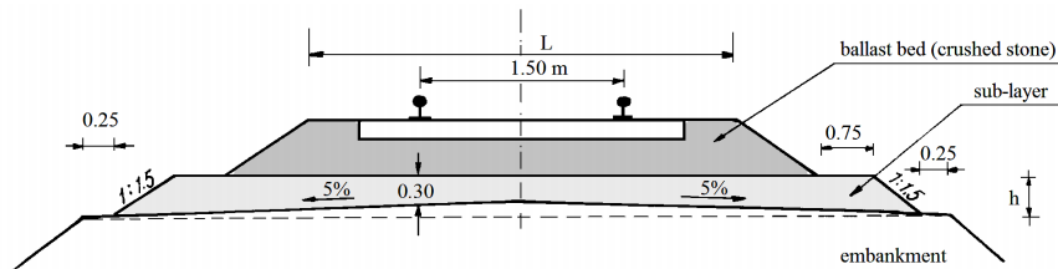


Figure 3. 1. Railway track (Ciotlaus et al. 2016)

The results of Ciotlaus et al.'s (2016) findings are presented in Table 3.5:

Layer	Layer's height [m]	Safety factor	Minimum safety factor
Sub grade: Sand	0.30		
Embankment: dust clay	4.00	2.49	1.30
	6.00	2.14	1.30
	8.00	1.96	1.30
	10.00	1.75	1.30
	12.00	1.65	1.30
Embankment: gravel with sand insertions	4.00	1.18	1.30
	6.00	1.14	1.30
	8.00	1.12	1.30
	10.00	1.11	1.30
	12.00	1.11	1.30
Embankment: rock fill	4.00	1.40	1.30
	6.00	1.34	1.30
	8.00	1.31	1.30
	10.00	1.26	1.30
	12.00	1.25	1.30

Table 3. 5. Safety factor (FS) for different embankments heights and soil types using Bishop's method (Ciotlaus et al. 2016)

From the research carried out by Ciotlaus et al. (2016), according to the results from Table 3.5, it is clear that different soil types and embankment heights can lead to various factors of safety. For all these three soil types, in the case of the same soil type layer, with the height of embankment increasing (from 4m to 12m), the safety factors are all decreasing. With the embankment fills of dust clay, under all heights simulated (from 4m to 12m), the stability is quite satisfactory (FS in the range of 2.49-1.65, and all of them above 1.3). In contrast, for the soil type of gravel with sand, the safety factor was found to be below the limit value of 1.3 for all studied heights. For the third case with rock fill soil type, the safety factor is above the minimum value 1.3 for heights up to 8m, above which the loss of stability is noticed between 10m and 12m. In addition, comparing to the heights with 8-meter and 6-meter under which FS is close to the critical value 1.3 (shown in Table 3.5), the relatively low height with 4-meter is the better choice.

In conclusion, based on Tables 3.1, 3.2, and 3.5, with the soil types presented, the rock fill soil type is the best choice for embankments fills due to their excellent erosion resistance, but the embankment heights cannot exceed 8m because of factor of safety concerns. Although the erosion resistance of gravel is good, concerning FS, the soil type of gravel with sand for embankments fillings is not recommended. Even though the dust clay has an excellent performance regarding FS, its poor natural erosion resistance cannot ensure a stable embankment. What's more, in the reality of constructability, based on current railway practice, the height of embankment in excess of 10m is unrealistic as well. Thus, considering all of the considerations mentioned above (natural erosion

resistance, optimal cost, stability, etc.) granular materials are a desirable candidate for new fill slopes and the maximum critical value of the height of railway embankment is 8-meter according to minimum Safety factor (FS).

From discussion above, the conclusions drawn can help choosing the correct soil type, the height and slope ratio of embankment for constructing stable embankments. For this thesis, modeling embankment slopes, assuming the material is gravel with sand, in accordance with the typical slope ratios shown in Table 3.2 and the typical slope ratio specified in AREMA's Manual for North America Railway Engineering (AREMA 2010). The values of horizontal to vertical (H:V) slope ratio can be assumed either 3H:1V or 2H:1V. Besides, under this condition, considering current railway construction practice, the slope stability and the optimal cost, the heights of embankment can have various choices but not in excess of 8m and the height below 4m (e.g., 1m, 2m, 3m, and 4m) is the better choice. Thus, these embankment parameters will be considered in the simulation chapter.

3.3 Parameters for Freight Trains

3.3.1 Loading from rolling stock

In the third decade of the 21st century, coupled with a decrease in construction of new railway lines and an increase in goods carried and heavier loads, it is a considerable problem for the existing railway lines to meet the growing demand. Thus, efficient planning is necessary to make decisions which can maximize utilization of train carrying capacity. Meanwhile, demand for transport capacities on railway lines is rising rapidly around the world, particularly, in the heavy traffic sector, where there is a significant increase. Heavy freight trains are those with an axle load of 25 metric tons and above or a total train weight of at least 5000 metric tons (Getzner 2020). Heavy traffic routes can be found all over the world such as the USA, Canada, Australia and China. Normally, under the heavy freight trains, the railway track foundation is subjected to static, cyclic and dynamic loading (Li et al. 2016). For this thesis, for convenience in simulation, it is assumed that the train model is static, in a stationary state, there is no need to consider the cyclic and dynamic loading. Static loading to the track foundation is comprised of live loads and dead loads. The live loads are equal to the train weight including the load carried by the train and the dead load, which is the weight of the track and sub-grade (Li et al. 2016). Hence, for static loading, the weight of a train (the dominant component of static loading) and its corresponding load carrying capacity are considered. Based on these loadings, loading per axle, there will be stresses on the track generating a vertical wheel-rail contact pressure. Particularly, heavy axle load (HAL) freight trains generate significant stresses on the track and sub-grade.

Up until the 1990s, the average heavy freight train in Canada was about 1.54 kilometers (5,000 feet) long and weighed 7000 tons (Deveau 2011). A modern railcar with two bogies and 4 axles has a gross capacity of 125.5 tons (286,000 lbs) moving in trains consisting of 100 cars or more (Quorum Corporation 2005). With the development of the society, there is an obvious increase the demand of goods carried and heavier loads in the 21st century, the carrying capacity has also increased. Table 3.6 below provides data for HAL freight trains around the world.

Country	Axle load (tones)	Train length (number of cars)	Future trend (train length or axle load)
United States and Canada	33	130-140	150-170 cars
Australia	35-40	200-240	333 cars
South Africa	26-30	200-216	332 cars
Brazil	27.5-32.5	330	37 tones
Sweden	30	68	
China	25-27	210	30 tones

Table 3. 6. Typical HAL freight trains around the world (Li et al. 2016)

According to the data from the above table, comparing to the 1990s, trains of the same specifications in the United States and Canada now consist of 130-140 cars with an average axle load 33 tons (Li et al. 2016), meaning the gross capacity has been increased to 132 tons which brings a vertical wheel-rail force of 1293.6 kN on track. Therefore, a constant static load of 33 tones (criteria for the United States and Canada) can be assumed in the simulations, which is considered as Heavy Axle Load (HAL) and correspondingly, with this Heavy Axle Load, the train is comprised of 130 cars, generating a vertical wheel-rail force of 1293.6 kN.

3.3.2 Track gauge

For the purpose of allowing trains to pass safely from one railway line or even railway network to another, there are size standards for railway coaches and freight cars. The maximum size and shape of the trucks that a rolling stock is mounted on is denoted as gauge (Roanes-Lozano 2013). In other words, the track gauge is the spacing of the rails on a railway track. The standard gauge of rails is 1435 mm for laying on ballasted track (Bonnett 1996) in most countries, including North America, UK and China (Chinese Railways 2009).

Country	Gauge (mm)	Gauge (in)
North America	1435	56.5
Europe	1435-1668	56.5-65.7
South Africa	1065	41.9
Australia	1524-1676	42-63
China	1435	56.5

Table 3. 7. Railway gauge values (Selig and Waters 1994)

3.3.3 The sleepers or cross ties

As discussed before, except for steel rails, the other two main components of railway tracks are the track bed and subgrade. The track bed is comprised of ballast and any sub-ballast layers while the subgrade is the natural soil stratum, or embankment soil, upon which the track bed is constructed. Steel rails, installed on crossties (railway sleepers) are set in a ballast layers, on which the rolling stock that fitted with metal wheels moves, as shown in Figure 3.2.

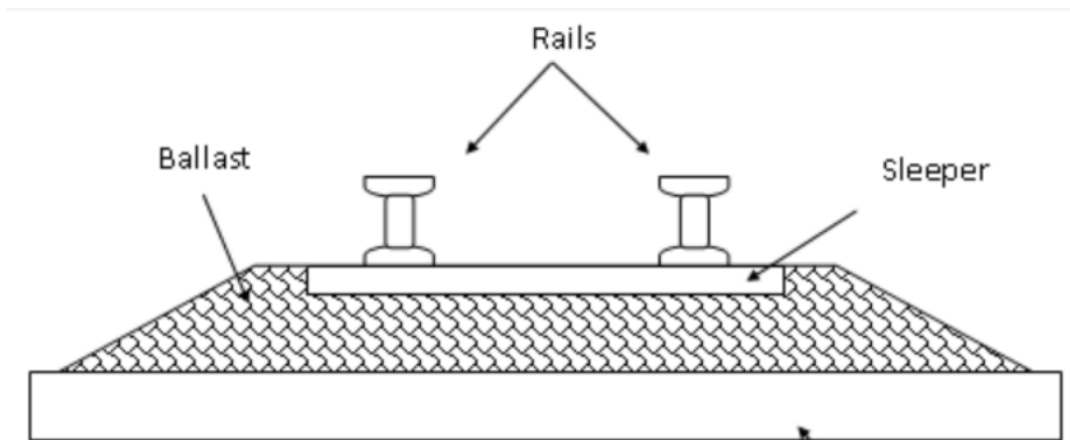


Figure 3. 2. The simple layout of a rails upon an embankment (Sujay 2017)

It is clear from Figure 3.2 that, in ballasted railway tracks, the steel rails installed on sleepers are set in ballast. Railway sleepers, sometimes are also called railway ties or crossties, mainly in the North American practice.

Railway sleepers were first made of timber, and then a limited number of steel sleepers were used, followed by the now popular concrete sleepers (Remennikov and Kaewunruen 2006). Generally, the rail sleepers are required to:

- Provide a base for rail seats and fastenings
- Spread wheel loads from rail to the underlying ballast
- Support the rail and maintain the rail gauge and shape, and prevent rail inclination and track instability
- Bear longitudinal, lateral and vertical forces
- Provide insulation between parallel rails
- Resist wearing and endure extreme weather conditions from cold to hot, and from rain to drought.

Owing to the different materials, the three most common types of sleepers are timber sleepers, steel sleepers and concrete sleepers. The traditional material used to manufacture railway sleepers is timber, which was accepted by most railways as standard up to about the middle of the twentieth century (Bonnett 1996). The advantages of timber sleepers are good resilience, ease of handling and manufacturing, electrical insulation and ease of adapting to non-standard situations. Normally, depending on different conditions, countries or regions all over the world have promulgated the standard design of timber sleepers for their own railway track. For example, the typical size of mainline railroad timber crossties used in United States is 229mm wide by 178mm thick in cross-section and 2591mm long or 7" × 9" × 8.5' long (Railway Tie Association 1919) and in the UK, the standard dimension for timber sleepers used are 127mm × 254mm × 2600mm long (Bonnett 1996).



Figure 3. 3. Timber sleepers (LooiNL 2007)

With the development of society and technology and the awareness of environmental protection, around the 1880s (Ferdous et al. 2015), steel railway sleepers were introduced (Figure 3.4) as an alternative to timber due to the scarcity of timber and the sensitivity of its use.

Whereas, in ballasted railway tracks, considering long-term performances, steel's high risk of corrosion, high electrical conductivity, fatigue cracking and the difficulty of packing within the ballast made it is an inferior material for sleepers. In such case, a railway system pays more attention to a cement-based concrete rather than timber and steel sleepers. As a substitute to timber and steel, concrete sleepers were developed during the late 1930's (Bonnett 1996) and mono block prestressed concrete sleepers (as shown in Figure 3.5) came from UK, were they first appeared in 1943 (Ferdous et al. 2015). Currently, concrete crossties are used extensively in heavy haul and high-speed rail track construction throughout the world. Another commercially available type of concrete sleeper is twin block sleeper, which is used extensively in Europe, especially in France. The twin block sleeper consists of two reinforced concrete blocks connected by a steel bar as shown in Figure 3.6 & 3.7 below.

As the sleepers play a significant role in rail networks and there is a considerable demand for sleepers every year throughout the world, in 2006, a worldwide survey conducted by the International Federation for Structural Concrete, which concludes annual demands for traditional three types sleepers in railway systems in various countries presented in Table 3.8 below.



Figure 3. 4. Steel railway sleepers (AGICO GROUP 2020)



Figure 3. 5. Mono block concrete sleepers (AGICO GROUP 2020)

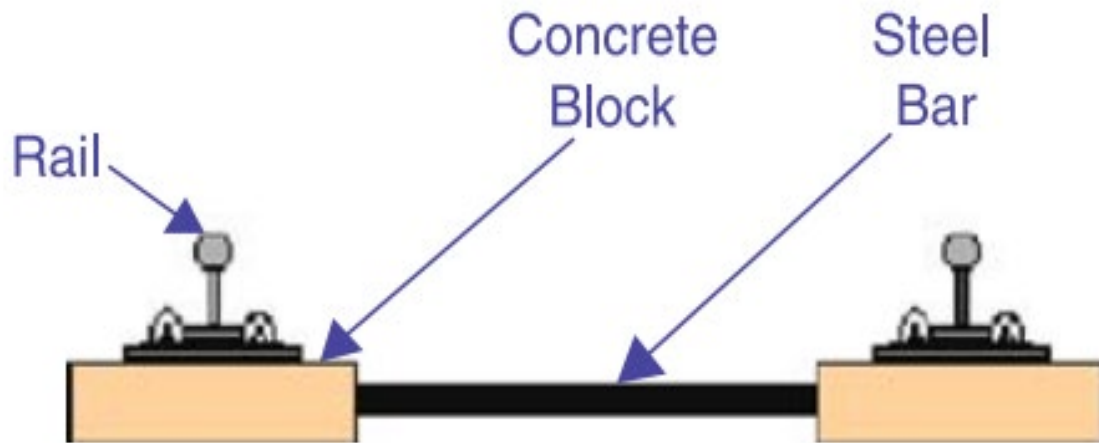


Figure 3. 6. Twin-Block concrete sleepers (Remennikov and Kaewunruen 2006)



Figure 3. 7. Twin-block concrete sleepers (AGICO GROUP 2020)

Country	Total sleepers in track ($\times 1000$)	Demands per year ($\times 1000$)		
		Concrete	Steel	Timber
Argentina	-	60	-	-
Australia	600,000	-	150	200
Austria	9000	200	70	100
Belgium	9912	400	2	20
Brazil	50,000	500	60	300
Chile	5300	200	-	-
China	115,000	3000	-	-
Colombia	5080	-	-	-
Czech Rep.	17,000	250	-	3
Denmark	-	150	-	-
France	60,000	800	0	400
Germany	70,000	1400	100	100
Greece	6150	30	5	3
Hungary	20,388	-	-	-
India	163,500	4640	-	-
Italy	40,000	2000	-	-
Japan	34,000	400	-	-
Malaysia	3000	-	-	-
Morocco	5000	-	-	-
Netherlands	8500	400	-	-
Norway	3000	60	-	-
Romania	16,000	12	-	-
Russia	150,000	3500	-	-
S. Africa	43,000	305	0	0
Spain	30,000	1200	0	30
Sweden	19,500	400	-	8
Switzerland	17,000	150	-	-
Taiwan	4000	120	0	12
USA	600,000	1000	10	13,000
UK	45,000	500	400	100
Venezuela	1225	-	-	-

Table 3. 8. A worldwide survey of sleepers in railway networks (International Federation for Structural Concrete 2006)

The data from this worldwide survey (Table 3.8) illustrates that concrete sleepers are used commonly in many countries except in USA where there is a major demand for timber sleepers. In the reality, most crossties used in North America are still wooden crossties, especially, in this thesis, within the study area of Ottawa Valley, Canada. The existing Ottawa Valley Railway is a Canadian railway that operates 150 miles (240 km) of track in the province of Ontario and Quebec with 1435 mm standard track gauge and wooden crossties, which operated by Genesee & Wyoming Canada Inc. since 1996.

In conclusion, based on the discussed above, within the models in this thesis, under a static 33 tones vertical load (heavy axle load) envisioned (North America criteria), a rail track with timber crossties in size of 178mm \times 229mm \times 2591mm long, along with 1435mm track gauge will be assumed.

3.4 Parameters Related to Mudflow

3.4.1 Impact force of mudflow

Considering the case of train derailment as stated previously, it is necessary to take the impact force generated by mudflow into account. Impact force caused by real-scale debris flow events exerted on obstacles have already been measured in the Jiangjia Ravine in China (Zhang 1993; Hu et al. 2011), at Mt. Yakedake in Japan (Okuda et al. 1977) and in the Illgraben torrent in Switzerland (Wendeler et al. 2007). Besides, impact pressures exerted by gravitational flows against obstacles

have been the subject of many experimental investigations. At present, two common types of empirical formulas exist for calculating the impact pressures exerted by gravitational flows against obstacles: hydrostatic models (Lichtenhahn 1973; Armanini 1997) and hydrodynamic formulas (Watanabe and Ike 1981; Zhang 1993; Egli 2005; Wendeler et al. 2007; Bugnion et al. 2010):

- Height-dependent pressure (hydrostatic formula)

$$p_{max} = k \cdot \rho \cdot g \cdot h \quad (3.1)$$

Where p_{max} denotes the maximum debris flow impact pressure with the parameter k as an empirical factor. ρ is the density of the debris flow, g is the gravitational acceleration and h is the total flow height.

- Velocity-dependent pressure (hydrodynamic formula)

$$p_{max} = C \cdot \rho \cdot v^2 \quad (3.2)$$

where v is the average velocity of debris flow with the empirical impact factor C . The impact empirical factor C depends on the flow type. For example, C ranges between 0.7 for watery flows and 1.0 for viscous flows monitored at the Illgraben torrent in Switzerland (Wendeler et al. 2007). In Switzerland and Hong Kong, guidelines of for constructing mitigation measures (Egli 2005; GEO Report 2000), the hydrodynamic formula is recommended for the calculation of debris flow impact pressure on obstacles, and for the impact coefficient C , the value is takes as 2 and 3, respectively. This formula states that the impact pressure is related to the rate of change of fluid momentum.

It is worth to note that the determination of empirical parameters (C and k) may have various values or error due to the complex condition and the complex components of debris flow. On the basis of these, the other existing calculation methods for a typical debris flow are summarized in Table 3.9:

Study	Calculation formula	Modified parameter	Hydraulic model
Lichtenhahn (1973)	$p_{max} = k\rho gh$	2.8-4.4	Hydrostatic model
Scotton and Deganutti (1997)	$p_{max} = k\rho gh$	2.5-7.5	Hydrostatic model
Armanini (1997)	$p_{max} = k\rho gh$	5.0	Hydrostatic model
Watanabe and Ike (1981)	$p_{max} = a\rho v^2$	2.0-4.0	Hydrodynamic model
Zhang (1993)	$p_{max} = a\rho v^2$	3.0-5.0	Hydrodynamic model
Wendeler (2007)	$p_{max} = a\rho v^2$	0.7-2.0	Hydrodynamic model
Bugnion et al. (2011)	$p_{max} = a\rho v^2$	0.4-2.0	Hydrodynamic model
Hubl and Holzinger (2003)	$p_{max} = 0.5\rho v^{0.8}(gh)^{0.6}$		Hydrodynamic model

Table 3. 9. A summary of calculation methods based on various empirical parameters for a typical debris flow

Here, in Table 3.9, there is a modified hydrodynamic formula given by Hubl and Holzinger (2003). They measured the impact forces of debris flow by employing miniaturized tests. In order to achieve a scale-free relationship, they further related the Froude number (F_r), which is the ratio of inertial and gravitational forces of the flowing mass, to normalized impact forces. On the basis of a correlation analysis, a modified hydrodynamic expression is given as:

$$p_{max} = 0.5\rho v^{0.8}(gh)^{0.6} \quad (3.3)$$

Among the investigations that already been carried out, the example of a large scale field testing of hillslope debris flow given by Bugnion et al. (2010), who used both of hydrostatic and hydrodynamic formulas, which was carried out in a disused quarry in Veltheim, Switzerland, where 50 m³ debris material mixed with water (approximately 100 metric tons) was released down along a 41m long, 8m wide channel with a slope inclination of 30°. In this test, the material density ranged between 1760 and 2110 kg/m³ and the flow heights were of the same order of magnitude as the size of the obstacles. In total 16 tests are carried out from September 2008 to September 2010. Surprisingly to note that the result of Veltheim test performed by Bugnion et al. (2010) shows that there is no apparent correlation between flow heights and impact pressure values, the dependency on flow height of the impact pressure is negligible. By contrast, the study found the pressures depend primarily on the flow speed, the hydrodynamic formula, which in turns to depend on distribution and size of particles. Even though the large-scale field experiments have many advantages like scaling considerations with regard to the process are not necessary, the expected volume of the debris flow makes the cost of designing the measurement setup intensive, with a long period and the parameters of flow and material are often unknown. For this reason, small scale laboratory experiments for measuring debris flow came into being. Within the small-scale laboratory experiments, scaling debris flows for physical modelling must take into account but difficult, a common approach to extrapolate from experimental scale to field scale. These extrapolations are often based on hydrodynamic approaches, assuming geometric as well as simple kinematic similarity, which is characterized by the dimensionless Froude number (Fr). On the basis of Froude scaling, Hubl and Holzinger (2003) proposed a modified hydrodynamic expression. As mentioned before, Scheidl et al. (2012) analyzed the impact pressures of granular and viscous debris flow by employing small scale laboratory experiments, accomplished with Froude numbers less than 3 ($Fr < 3$). After all the tests executed by Scheidl et al. (2012), the general form of the dynamical impact model shows more plausible results with comparison of that of a general hydrostatic one. Therefore, from experimental scale to field scale, the hydrodynamic model is recommended for measuring the impact force of debris flows.

In addition to the flow speed, considering the influence of distribution and size of particles on the impact force of debris flows, based on existing hydrodynamic theory, He et al. (2016) conducted a more recent investigation. Within their studies, regarding debris flow is a typical two phase (solid-fluid) fluid flow that consisted of a various distribution of different grain size and their different mobility, the impact force of debris flow was mainly divided into three parts: 1) the dynamic pressure provided by the debris slurry (mixture of fine particles and water); 2) the impact force of coarse particles; 3) the impact force of boulders. The size of solid particles is classified in Figure 3.8: fine particles with a grain size less than 10mm, boulders are over 500mm and a transition size of coarse particles between fine particles and boulders.

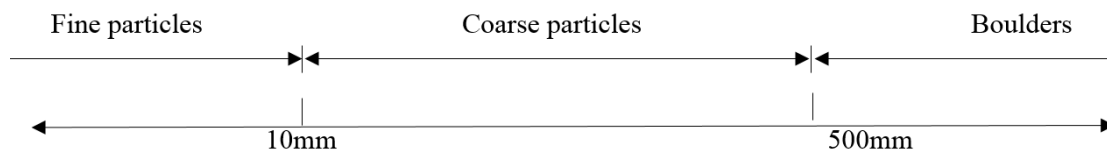


Figure 3. 8. Standard particle size of debris flow (He et al. 2016)

Within their conditions assumed (e.g., the solid volume fraction was 0.3, density of fluid and solid was 1200 kg/m^3 and 2400 kg/m^3 respectively, the depth of the flow was 2m, with an average flow velocity 5 m/s), the results show that the impact forces caused by boulder were the largest followed by coarse particles and the dynamic pressure produced by slurry was minimal, which directly reveals that the grain size distribution plays an important role in impact force of debris flow. On basis of hydrodynamic model, the method proposed by He et al. (2016) is new and obviously justified, since their experiments focus on the impact forces of solid-fluid mixture exert on an obstacle rather than on the flow dynamics of debris flow. What's more, it is worth noting that compared to the existing two typical impact force formulas, this theory can avoid the errors of the determination of empirical parameter that occur due to the complex components of debris flow. On basis of this, to serve the purpose of better estimating the impact force generated by debris flow occurring in the study area, it is necessary to define the grain size distribution in it.

Normally, rain induced debris flow is composed of water and the natural solid material of the hillslope. The complex components of debris flow lead to various orders of magnitude of impact forces as discussed previously. Hence, as the study area in this thesis, the natural sediments of hillslopes in Ottawa Valley need to be discussed. The Ottawa Valley refers to a geographic area that merges with the St. Lawrence Lowlands from the Ottawa River to the Saint Lawrence River as far east as the island of Montreal, which can also denote the geographic area from Ottawa to Montreal and the surrounding area. In the twentieth century, natural slopes in the Ottawa Valley has been studied by several investigators (Sangrey and Paul 1971; Lo and Lee 1973; Mitchell and Markell 1973). Since then, a better understanding of the causes of debris flow can be acquired based on a regional geologic map, which shows the distribution of sensitive clay and associated landslides in Ottawa Valley was presented by Fransham et al. (1977):

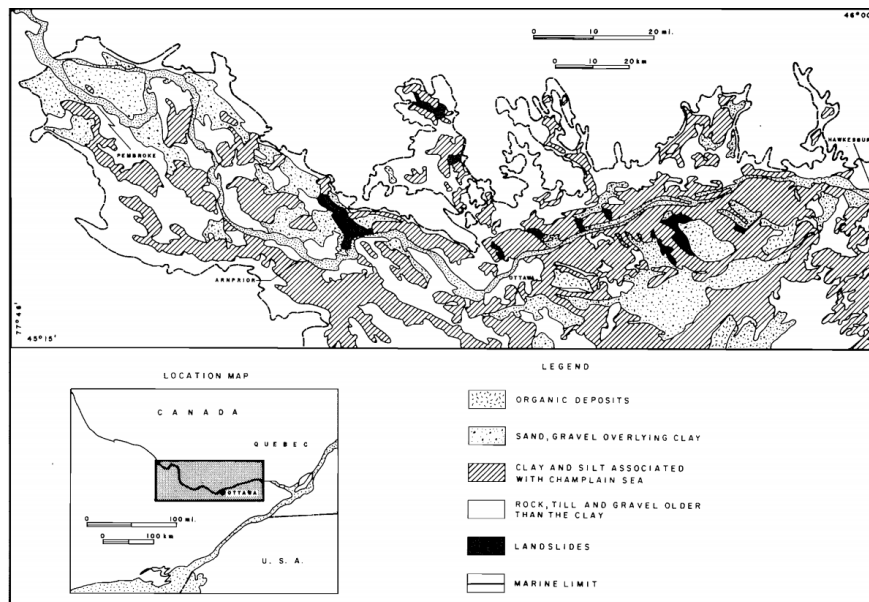


Figure 3. 9. Distribution of sensitive clay and associated landslides in Ottawa Valley (Fransham et al. 1977)

In this map (Figure 3.9), the soils in Ottawa Valley can be mainly divided into four types:

- Organic deposits
- Sand and gravel overlying clay
- Clay and silt associated with the Champlain Sea, and
- Rock till and gravel

It is apparent that the Champlain clay, which is the fine-grained sediment, also commonly called as Leda clay takes major counts of natural soil condition of Ottawa Valley, and the most of landslides mainly took place within or around the Champlain clay section. Depending on the stratigraphy, sensitive clay slopes in Ottawa Valley have been classified into two geological setting types (Fransham and Gadd 1977), as shown in Figure 3.10:

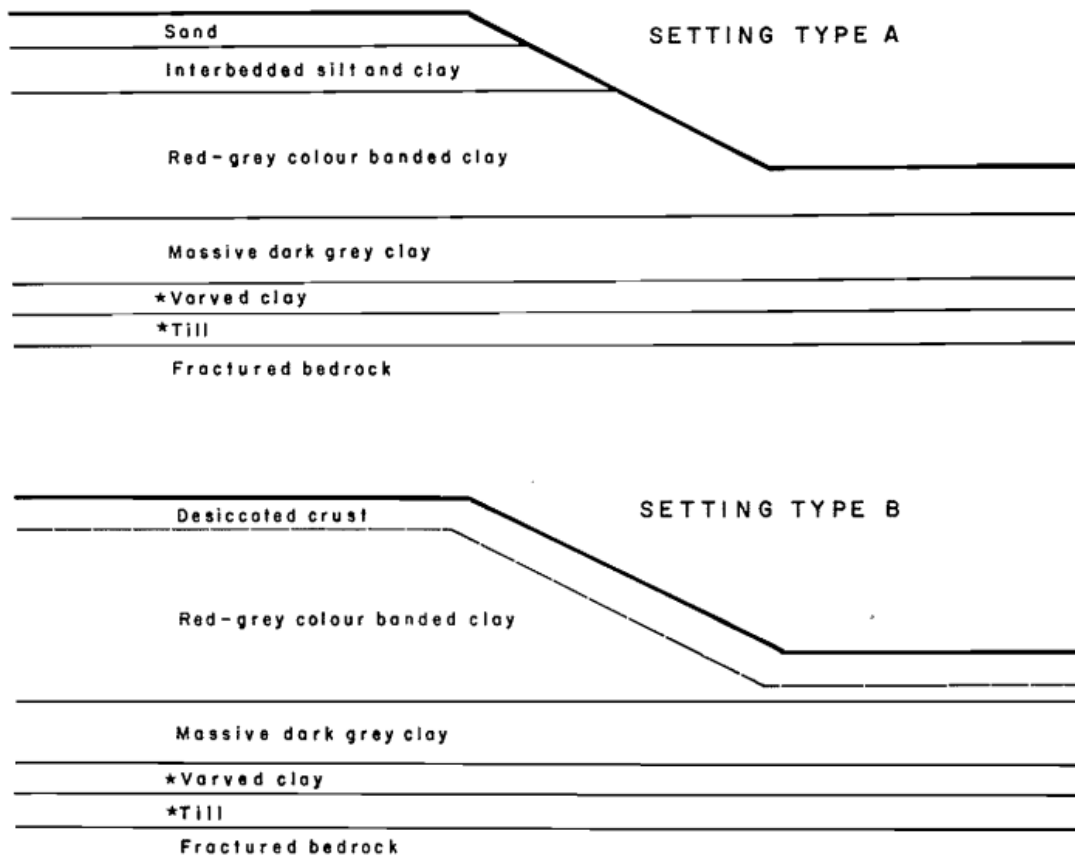


Figure 3. 10. Classification of sensitive clay slopes (Fransham and Gadd 1977)

The apparent difference between these two types is the presence of a sand layer on the surface underlain by a silt and clay layer in setting type A, on the contrary, type B only have a topping layer of desiccated crust. Depending on the database, most of the large slides in Ottawa Valley have occurred in slopes of setting type A. Since grain size is classified as clay if the particle diameter is $<0.002\text{mm}$, as silt if it is between 0.002 mm and 0.06mm , or as sand if it is between 0.06mm and 2mm , hence, according to the criteria in Figure 3.8, the solid phase of debris flow occurs in Ottawa Valley are mainly composed of fine particles (grain size less than 10mm).

As is well known, debris flows are non-Newtonian fluids and can be classified various types depend on different criteria. Regarding material involved, debris flows can be classified into three common types: mud-rock flow, mudflow and water-rock flow (Zhang 1993). The grain size distribution of these three types are presented in Table 3.10.

Debris flow type	Size distribution % by weight				
	200-20 (mm)	20-2 (mm)	2-0.1 (mm)	0.1-0.005 (mm)	<0.005 (mm)
Mud-rock flow	100	57.0	28.5	14.0	5
Mudflow			100	84.9	17
Water-rock flow	100	67.5	39.0	17.6	6

Table 3. 10. Grain size distribution of mud-rock flow, mudflow and water-rock flow (Zhang 1993)

The Table 3.10 states that grain sizes in mudflows are mainly from 0.005mm to 2mm, according to the information shown in Figure 3.8, revealing that the solid phase of mudflows is comprised of fine particles. Therefore, it is not hard to infer that under sufficient natural fine particles (Champlain clay) soil conditions, the area of Ottawa Valley is prone to mudflows at the condition of a heavy rain, which are the sandy but more watery counterparts of low-viscous debris flow.

As mentioned previously, the grain size distribution plays an important role in impact force of debris flow, here, as counterparts of low-viscous debris flow, also for mudflow. Within mudflows, fine particles (solid phase) and water form a relatively uniform slurry. Considering the effect of grain size distribution for impact forces, although the dynamic pressure produced by slurry is much smaller compared to that of boulders and coarse particles, fine particles is the only component of the solid-phase within mudflows, hence, the impact forces produced by slurry cannot be ignored which comprises the mudflow's impact force.

3.4.2 The viscosity of mudflow

A mudflow is a mass movement composed of fine-grained soil particles mixed with water, as a non-Newtonian fluid, mudflow has yield stress and viscosity (rheology parameters). However, normally, as input parameter in the fluid simulation, the viscosity of mudflow is difficult to obtain by using a conventional viscometer. Accordingly, Widjaja et al. (2014) proposed recommendation values of viscosity for mudflow by comparing two laboratory tests: vane shear test and flow box test. Within these two laboratory tests, five water contents around the liquid limit were used. Here, it is necessary to mention that the solid phase of mudflow is mainly comprised of fine-grained soil particles in a viscous liquid state, thus, water content could be equal to or higher than the liquid limit. Firstly, the yield stress value was derived from the vane shear test, which was used in the flow box test later to obtain the viscosity value.

As we all know, water is a typical Newtonian flow which is governed only by viscosity and cannot resist shear stress, while, in mudflow, a non-Newtonian flow, flow is governed both viscosity and yield stress. And only when shear stress is higher than yield stress, the mudflow will occur.

Typically, rheology models used for non-Newtonian fluid include the Bingham plastic model and the yield-pseudoplastic model (O'Brien and Julien 1988). Among them, Bingham model exhibit a linear stress-strain relationship at shear stress (τ) in excess of the yield stress (τ_y). Therefore, Bingham model can be adopted for mudflow. The equation describing Bingham fluids is:

$$\tau = \tau_y + \eta \left(\frac{du}{dy} \right) \quad (3.4)$$

Where viscosity η is measured as a gradient of the line from the relationship of shear stress τ and shear strain rates du/dy .

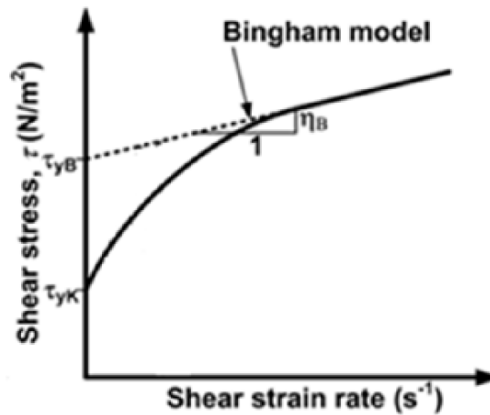


Figure 3. 11. Bingham Model (Widjaja et al. 2014)

Then, based on the Bingham model, the fine-grained soil sample with water content in a range from 0.8LL-1.2LL used in the vane shear test to obtain the rheology parameters. Conventionally, the rheology parameters may be obtained from conventional laboratory viscometers, but due to the range of applying the water content around the liquid limit is hard to measure, Widjaja and Lee (2013) developed a new viscometer in the flow box test which could give a wider range of water content in both plastic and viscous liquid states (liquidity index LI from 0.1-2.3) for elucidating the behavior of mudflow. On the basis of Bingham model and Terzaghi's trapdoor theory, the displacement profile and viscosity value could be derived.

As a consequence, by comparing the data obtained from these two laboratory tests and further validating from real deposition of mudflow and software simulation. The result shows that the viscosity value of mudflow from the flow box test is relatively reliable and is very close to the real deposition of mudflow which is in the range of 0.1 Pa-s-2Pa-s (1 poise - 20 poise) at liquid limit which is two orders of magnitude larger than the viscosity of clear water ($\eta_{\text{water}} = 0.01$ poise).

3.5 Parameters Influencing Impact Force

Like aforementioned, the Ottawa Valley area of this research is prone to mudflows at the condition of a heavy rain, consisting of slurry of water and fine particles. The slurry characteristics within a mudflow depend on the constituents forming the slurry phase such as silt, clay, and fine particles. Assuming an average velocity v_f of slurry, the depth of flow h with the width b of transverse force surface, the momentum theorem is:

$$(p_f bh)\Delta t = (\rho_f bhv_f \Delta t)v_f \quad (3.5)$$

Where p_f means the dynamic pressure of the slurry, ρ_f is the density of slurry and Δt is the impact time. Therefore, the dynamic pressure exerted by slurry on an obstacle can be expressed as:

$$p_f = \rho_f v_f^2 \quad (3.6)$$

In general, in viscous debris flow, solid-phase particle distribution is more uniform (He et al. 2016) which could be effectively modeled by employing a single equivalent phase model of a viscoplastic fluid. In addition, as stated in previous section that mudflows occur in study area are actually a uniform mixture slurry of water and fine particles, which is the sandy but more watery counterparts of low-viscosity debris flows. Thus, the mudflow in this study can be envisioned as a single-phase model of a uniform slurry mixed by water and fine particles.

Since the different grain particles in debris flow can produce different forces as mentioned before, while, in the mudflow simulated in this thesis, the solid phase only has fine particles which mix water form uniform slurry, therefore, the dynamic pressure p_f produced by slurry is the impact pressures P exerted by mudflow, the velocity v_f of slurry is the velocity v_m of mudflow and ρ_f is the density of mudflow ρ_m . Then, Eq. 3.6 can be represented as:

$$P = p_f = \rho_m v_m^2 \quad (3.7)$$

On basis of the elements that could affect the impact forces discussed previously, under the circumstances of certain grain size distribution, it is apparent that the flow velocity plays key role in the impact pressure. Since the mudflow simulated is assumed as a uniform flow, the flow velocity could be affected by various parameters according to one of the most commonly used equations known as the Manning's Equation.

The Manning's equation (SI: International System of Units) is an empirical formula that applies to estimate the average velocity of uniform flow in open channels, which was first introduced by the French engineer Philippe Gauckler (1869) and later developed by Irish engineer Robert Manning in 1889, and presented as:

$$v = \frac{1}{n} R^{\frac{2}{3}} \theta^{\frac{1}{2}} \quad (3.8)$$

Where v is the velocity of flow, n is the roughness coefficient which represents the roughness or friction applied to water flow by the channel (also called Manning's Roughness Coefficient), R represents hydraulic radius (the flow depth d) and θ is the channel slope. Obviously, in addition to the acceleration due to gravity, parameters of terrain roughness, flow depth and natural slope steepness (slope of channel) can affect the velocity of flow, further, affecting the impact forces generated by flow, hence, these parameters will be considered in simulation.

Additionally, in the research, assuming railway lines are constructed near slope in mountainous area, the buffer plane D is constructed between natural hillslope and railway embankment (shown in Figure 3.12) contributing to mitigation against the potential impact of mudflows. Concerning the value of flat natural bedding plane D, the mudflow will easily impact the train on top of the railway embankment if the distance is too short (e.g., ~1m), on the contrary, mitigation measure like a long buffer plane D built is helpful to retard mudflows' movement, even it is possible that

the mudflow cannot reach at the top surface of embankment. Thus, the effect of buffer distance D on mudflow should be investigated, the value of D is assumed 1m, 2m, 4m, and 6m in the research.

To sum up, in order to simulate the scenes of mudflows hitting trains using SPH based simulation tool, a slope at the condition of the natural fine particle soil will be simulated, along with the railway embankment and buffer plane mentioned earlier. The simple layout of terrain environment in models is envisioned as shown in Figure 3.12 below:

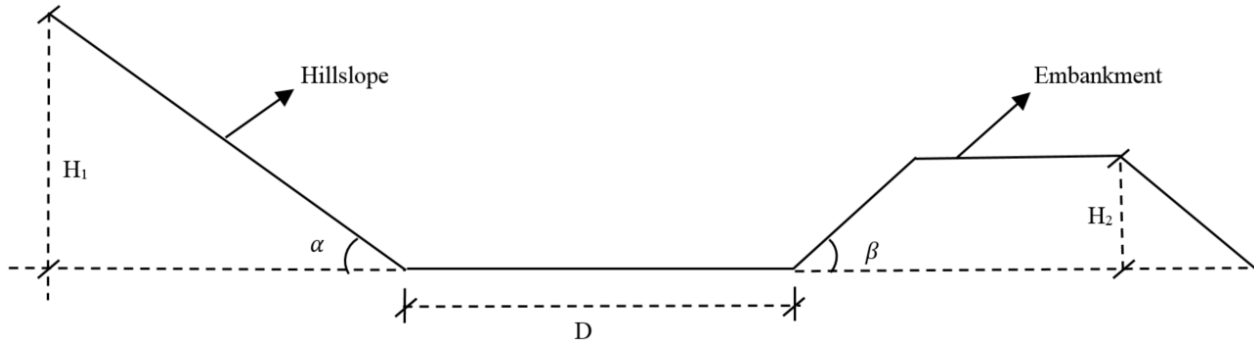


Figure 3. 12. Layout of terrain condition in model

Where H_1 is the height of hillslope with an angle α , H_2 is the height of the railway embankment, β presents the slope ratio of railway embankment. The middle plane D is the straight-line distance from the bottom of hillslope to the bottom railway embankment which is natural bedding plane parallel to the land surface.

Then a mudflow with a certain density at rest on the top of hillslope start to fall. As mentioned above, apart from the constant acceleration due to gravity, the changes of mudflow velocity could be achieved by changing hillslope inclination or terrain roughness, further, the impact force exert on the train could be observed and analyzed. Applying the assumption of these various parameters, different models can be created utilizing DualSPPhysics software (based on SPH method), their effect on the impact force generated by mudflows and the derailment potential of railway cars could be investigated.

Chapter Four: Model Calibration and Verification

4.1 Introduction

Before carrying out the simulation of mudflows impacting railway cars, the mudflow model needs to be calibrated against the experimental results and the accuracy of the model needs to be validated. An experimental debris flow test will be modeled using SPH as a reference with the aim of exploring the range of values assigned to main model parameters like mudflow properties and their effect on the simulation results. It was concluded that the values assigned to some key model parameters, such as artificial viscosity, are very important to ensure a realistic simulation.

4.2 Variables Considered in the Calibration Test

Even though SPH-based models have been already applied for engineering purposes (e.g., Rogers et al., 2010; Barreiro et al., 2013; St-Germain et al., 2013; Altomare et al., 2015), the selection of proper values for some key model parameters might be case-dependent, which will inevitably affect the model results, so do for DualSPHysics, in which the “Artificial viscosity coefficient” and “Initial particle distance” are key case-dependent ones. Hence, these two parameters are selected for the parameter calibration of DualSPHysics.

4.2.1 Artificial viscosity coefficient

Among the various parameters involved in DualSPHysics, one of the most important parameters in the simulation of the fluid is artificial viscosity. The initial aim of artificial viscosity coefficient α proposed by Monaghan (1992) is to be a tuning factor in order to introduce the proper dissipation. According to the recent research proposed by Padova et al. (2014) in which they focused on the effects of the artificial viscosity on the propagation and breaking of regular waves. It was concluded that the value of the artificial viscosity coefficient α can drastically modify the results of the simulation. However, as a tuning coefficient, the proper value for α is not constant for each case. For example, empirically, the value of $\alpha=0.01$ has proven to give the best results in the validation of wave flumes to study wave propagation and wave loadings exerted onto coastal structures (Altomare et al. 2015 & 2017). While in the simulation of other cases such as dam-breaks, the interaction of fluid with boundaries during dam propagation becomes more relevant and the value of α should be changed according to the resolution (“dp”) to obtain accurate results. Therefore, it is important to test a range of values for the artificial viscosity coefficient to reach a value or a range of values which provide the closest result to that in physical experiments and attain satisfactory simulation results for mudflow model.

As a final note, artificial viscosity, is not a property any fluid has, it should be considered as a tuning factor varies with particle resolution (“dp”), which is able to stabilize SPH simulation without enormous numbers of particles and get results comparable to the experiments which have been conducted.

4.2.2 Initial particle distance

The initial particle interspace, dp, is another key case-dependent parameter, which defines the distance between particles which is initially used in SPH to locate the particles within the domain

at $t = t_0$. Once the simulation starts, the fluid particles are free to move. The selection of the value of dp determines the total amount of fluid and boundary particles, hence, on the other word, dp being an expression of the model resolution. Convergence studies are usually carried out to analyze the influence of the model resolution on the results. This has been done also in SPH and DualSPHysics (Altomare et al. 2015). However, the optimal value of the initial particle relative distance is still case-dependent. Empirical experience suggested that, for wave propagation purposes, a value of dp should be at least $1/10$ of the water height H (Roselli et al. 2018). Several authors, such as Altomare et al. (2015) and Padova et al. (2014), show that increasing the spatial resolution (i.e. using smaller values of dp) improves the numerical model accuracy. In other words, resolution and the value of dp have a relationship in DualSPHysics. The smaller values of dp is for the higher the resolution should be in order to achieve better results. However, convergence has not yet been completely proved in SPH and the choice of this parameter influences the contribution of artificial viscosity terms in the equations of Eq. 2.15 and Eq. 2.16 (Padova et al. 2014).

4.3 Calibration Test

To apply correct values to the abovementioned parameters in order to perform a realistic simulation, a suitable real-life project or experimental test had to be utilized by which the SPH-based simulation program, DualSPHysics, could be calibrated and verified. Utilizing a reference experimental test, a form of a simulation would be created which could provide useful calibrating information regarding the changes in the simulation results by changing the values of the aforementioned parameters. The reference experimental test was chosen as developed by Bugnion et al. (2010). In total 16 tests were performed in a rock quarry near Veltheim, Canton Aargau, Switzerland. A 41m long, 8m wide channel was constructed on the side of this rock quarry. This channel on the hillslope was excavated down to the bedrock surface, which is a natural bedding plane parallel to the land surface, with an average slope inclination of 30° (Figure 4.1). The sidewalls of this channel were 1m high and consisted of soil material which is generally not entrained by the flows. Within each test, a volume of 50m^3 debris flow material was released and it flowed down the slope.

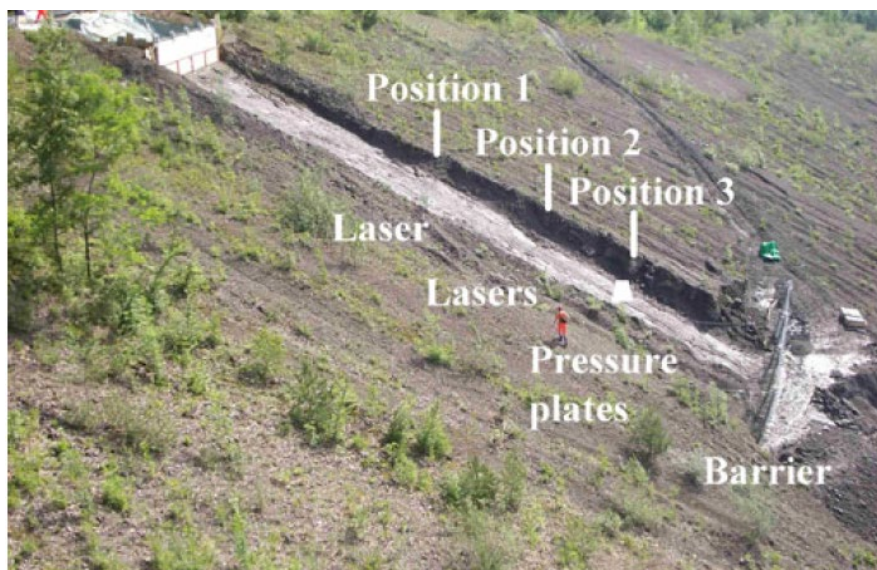


Figure 4. 1. The slope in large-scale field test (Bugnion et al. 2010)

Two vertically oriented laser distance sensors were instrumented along the channel (shown in Figure 4.1) to determine the flow heights at the middle of the channel which was located 14m at position 1 and 26m at position 2 downstream from the starting point (distances were measured parallel to the slope), and were used to compute the front velocity of flows. At position 3 (shown in Figure 4.1), four meters downstream of position 2 at 30m downslope, two pressure plates were installed in the center of the channel perpendicular to the flow direction to measure impact pressures which were square in shape with 120mm and 200mm side length ($A=0.0144\text{m}^2$ and 0.04m^2) respectively. The pressure sensors were protected from the flowing material by two steel plates separated by an elastomer layer (Figure 4.2).

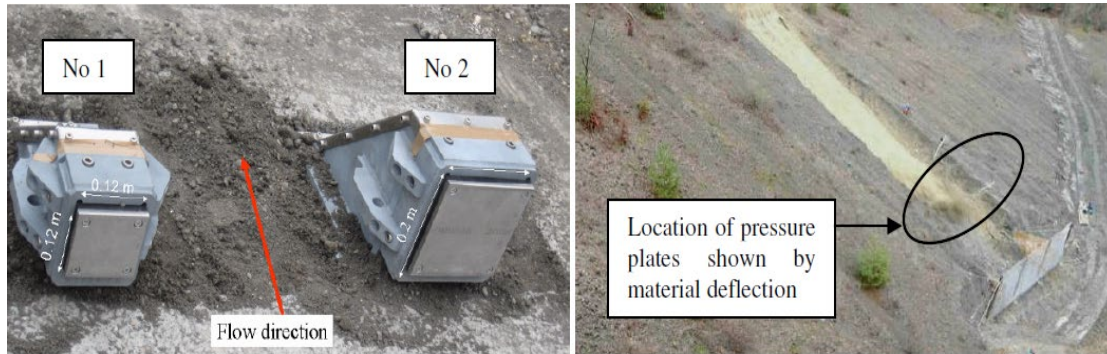


Figure 4. 2. Pressure plates used in the field test to measure impact pressure (left side) and (right side) debris flow impacting the pressure plates (Bugnion et al. 2010)

Downstream of the two pressure plates, at the lower end of the channel, a 15m long and 3.5m high flexible steel mesh barrier was set (shown in Figure 4.1) to limit the runout of flows. Thus, during the process of flowing down, the impact pressure and velocity of debris flow can be measured. Since the field tests carried out by Bugnion et al. (2010) were performed with different composition of debris flow, therefore, the debris flow material samples were collected after each test was finished and analyzed in laboratory to determine grain-size distribution, density and water content. Among all 16 tests, the density of the debris mixtures ranged between $1,760\text{ kg/m}^3$ and $2,110\text{ kg/m}^3$ and the water content between 14% and 28% (percentage of mass). The mass fraction of fine particles and gravel varied between 21% and 48% and 16% and 59%, respectively. As a result, based on Bugnion et al. (2010) investigation by using a field-scale flows test, one can find that the maximum impact pressure values correlate with the square of the speed and validate the hydrodynamic model. Moreover, within the 16 tests, due to the different composition of debris flow material, comparing to the releases with a large fraction of coarse particles, debris flow releases with large fines content (i.e., clay and silt fraction larger than 40%), the front velocities of these releases are lower on average and display scatter but correlate with the liquidity index. While it is worth to mention that, comparing to a numerical modelling simulation, as in the Bugnion et al. (2010) field research, the composition of the raw debris flow materials (bedrock and soil material) are directly collected from the quarry, which is not a constant and expected to vary from one test to another. What's more, the velocity tested in the Bugnion et al. (2010) field test is not directly measured by sensors, which is computed from the passing times and distances between sensors. On the other hand, during transportation from quarry to the field site and movement on the slope, water loss of the debris flow material is inevitable and difficult to quantify. Thus, for all these reasons, the pressure and velocity results modeled from the numerical simulation cannot be as the

same as that in field tests. However, no matter what the values of velocity or pressure are, regarding the debris flow, viscous debris flow or mudflow, the impact pressure values always correlate with the square of the speed by introducing the impact coefficient C (hydrodynamic model), which is validated in the field research performed by Bugnion et al. (2010). As mentioned in the previous chapter about key parametric studies, the hydrodynamic model (Eq. 3.2) is the most popular one for calculating the dynamic pressure of the slurry, because the debris flow velocity and coefficient C are more easily acquired. It is mainly derived from fluid momentum balance and the Bernoulli equation, which can be applied to calculate impact pressure of most fluids, even in the case of pure water and saturated mixtures. The key issue for the hydrodynamic formula is the determination of the impact coefficient C , which is used to represent the difference of flow regime and proportions of granular composition. On the other words, the value of impact coefficient C depends on the types of flow or some sort of debris flow. As for the impact coefficient C , some empirical values which have been already estimated based on laboratory tests and field observations shown in Table 4.1.

Resource	Empirical coefficient C	Description
Watanaba and Ikeya (1981)	2.0	Estimated with the data measured in Nojiri Ravine, Japan, characterized by laminar flow and fine-grained material (mudflow).
Hungr et al. (1984)	1.5	Back analysis of the stony type debris flow in British Columbia, Canada.
Mizuyama (1979)	1.0	Derived from jet impact theory, applied in Yakedake, Nigorisawa Urakawa debris flow in Japan.
Armanini (1997)	0.45-2.2	Estimated with the data measured in laboratory experiments, the material is a mixture of PVC and water with densities 1080–1300 kg/m ³ .
Zhang (1993)	2-5	Estimated with the data measured based on field measurements of over 70 debris flow in Jiangjia Ravine, China, characterized by viscous debris flow.
Egli (2005)	2	Swiss guidelines for constructing mitigation measures for the calculation of debris flow impact pressure on obstacles

Table 4. 1. Empirical coefficients in hydrodynamic models

Combination these empirical impact coefficient values and the values of impact coefficient C (0.5-2) from the Bugnion et al. (2010) field observations for viscous debris flow (release 4, 9 and 16), it is not hard to find that about 2.0 is the optimal value of impact coefficient C for viscous debris flow with large fines content (i.e., clay and silt fraction larger than 40%). Since mudflows are the sandy but more watery counterparts of low-viscous debris flow whose soil-phase is mainly composed of fines particles (clay and silt fraction larger than 40%), hence, the value of 2.0 is the optimal value of impact coefficient C for the mudflow fluid type in hydrodynamic model for computing the flow impact pressure.

Based on Bugnion et al. (2010) research, a slope was created in DualSPHysics (Figure 4.3a) which has the same geometric parameters as in the field test, in order to perform the similar tests to calibrate the DualSPHysics code by comparing the results obtained from the tests with the ones in the reference field research and further validate the hydrodynamic formula Eq. (3.2) stated in Chapter 3 for mudflow's fluid type. This slope was a 41m-long, 8m-wide and had an inclination of 30° . As the same set in the field test, there is a pressure sensor with a square surface $A=0.04\text{m}^2$ (the large pressure plate) in the middle of the channel, at the 30m downslope position to measure the velocity and impact pressure. At the lower end of the channel, a 15m long and 3.5m high flexible steel mesh barrier is set to stop the debris flow moves (Figure 4.3b). Since the objective of this current work is to estimate the behavior of mudflow which is the sandy but more watery counterparts of low-viscous debris flow with large fines content (clay and silt fraction larger than 40%). Thus, the calibration tests are mainly focus on the debris flow releases with large fine particles content within Bugnion et al. (2010) field tests (releases 4, 9, and 16). It should be mentioned that due to the DualSPHysics uses the SPH method to calculate the interactions of fluid particles with the boundary particles (pressure sensors), as the main DualSPHysics and physical calibrating parameters, the higher the values for the aforementioned variables, the longer of simulation time will be.

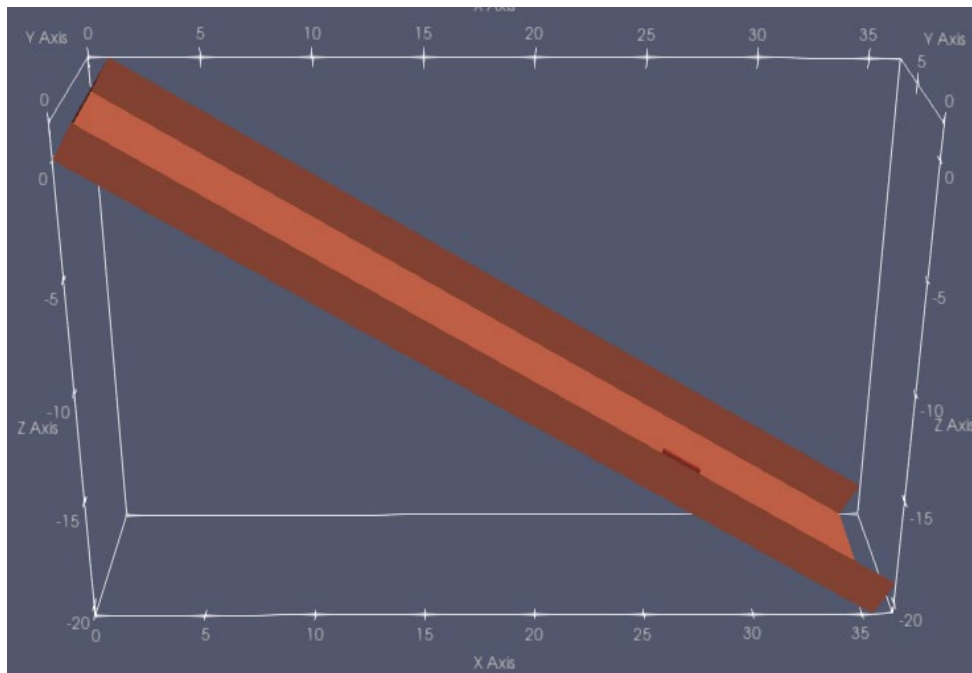


Figure 4. 3. a) The slope modeled in DualSPHysics

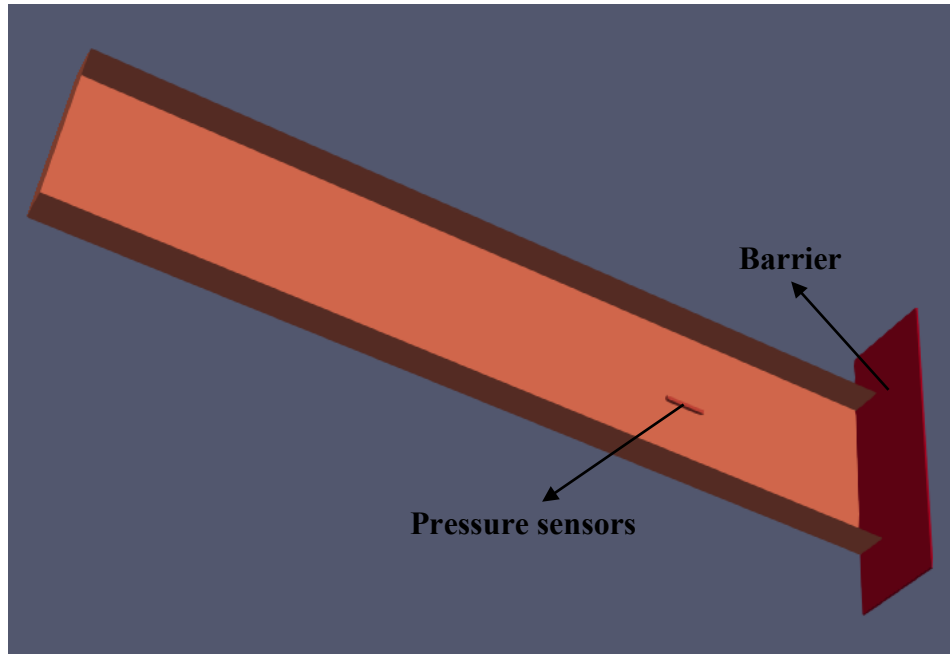


Figure 4. 3. b) The slope modeled in DualSPHysics with a pressure sensor at 30m downslope position and a barrier at the end of the channel (continued)

Since the default values for the aforementioned parameters used in DualSPHysics code are assumed for water (such as artificial viscosity), which will result in using unrealistic values of the debris flow characteristics to define the mudflow. Thus, the main objective of the calibration test is to test a range of values for the artificial viscosity and dp to reach a value or a range of values which provide the closest result to the real-life processes for the mudflow simulations. Therefore, the calibration tests will be performed in two steps with the goal of finding the optimal combination values set of artificial viscosity and dp to represent the real-life mudflow process. To serve the purpose of the calibration tests, the value of one of the parameters will be considered as variable and the values for the rest of parameters (such as dp) are taken as constant. Thus, different series simulation will be performed within two steps:

1. The first step was implemented by performing the first series of simulation, with the aim of achieving an overall understanding of the general regime of changes in the flow velocity, the impact pressures or the impact coefficient C with the fluctuation in the artificial viscosity parameters applied in DualSPHysics code. Considering to achieve this goal, a range of artificial viscosity values were chosen for parameters. Because the goal of this series of simulations is to understand the effect of changes in artificial viscosity, hence the other parameters should be the constant.

One of the most important aspects in the movement of the fluid is its density. Density is the proportion of mass over volume. Density in DualSPHysics is one of the few parameters that has the physically accurate value and dimensions. Since the default value for density in DualSPHysics is 1,000 which corresponding to the actual density $1,000 \text{ kg/m}^3$ for water. Comparing to water, as one more dense and viscous fluid, mudflow has higher a value. Based on the reference test, the field research performed by Bugnion et al. (2010), combing

with the mudflow physical properties definition discussed previously, the density validated in Bugnion et al. (2010) field investigation for mudflow is $1,850 \text{ kg/m}^3$, therefore, the fluid density of $1,850 \text{ kg/m}^3$ will be set in simulations.

According to the documentation of DualSPHysics regarding the particle resolution, it will take a considerable amount of time (even up to three days) for DualSPHysics to process each simulation if the value of dp is too small (higher resolution). While the mudflow's fluid cannot be simulated correctly if the resolution is too low (the greater value of dp). Hence, regarding the documentation of DualSPHysics and experiences validated by others using DualSPHysics, for wave propagation purposes, the ideal resolution (optimal value of dp) for the simulations without changing the scales in the platform would be a value of at least $1/10$ of the water height H . As the initial the fluid height is 1.25m , thus $dp=0.125\text{m}$ will be set in the first series simulations.

Artificial viscosity is the crucial factor need to be considered in this series, it is one of the parameters applied in DualSPHysics which has not been assigned a realistic value. Different types of fluids have different viscosity values. Since all example simulations shown in DualSPHysics using the default value to simulate water, the default value of the artificial viscosity applied in DualSPHysics being 0.01 for water with the actual viscosity of $1 \times 10^{-3} \text{ N} \cdot \text{s/m}^2$ (0.01 poise), therefore, the effect of the fluid changing from being a bit more viscous to being far more viscous than water was necessary to be observed. Hence, the assumed artificial viscosity values for mudflow starts from 1 to 20 which corresponding to mudflow's viscosity value of approximately $1 \sim 20$ poise as mentioned in the key parametric studies of Chapter 3 and the increment value of 2.5 is used to increase steadily the value of artificial viscosity for each subsequent test. This range of values were selected due to the definition of mudflow physical properties, discussed previously and combined with the recommended values for the viscosity of mudflow mentioned in the third chapter of this work (comparing to the standard viscosity value for water).

2. After having performed the first series of simulations and understood the general behavior of changes in the simulation results as a matter of artificial viscosity factors in the previously defined range, the second step will be implemented to find out the effect of changes in another individual parameter (dp) on the results of the tests. As mentioned previously, the initial space between the particles (dp) determines the total amount of fluid and boundary particles, hence being an expression of the model resolution and the choice of this parameter influences the contribution of artificial viscosity term which could further influence the whole fluid behavior. In other words, the selection of the value of dp determines the total time of the simulation, the effect on the aspect of visualization in post-processing and the effect of the changes in the flow velocity, further influence the impact coefficient C . Thus, in the second step, the parameter dp will be considered as variable, and hence two series simulations will be performed:
 - Due to the value of dp is set as 0.125m in the first step, as mentioned previously, dp is an expression of the model resolution, smaller dp leads to a higher resolution which could help to achieve accurate results and more vivid visualization in post-processing aspect (animation), hence, within this series simulation, the value of dp will be decreased by 0.025m in each following test while the other parameters will

be constant (artificial viscosity will be held constant at the value of 5). This way, as the variable parameter dp changes, the overall effect on the resolution (whether it could simulate a real-life process of mudflow) and the values of impact coefficient C whether the value increases or decreases can be studied, compared and analyzed.

- Following the first series simulation in the second step, the second series of simulations will be performed with the aim of finding out the optimal combination values of artificial viscosity and dp to represent the real-life mudflow process, which is also the ultimate goal of the calibration test. During the previous simulations, how individual parameter affect the flow of the mudflow are already observed. However, since the final aim of all the performed tests is to be able to calibrate the DualSPHysics program, gain the knowledge of simulating samples of mudflow and find out the optimal values for simulating mudflows, to implement this goal, the simulations performed previously are not sufficient, thus, based on the previous tests results, the second part within the second step will be conducted by comparing different set combinations of parameter dp and artificial viscosity. All aforementioned parameter values will be set successively, for example, when the value of dp equals 0.125m, the artificial viscosity from 1 to 20 will be applied one by one, and then, 0.1m is assigned to dp , at the same time, there is a steadily increase in artificial viscosity valued between 1 and 20. The increasing unit pattern will be the same as that in the previous simulations.

Same as in Bugnion et al. (2010) field test, for running all simulations mentioned before, when the appropriate values are chosen, the mudflow with constant volume and the assigned physical properties will be released from the top of the created slope, flowing down the slope under gravitational acceleration, hitting the pressure sensors set on the slope and be stopped by the barrier at the end and the simulated flow material would come to rest as the result of the interaction. In the process of each simulation, the velocity of mudflow in assigned position and the impact pressure exerted by mudflows on the pressure sensors (one exact position on the pressure sensors) will be computed and measured by the code applied in DualSPHysics and after that, using the hydrodynamic model presented in Chapter 3 (Eq.3.2) the impact coefficient C would be calculated for each simulation.

4.4 Calibration Test Results

Similar to the Bugnion et al. (2010) field experiments, the velocity of mudflow and the impact pressure will be measured and computed by DualSPHysics at the same position each time, the instant that mudflows impact the pressure sensors.

4.4.1 Tests with changes in artificial viscosity

The first series tests are performed with a range of values in artificial viscosity applied in DualSPHysics with predefined equal increases in the value to examine how differently the DualSPHysics code simulates the mudflow with different properties. The following table shows the input data:

Test	Artificial viscosity	Density (kg/m ³)	The value of dp (m)
1	1	1850	0.125
2	2.5	1850	0.125
3	5	1850	0.125
4	7.5	1850	0.125
5	10	1850	0.125
6	12.5	1850	0.125
7	15	1850	0.125
8	17.5	1850	0.125
9	20	1850	0.125

Table 4. 2. Input data for the first series of calibration tests

The particle distance (dp) in this series tests are set to 0.125m, which eventually makes 25,858 of boundary particles and 44,572 of fluid particles. The following are the diagrams obtained in the tests (Figure 4.4). The information observed in the diagram shows that: the higher values for artificial viscosity suggest that the speed at which the mudflow would decrease as the time passed (Figure 4.4a), while the impact coefficient C would increase (Figure 4.4b). These results meet the real physical behavior of viscous fluid that, under the same force effect (gravity acceleration), higher viscosity of fluid leading to slower movement. What's more, according to the hydrodynamic model, the theory that more viscous fluid corresponds to a higher value of impact coefficient C can also be validated.

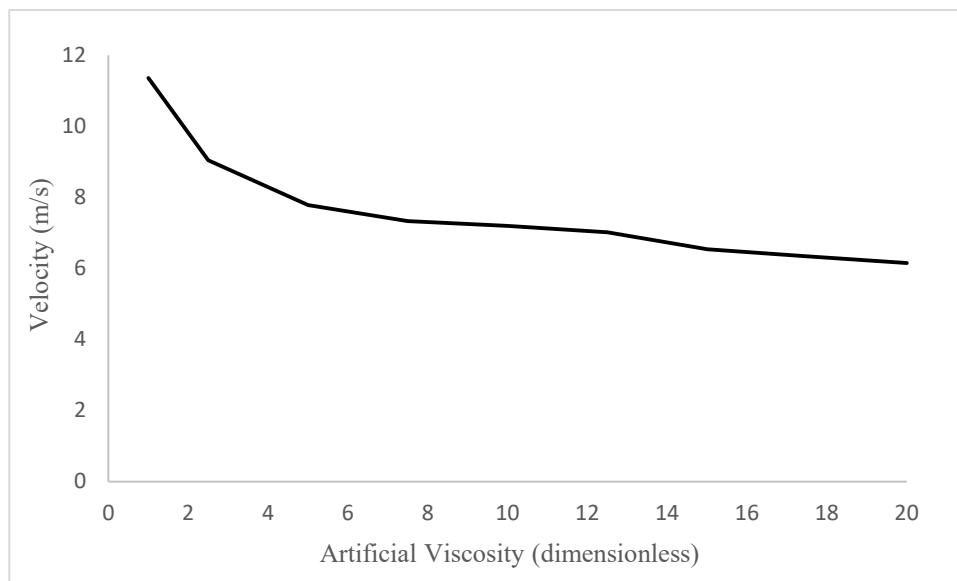


Figure 4. 4. a) Diagram of velocity versus atrificial viscosity for the first series simulations

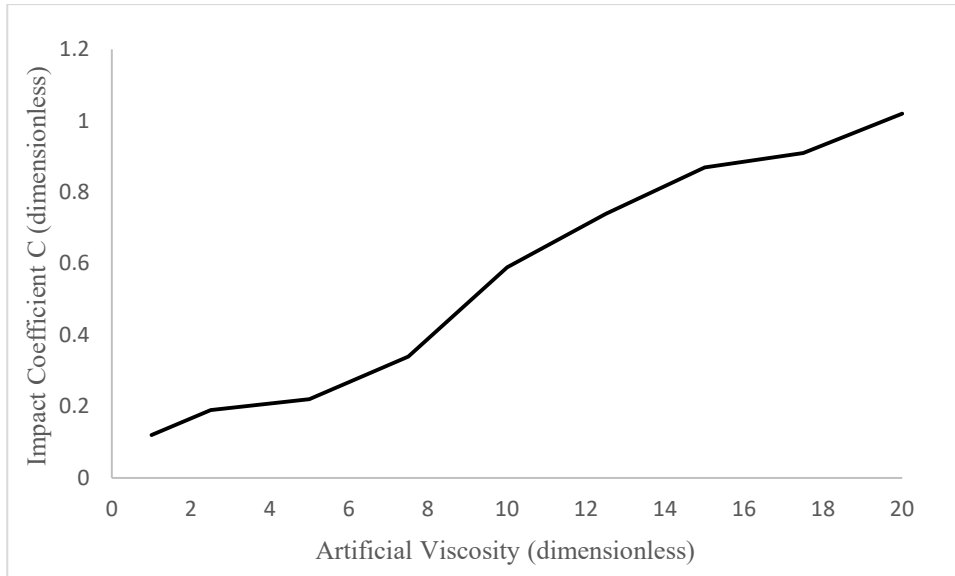


Figure 4. 4. b) Diagram of impact coefficient C versus artificial viscosity for the first series simulations (continued)

While it is evident in Figure 4.4b that the maximum value of impact coefficient C is less than 1.2 even the highest artificial viscosity value (20) is applied, according to the optimal impact coefficient value for mudflow type fluid in hydrodynamic model should be 2, meaning that the validation from only these data is insufficient even though these data provide useful information. As it is a real-life engineering simulation, not only the data comes out, the resolution is also essential to be considered which determines whether the realistic process of mudflows can be simulated. According to the post-processing tool, Paraview, which is suggested to use in DualSPHysics manual, the whole process of the simulation can be shown in Figure 4.5 below (three examples of the first series simulations). It is apparent that the distance between fluid particles is too large to present the real mudflows state under a higher artificial viscosity, such space between fluid particles results in separation phenomena in fluid, and the whole fluid cannot move uniformly, smoothly and continuously as shown in three figures of Figure 4.5. Most importantly, accompanying with the increasing value in artificial viscosity, the separation phenomena become more and more concerning (Figure 4.5b & 4.5c) which cannot guarantee the uniformity of the flow. On the contrary, even though a smaller artificial viscosity makes fluid flow a bit more liquid, uniform, continuous and smoother, the separation phenomena still exists and the interstice in fluid is evident as presented in Figure 4.5a. Besides, not only the fluid particles, the apparent spaces among boundary particles (the lines shown on the slope surface) are also cannot be ignored.

All of these could indicate the lower resolution in this series simulations, the value of $dp=0.125m$ is apparently not suitable for simulating mudflows and the results come out is inaccuracy under this condition. Therefore, the effect of changes in the particle distance (dp) for the whole simulation will be investigated in the following content.

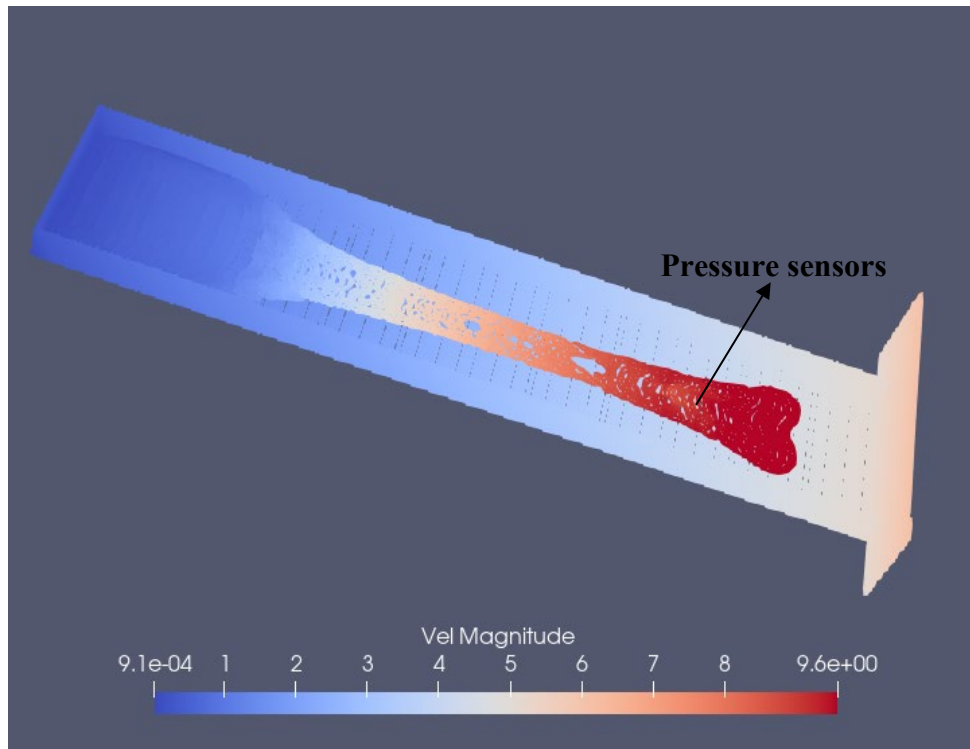


Figure 4. 5. a) The fluid behaviour when $d_p=0.125m$ with artificial viscosity=5

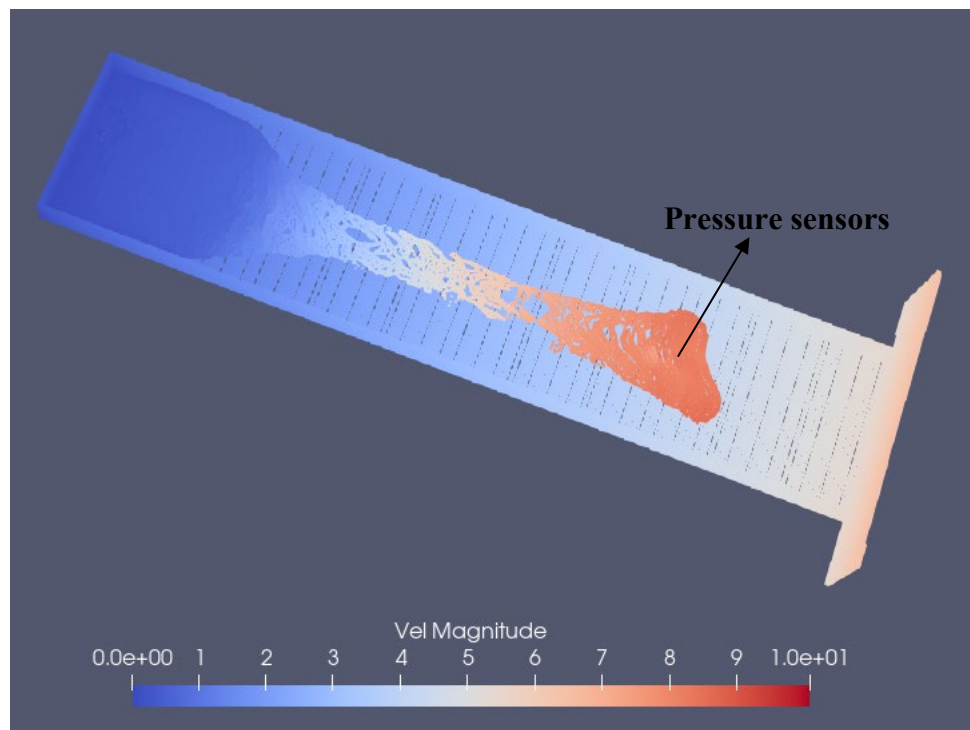


Figure 4. 5. b) The fluid behaviour when $d_p=0.125m$ with artificial viscosity=10

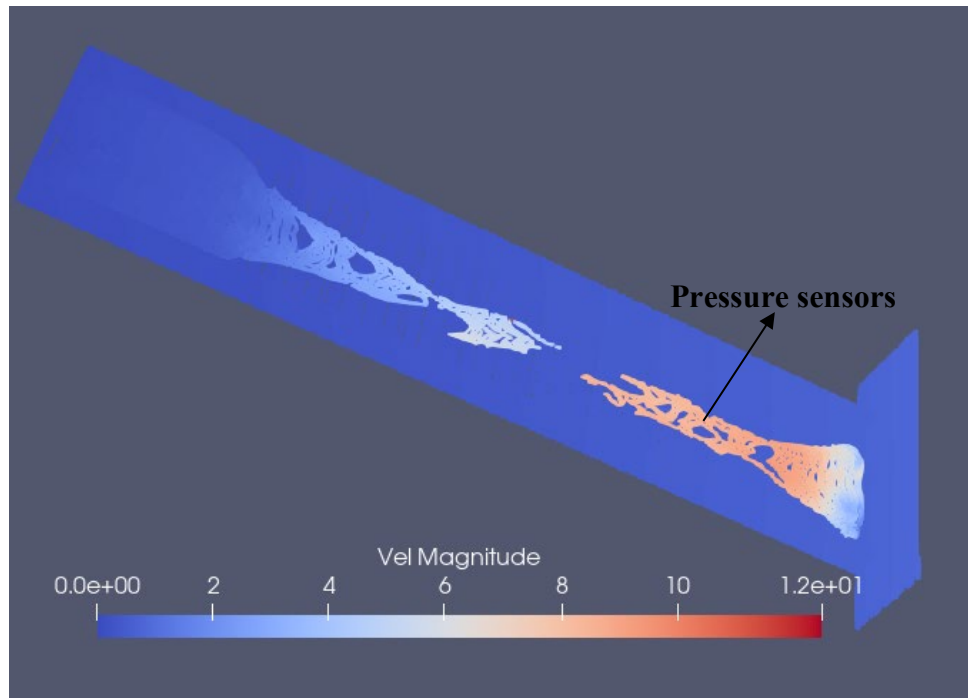


Figure 4. 5. c) The fluid behavior when $dp=0.125m$ with artificial viscosity=15 (continued)

4.4.2 Tests with changes in the value of dp

Based on the abovementioned observations in the first series simulations, considering the definition of dp in the documentation of DualSPHysics as well as the choice of parameter dp will influence the contribution of artificial viscosity which could further affect the flow velocity, impact pressure and impact coefficient C . Then, the second set of calibration tests are performed to observe the sensitivity of the simulations to changes in the value of single dp parameter and therefore, while the value of dp is chosen as the variable, remaining parameters are held constant. Same as the former simulations, density is still set to the value $1,850 \text{ kg/m}^3$. With regards to the artificial viscosity, according to the results and observations within the first series simulations, the value of 5 will be chosen which is not too small that leads to the fluid behavior just like the water and not too high which may result in the separation phenomena.

As was observed in the previous simulations, larger value of dp brings out the lower spatial resolution of mudflow simulation, combining with the interpretation of dp mentioned previously: increasing the spatial resolution by using smaller values of dp could improve the numerical model accuracy. Therefore, for the purpose of solving the spatial resolution issue and improve the accuracy of the whole simulation, the decreasing changes in the single parameter dp will be performed. In order to avoid the large fluctuation in the spatial resolution, the value of dp will be decreased gradually by $0.025m$ in each of the following test. Here, it is necessary to mention that a smaller value of dp (higher resolution) for the simulation will require more particles to be created which results in higher number of particle interactions to be calculated and therefore it is normal for DualSPHysics program to take more time to process the simulation. The input values for the Test A series in the second step of calibration tests with changes in the single dp parameter are shown in Table 4.3:

Test	The value of dp (m)	Density (kg/m ³)	Artificial viscosity
A	0.125 to 0.025 Reduction:0.025	1850	5

Table 4. 3. Values for the Test A series in the second step of calibration tests with changes in dp

The value chosen for the constant parameter like density is relative to the Bugnion et al. (2010) field tests which is assigned a realistic value to mudflows. The default value for artificial viscosity in DualSPHysics program being 0.01, which is for water, combining with the results from the first series simulation performed previously, the value of 5 that is a representative of a more viscous material than water such as debris flow. Hence, this value is assigned to artificial viscosity as the constant value in this series of simulations to observe the effect of changes in parameter dp on the impact coefficient C and resolution aspect. The results of the simulations with the abovementioned parameters can be observed in Figure 4.6 & 4.7 below:

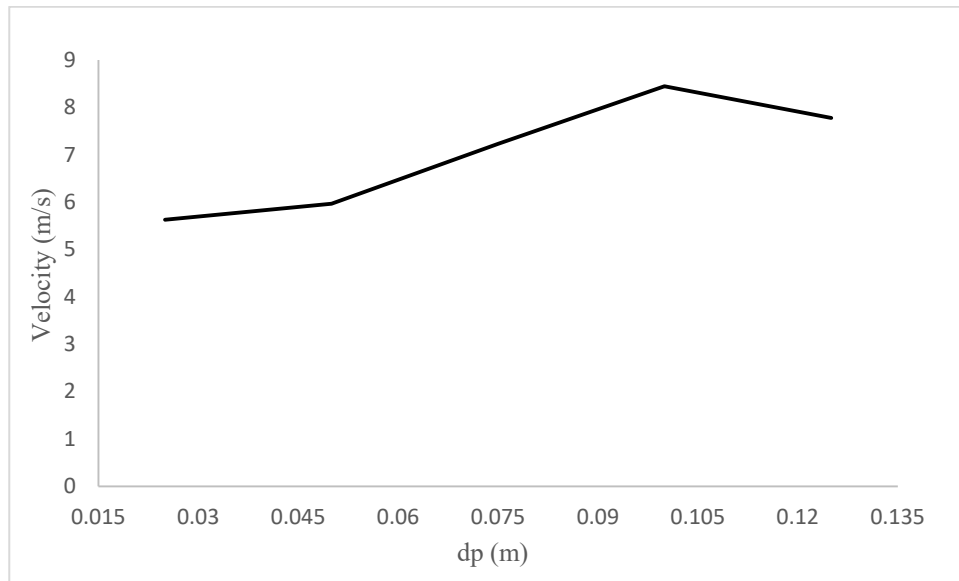


Figure 4. 6. a) Diagram of velocity versus dp for Test A

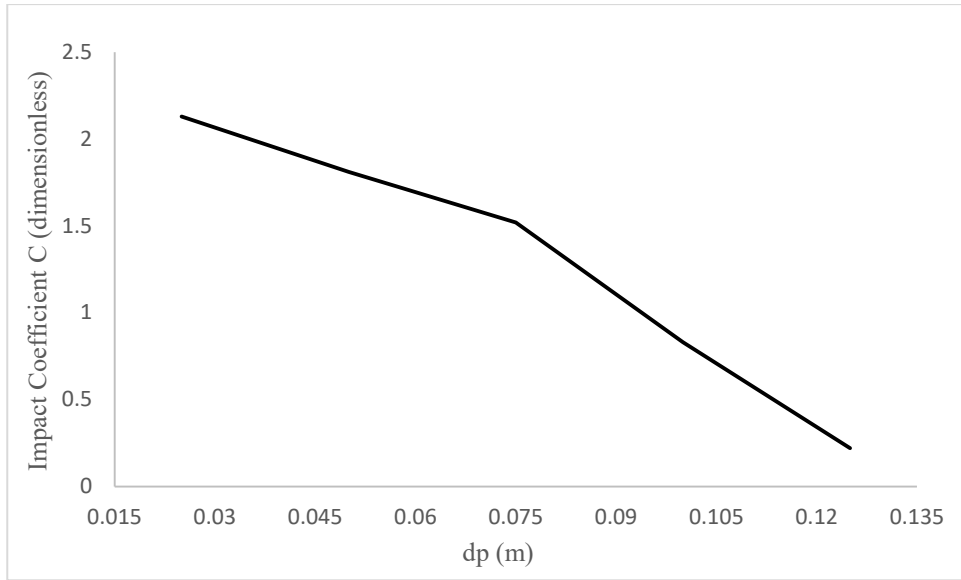


Figure 4. 6. b) Diagram of impact coefficient C versus dp for Test A (continued)

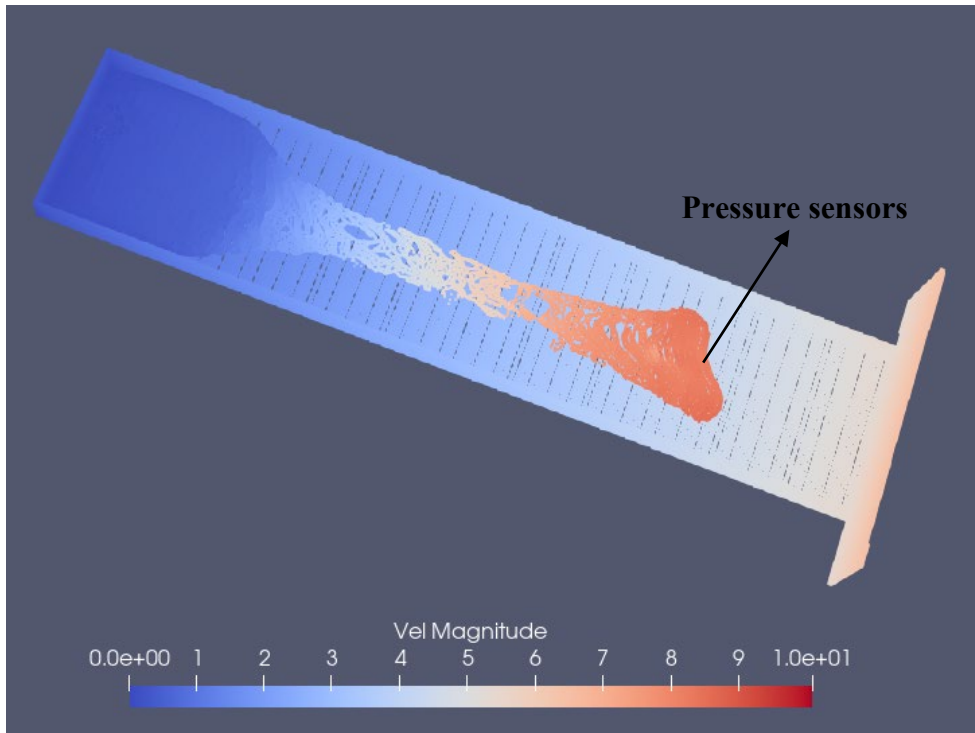


Figure 4. 7. a) The visualization snapshot with $dp=0.125m$ (the instant that the mudflow hits the pressure plate)

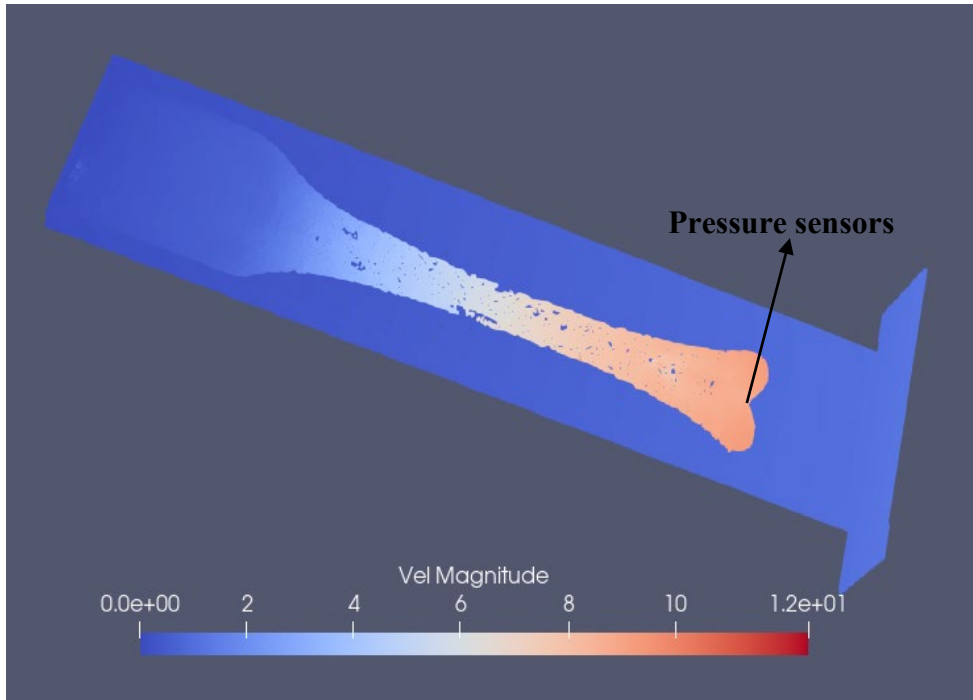


Figure 4. 7. b) The visualization snapshot with $dp=0.1m$ (the instant that the mudflow hits the pressure plate) (continued)

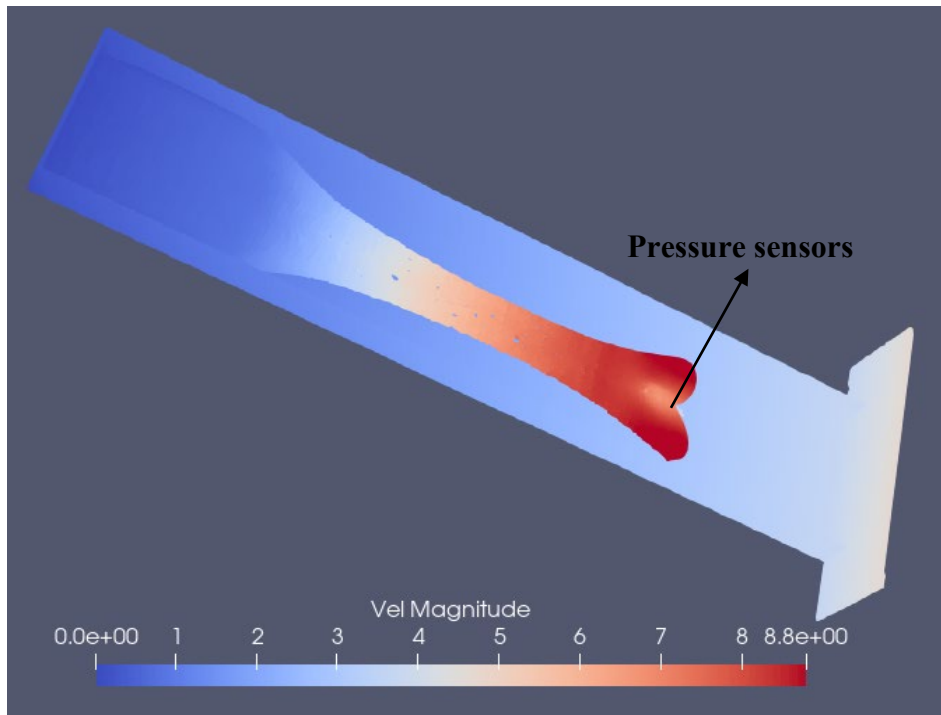


Figure 4. 7. c) The visualization snapshot with $dp=0.075m$ (the instant that the mudflow hits the pressure plate) (continued)

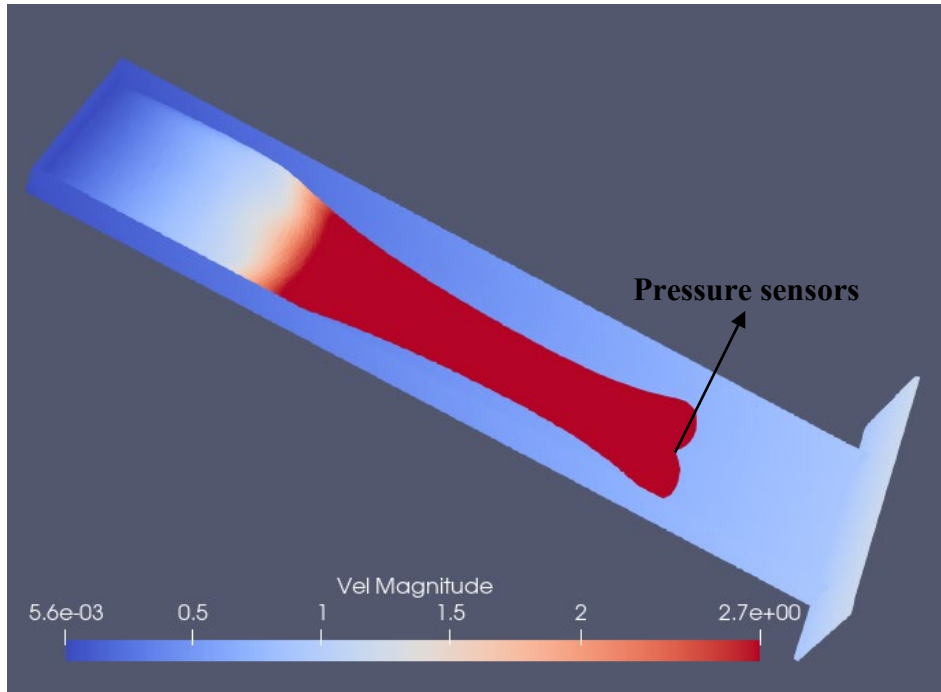


Figure 4. 7. d) The visualization snapshot with $dp=0.05m$ (the instant that the mudflow hits the pressure plate) (continued)

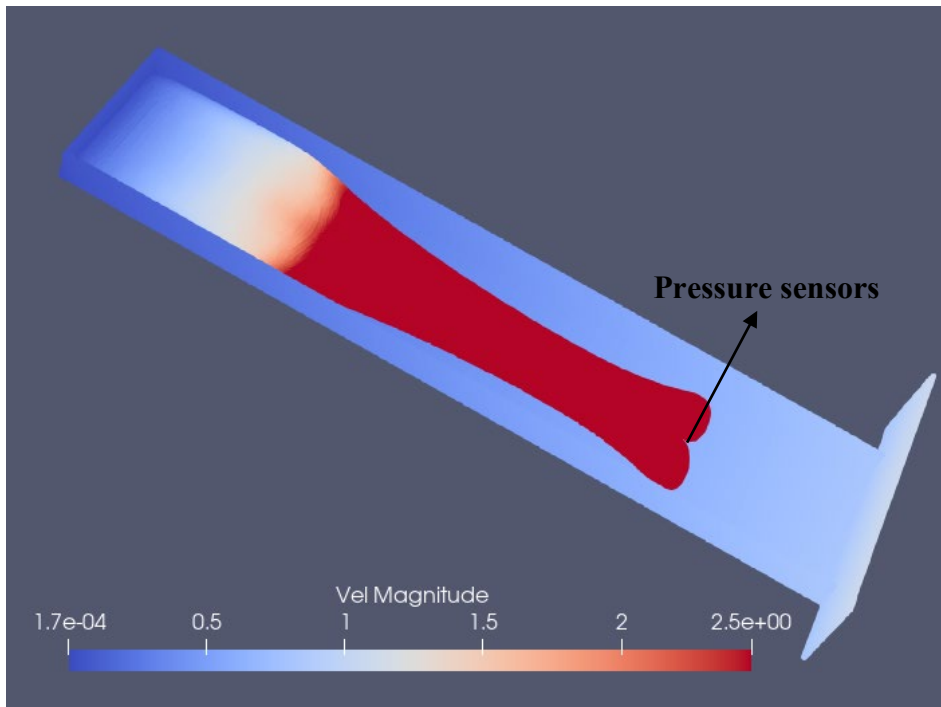


Figure 4. 7. e) The visualization snapshot with $dp=0.025m$ (the instant that the mudflow hits the pressure plate) (continued)

Owing to the setting of the entire model is exactly the same as that in experimental field test, the pressure plate indicated in Figure 4.3b ($A=0.04\text{m}^2$ and height equals 295mm) is often completely submerged when the debris flow hits it, which is the case most of the time as shown in Figure 4.7. Diagrams shown in Figure 4.6 present the results obtained in Test A, under which the artificial viscosity equals 5. The trend in the diagram (Figure 4.6b) presented showing that as the value of dp increases there is a decline in the impact coefficient C and a gradual increase in flow velocity (Figure 4.6a) in a positive linear manner. Conversely, there will be an increase in impact coefficient C and a decrease in fluid velocity by reducing the value of dp . One more interesting observation is, according to Figure 4.7, the visualized results of the simulations present a different effect when the different values are assigned to parameter dp : it is apparent that the whole resolution of the simulation becomes better with a smaller value of dp . With the rest of the parameters hold the constant, comparing to the simulation performed under the condition of dp equals 0.125m (Figure 4.7a), within the four other snapshots presented in Figure 4.7b to Figure 4.7e, it can clearly be seen that the interstice between fluid particles becomes smaller and smaller and even disappear (when dp is 0.05m) as the value of dp decreases, so did for the separation phenomena and the whole fluid becomes more uniform, viscous and continuous.

It is worth noting that the impact coefficient C at the condition of $dp=0.05\text{m}$ and $dp=0.025\text{m}$ is close to the value 2 which is the optimal impact coefficient value for the mudflow-fluid type in hydrodynamic model. The results shown in this series tests provide strong validation that: 1) the smaller values choice of dp is the crucial reason for getting the better spatial resolution (especially in animation aspect); 2) Along with the higher spatial resolution (smaller value of dp) implemented in the simulation, the whole numerical model could be improved which could present more realistic simulation effect with more accuracy results.

4.4.3 Tests with different combination set values

Having observed the effects of changes in each one of the parameters individually on the flow of mudflows, it could be concluded that the impact coefficient C will be larger by increasing the parameter artificial viscosity or reducing the value of dp and the better resolution with the more accuracy numerical results can be achieved by the smaller value of parameter dp . Since the final aim of the calibration test is to find out the optimal combination set values of artificial viscosity and dp to present the real-life mudflow process to maximum degree, hence, the purpose of this series of tests is to find the optimal combination values of artificial viscosity and dp applied in DualSPHysics to achieve the optimal impact coefficient value, thus ensuring that the fluid simulated in the model can be as close as possible to the actual mudflow process. In this part, the effect of the combination abovementioned parameters with different values will be performed, compared and observed. To obtain a result as the optimal combination values, the quantity of simulations is important. The more simulations are run the more accurate would the results be. On the other hand, time is a limiting factor for the quantity of the simulations. As it is previously mentioned, it would take DualSPHysics a great amount of time to simulate the flow of materials with characteristic like mudflows as a result of the higher values than water assigned to the parameters in the simulation tool. Therefore, in order to maintain the quantity and the quality of the tests as many as 36 tests were performed. The results details of the performed simulation are provided in the Table 4.8 below.

Owing to the d_p with the value of 0.125m is obviously not proper for simulating mudflows which has already been verified in the first series simulations, the value of $d_p=0.125m$ will not be applied in this series simulations and 0.1m will be the starting value assigned to d_p and still be reduced steadily by the decrements of 0.025m. For the artificial viscosity, the set of this parameter will be the same as the first series tests. The rest of the parameters have the same values as the previous test. The following tables show the input data performed in this part.

The input data for Test B:

Test	The value of d_p (m)	Density (kg/m^3)	Artificial viscosity
B	0.1	1850	1 to 20 Increments:2.5

Table 4. 4. Values for the Test B series under the condition of $d_p=0.1m$ and artificial viscosity from 1 to 20

The input data for Test C:

Test	The value of d_p (m)	Density (kg/m^3)	Artificial viscosity
C	0.075	1850	1 to 20 Increments:2.5

Table 4. 5. Values for the Test C series under the condition of $d_p=0.075m$ and artificial viscosity from 1 to 20

The input data for Test D:

Test	The value of d_p (m)	Density (kg/m^3)	Artificial viscosity
D	0.05	1850	1 to 20 Increments:2.5

Table 4. 6. Values for the Test D series under the condition of $d_p=0.05m$ and artificial viscosity from 1 to 20

The input data for Test E:

Test	The value of d_p (m)	Density (kg/m^3)	Artificial viscosity
E	0.025	1850	1 to 20 Increments:2.5

Table 4. 7. Values for the Test E series under the condition of $d_p=0.025m$ and artificial viscosity from 1 to 20

The results obtained from different tests are presented in Table 4.8 below:

Test	The value of dp (m)	Density (kg/m ³)	Artificial viscosity	Velocity (m/s)	Pressure (kPa)	Impact coefficient C
B	0.1	1850	1	11.64	138,356	0.55
	0.1	1850	2.5	9.02	87,626	0.58
	0.1	1850	5	8.45	110,6	0.83
	0.1	1850	7.5	7.77	11,561	1.03
	0.1	1850	10	7.60	106,856	1.08
	0.1	1850	12.5	7.80	112,554	1.07
	0.1	1850	15	7.55	105,454	1.12
	0.1	1850	17.5	6.82	86,048	1.46
	0.1	1850	20	7.38	100,759	1.53
C	0.075	1850	1	9.3	90,5	0.57
	0.075	1850	2.5	6.42	8,996	1.15
	0.075	1850	5	7.23	147,116	1.52
	0.075	1850	7.5	6.26	138,541	1.91
	0.075	1850	10	6.20	188,428	2.65
	0.075	1850	12.5	6.19	212,689	3.01
	0.075	1850	15	5.68	147,910	3.43
	0.075	1850	17.5	5.55	163,582	3.92
	0.075	1850	20	5.31	169,877	4.32
D	0.05	1850	1	8.76	178,875	1.26
	0.05	1850	2.5	7.43	16,47	1.63
	0.05	1850	5	5.97	119,295	1.81
	0.05	1850	7.5	5.52	144,210	2.25
	0.05	1850	10	5.38	138,151	2.58
	0.05	1850	12.5	5.24	141,214	2.78
	0.05	1850	15	5.01	150,450	3.24
	0.05	1850	17.5	4.89	162,351	3.67
	0.05	1850	20	4.68	162,483	4.01
E	0.025	1850	1	7.26	153,089	1.57
	0.025	1850	2.5	5.98	122,390	1.85
	0.025	1850	5	5.63	124,902	2.13
	0.025	1850	7.5	5.36	131,811	2.48
	0.025	1850	10	5.08	134,154	2.81
	0.025	1850	12.5	4.72	124,881	3.03
	0.025	1850	15	4.38	120,669	3.40
	0.025	1850	17.5	4.02	115,401	3.86
	0.025	1850	20	3.89	119,256	4.26

Table 4. 8. Results of the models simulated with different combinations of artificial viscosity and dp

Furthermore, not only requiring more accuracy the results, owing to it is a real-life engineering simulation, the resolution is also an essential aspect needs to be considered which determine

whether the real process of mudflow can be properly simulated. Therefore, some snapshots of the simulations process from different series tests are presented in Figure 4.8 as follows:

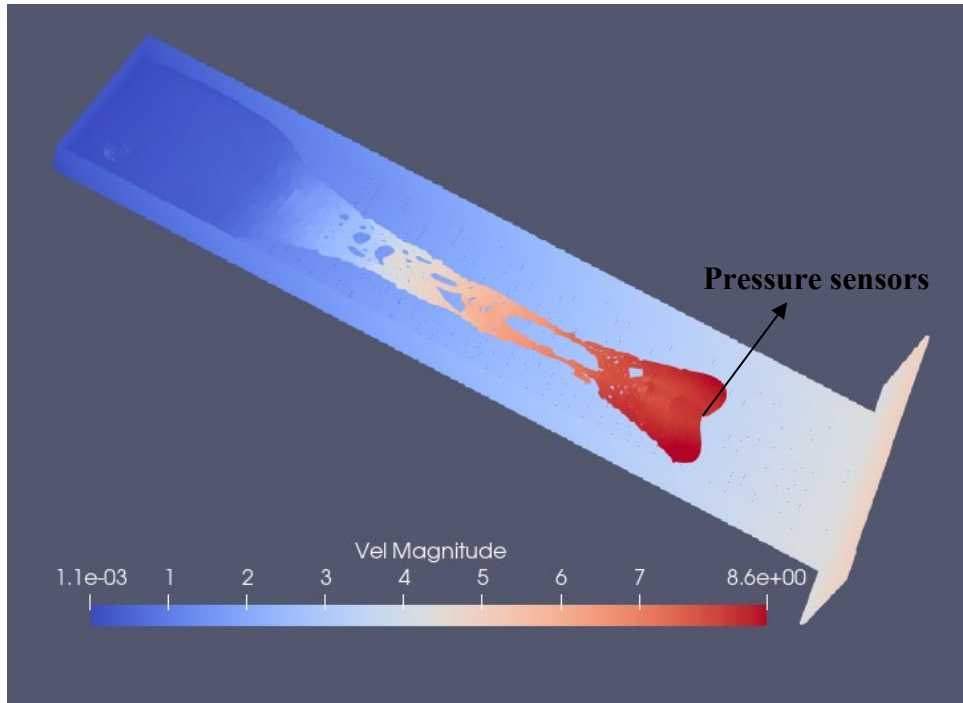


Figure 4. 8. a) Test B series with $d_p=0.1\text{m}$, artificial viscosity=15

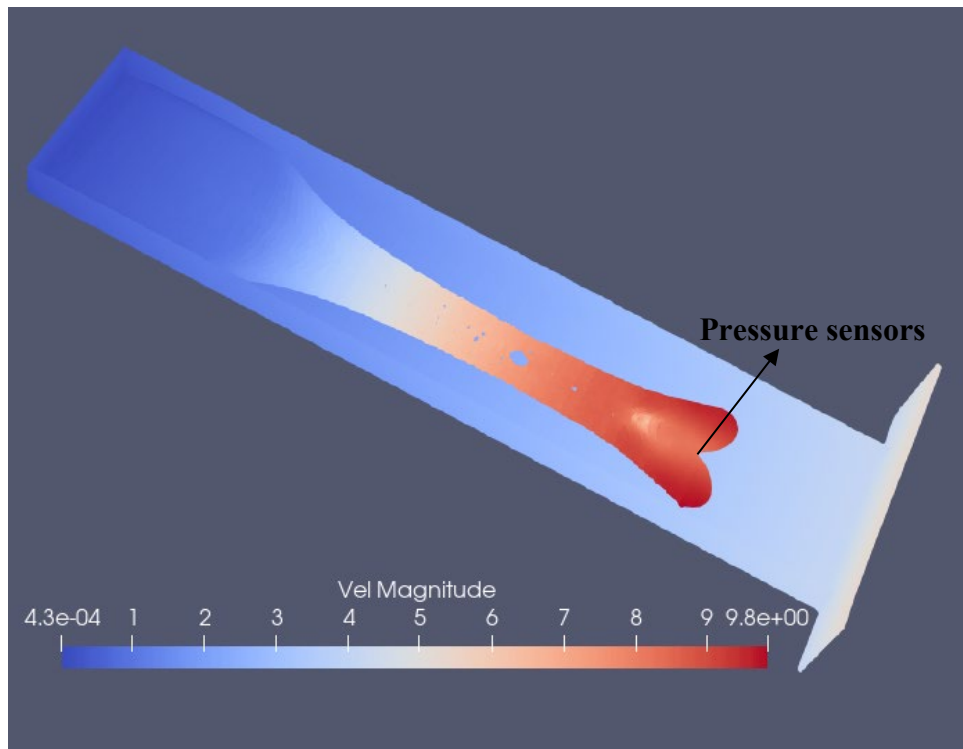


Figure 4. 8. b) Test C series with $d_p=0.075\text{m}$, artificial viscosity=7.5

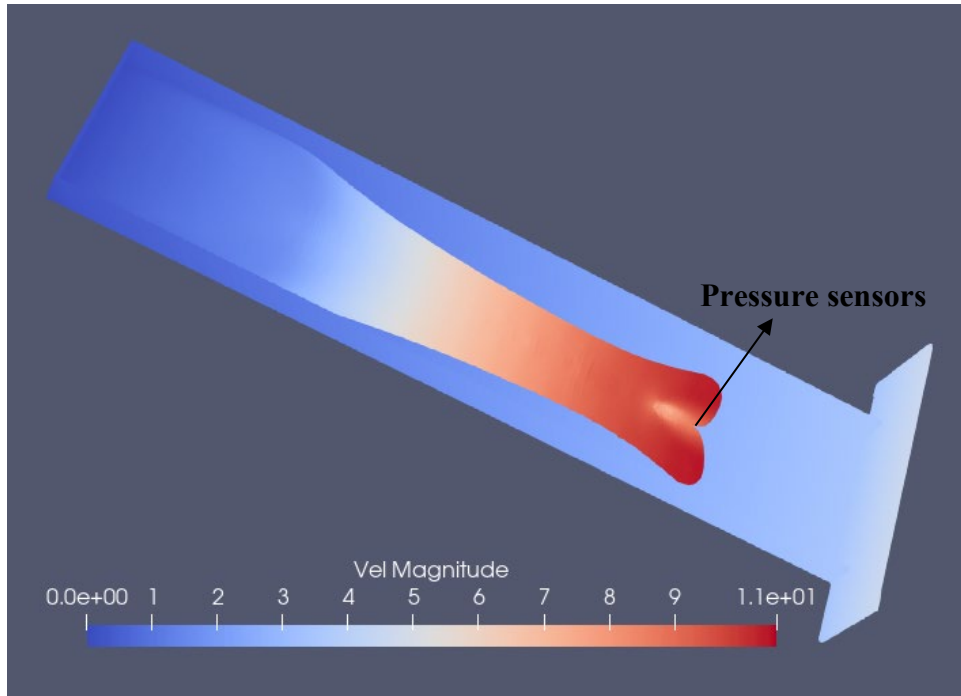


Figure 4. 8. c) Test D series with $dp=0.05m$, artificial viscosity=5 (continued)

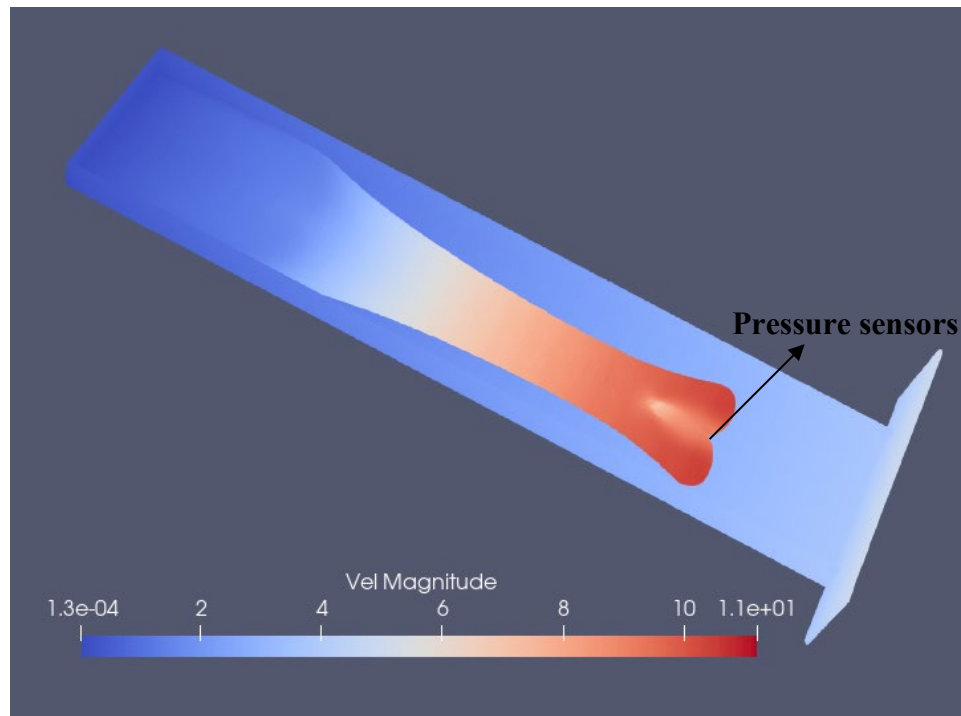


Figure 4. 8. d) Test E series with $dp=0.025m$, artificial viscosity=2.5 (continued)

After performing all these simulations as many as 36 tests, by comparing the results obtained and animation effect from different test series, four brief conclusions can be presented:

- For Test B series simulations, although the impact coefficient C increases along with the increasing in the artificial viscosity as predicted, the maximum impact coefficient value under the maximum artificial viscosity (20) is 1.53 which is less than 2. Moreover, for all simulations within Test B, the visible voids between fluid particles always exists, this leads to the fluid discontinuities. The visible gap evidently increases as the artificial viscosity increases to 15 (Figure 4.8a) or greater than 15 which directly results in separation phenomena (same as shown in Figure 4.5c). The fluid breaks up from middle and is divided into two parts, only a small portion of the fluid slides to the bottom of the slope due to gravity and the rest stand still due to excessive artificial viscosity. This shows that using excessive values of artificial viscosity coefficient lead to low diffusivity.
- Comparing to Test B series simulations, when a smaller value of dp is applied (0.075m) in simulation of Test C, the void spacing issue among fluid particles can be improved but still exists (Figure 4.8b) and the same problem occurs like that in the simulations of Test B when the value of artificial viscosity is more than 15. And in this series of simulations, the closest value around 2 (the optimal impact coefficient) shows up (1.91) when artificial viscosity equals 7.5, another one equals 2.65 when artificial viscosity is 10. From the data presented in Table 4.8, the increment in the impact coefficient of Test C is larger than that in Test B.
- Same as the trend happens in the former two series simulations, Test D series simulations experienced the same process: the impact coefficient increases as the artificial viscosity becomes larger. Surprisingly, the spatial resolution issue disappeared in this series test and the fluid simulated by DualSPHysics is uniform, smooth and continuous (Figure 4.8c), the whole behavior of the fluid just like the mudflow occurs in real-life. And within this series, the value closest to 2 is 1.81 in case of artificial viscosity equals 5, another one equals 2.25 under the condition of artificial viscosity is 7.5.
- The Test E series simulations show similar results (Figure 4.8d) to Test D, the value of the impact coefficient closest to 2 in Test E is 1.85 as artificial viscosity equals 2.5, and the other is 2.13 under the condition of artificial viscosity is 5. But in terms of the operation time, it takes five times longer than Test D.

Comparing the results (presented in Table 4.8) and observations (shown in Figure 4.8) obtained from the different series simulations, it is observed that the artificial viscosity value greater than 15 should not be considered for mudflow simulation in DualSPHysics. Moreover, when dp equals to 0.05m with artificial viscosity ranges from 5 to 7.5, or $dp=0.025m$ with artificial viscosity ranges from 2.5 to 5, the whole resolution of the model simulated becomes better and the value of C is closer to 2, meaning the simulated fluid in the model is closer to mudflow-fluid type. The details of the model simulated under these two conditions are shown below:

The value of dp (m)	Fluid particles	Boundary particles	Computational time (second)	Artificial viscosity	Impact coefficient C
0.05	401,703	305,716	3600	5	1.81
				7.5	2.25
0.025	1,482,662	3,239,276	21,600	2.5	1.85
				5	2.13

Table 4. 9. Models simulated with different combinations of artificial viscosity and dp

It is observed that although the smaller value of dp can have a higher resolution and more accurate results, as it is previously mentioned, it would generate more particles and take DualSPHysics a great amount of time to simulate. For example, there are 305,716 boundary particles and 401,703 fluid particles generated under the condition of $dp=0.05m$, whereas, when dp equals to $0.025m$ which ultimately makes 3,239,276 of fluid particles and 1,482,662 of boundary particles. This will take DualSPHysics around 6 hours to run each simulation when $dp=0.025m$, while one hour will be required for dp equals to $0.05m$ under the same condition. Furthermore, it is worth mentioning that, there is no large differences from these two series simulations (Test D & E), no matter on the results obtained or on the spatial resolution (visual simulation shown in Figure 4.8). Therefore, considering the point that having the highly efficiency, lower cost (less time) as well as assuring the whole quality and accuracy of the simulation at the same time, the value of dp equals to $0.05m$ will be the optimal choice for the resolution of mudflow simulation, and the artificial viscosity should be between 5 and 7.5 (the impact coefficient from 1.81 to 2.25).

Since the optimal impact coefficient C is 2 for mudflow-fluid type in hydrodynamic model as discussed previously and the two closest results obtained now in the calibration tests is 1.81 and 2.25, respectively. Hence, in order to gain a more accurate result, a few simulations will be further performed between 5 and 7.5 of the artificial viscosity in case of $dp=0.05m$. In the previous series of simulations, the increment of the artificial viscosity was in unit of 2.5. The smaller increment will be adopted: set in unit of 0.5. The input data applied in DualSPHysics are presented as follows:

Test	The value of dp (m)	Density (kg/m^3)	Artificial viscosity
F	0.05	1850	5
	0.05	1850	5.5
	0.05	1850	6.0
	0.05	1850	6.5
	0.05	1850	7
	0.05	1850	7.5

Table 4. 10. Values for the Test F series under the condition of $dp=0.05m$ and artificial viscosity from 5 to 7.5

And the results are obtained in Table 4.11 below:

Test	The value of dp (m)	Density (kg/m ³)	Artificial viscosity	Velocity (m/s)	Pressure (kPa)	Impact Coefficient C
F	0.05	1850	5.0	5.97	119,295	1.81
	0.05	1850	5.5	5.92	130,507	1.84
	0.05	1850	6.0	5.76	126,070	2.05
	0.05	1850	6.5	5.65	123,566	2.09
	0.05	1850	7.0	5.56	120,276	2.10
	0.05	1850	7.5	5.52	144,210	2.25

Table 4. 11. Results from the Test F series under the condition of dp=0.05m and artificial viscosity from 5 to 7.5

Since the visualization of simulations performed with different values of artificial viscosity in this series as the same as shown in Figure 4.8c (when artificial viscosity equals to 5), hence, the snapshots will be not presented. Comparing to the Test D series, as expected, as the interval value of artificial viscosity is narrowed, the obtained impact coefficient values are getting closer to 2. When the artificial viscosity applied is 6, the closest value to the desired impact coefficient C (2) is obtained, that is, C=2.05.

Therefore, according to all simulations performed previously (Test 1- 9 & Test A-F), the optimal combination values utilized in DualSPHysics to represent the real-life mudflow process appears when dp equals to 0.05m and the value of 6 assigned to artificial viscosity. This combination set of values is not too high that there is no need to take so much time for the program to process each simulation and it was not too low which can serve the goal of simulation correctly and vividly which implies the fact that DualSPHysics performed the desired simulation for the aforementioned set of values and the DualSPHysics program can well perform the real-life engineering simulation.

Chapter Five: Parametric Model Studies and Interpretation of Result of Mudflows Impacting Trains

5.1 Introduction

According to previous studies mentioned in the literature review chapter, the geomorphic phenomenon of mudflows triggered by heavy rainfall on natural or man-made hillslope are prone to occur in Ottawa Valley and St. Lawrence Lowlands in Canada. Owing to the particular terrain comprised of Champlain (Leda) clays (fine-grained sediments) are the core composition of mudflows. Hence, it is quite possible that railway tracks that traverse these areas would be affected by mudflows. In order to observe the danger posed by mudflows on railway infrastructure, the investigation of the impact force exerted by a mudflow on the railway cars is important. In the field of solving practical engineering problems, impact forces exerted by gravitational flows against obstacles have been the subject of many experimental investigations, where these experimental tests refer to field measurements or laboratory experiments. With recent developments of coupling a fluid flow model with rigid body dynamics, it is possible to examine the interaction of fluid flow with solid objects by using a simulation tool instead of measurements on site or in the laboratory. Model calibration was performed in the preceding chapter, demonstrating that the capacity of the chosen simulation tool (DualSPHysics) based on SPH. It was used to model a situation in which a relatively viscous fluid flows down, as a result of gravitational acceleration, from a stationary position. The calibration study also provided the information on how the changes in fluid parameters in the simulation tool affect the outcome and therefore, paved the way for implementation of the case studies' environment and the properties of the mudflow in the simulation tool in order to be modeled. Therefore, on basis of that, the scenarios of a mudflow impacting railway cars could be simulated by DualSPHysics and the potential destructive power exerted on trains could be computed. Furthermore, by performing parametric model studies, it could be envisioned that the effect of parameters describing fluid properties and terrain geometry on mudflow's behavior and its corresponding destructive power could be observed and analyzed.

The following sections provide a detailed description of the modeling studies and the evaluation of potential danger that a mudflow pose on trains. The necessary considerations in modeling implementation are considered first, followed by an account of scene creation and assignment of key parameters, and concluded by the interpretation of results.

5.2 Considerations in Model Implementation

To create models akin to the physical experiment as possible, and analyzing the effect of slope and embankment geometry on the impact force generated by the mudflow, some key parameters had to be implemented in the modeling tool as precisely as possible, as they would greatly influence the outcome of the simulation. These parameters relate to the terrain of hillslope, railway embankment and mudflow material properties. The parameters describing the terrain environment as presented below, in Figure 5.1, where H_1 is the height of the hillslope, α is the hillslope inclination, D represents the buffer distance from the toe of hillslope to that of the railway embankment, the slope ratio of railway embankment H:V (horizontal:vertical, that is, $\cot \beta$), the railway embankment height H_2 , and the terrain roughness n .

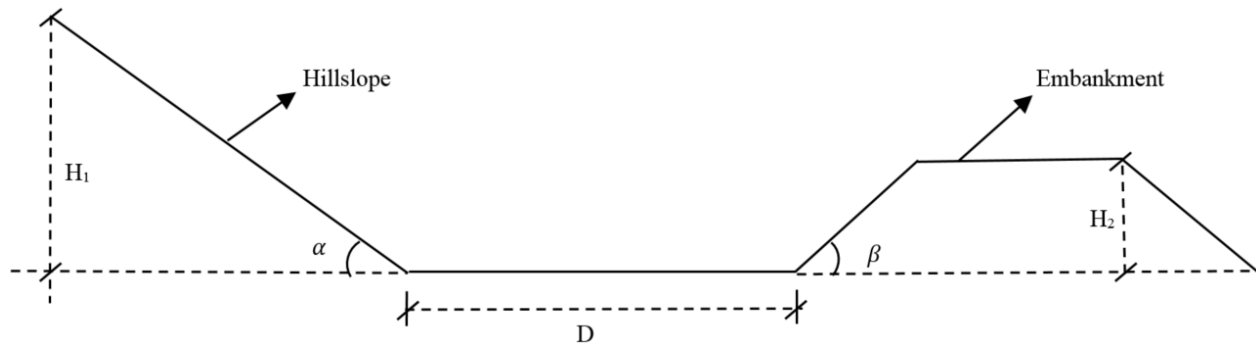


Figure 5. 1. The sketch of the terrain environment in the model

5.2.1 The hillslope terrain

In case of a mudflow impacting railcars, the terrain of a hillslope plays an important role. The characteristics of the terrain influence the manner in which the mudflow run out and advance. The aspects on which the terrain can have influence include the velocity at which the mudflow travel, the direction of flow, the run-out distance and the area the mudflow cover both lengthwise and breadthwise. Among of these aspects, the flow velocity directly determines the impact force generated by the mudflow according to the previously explained Hydrodynamic Model (Eq. 3.2) in Chapter 3. While, the flow's velocity primarily depends on the hillslope inclination and terrain roughness based on Manning's Equation (Eq. 3.8). Generally, parameters describing a natural hillslope, including slope angle and terrain roughness, are a constant which is normal and cannot be easily changed by human activities. This is the limitation for large-scale field experiments that can only be performed in existing conditions, also for laboratory experiments that cannot reproduce the natural terrain environment exactly. Compared to this, the advantages of simulations by a simulation tool are obvious, which can artificially regulate the data that cannot be easily changed in nature (like slope angle) while ensuring the authenticity of the simulation so that its effect on numerical results can be analyzed. Thus, compared to field observations and laboratory experiments, in a numerical simulation study, the effect of hillslope terrain on the impact force exerted by the mudflow on a railcar could be easily observed by changing the slope angle α or its corresponding terrain roughness n .

5.2.2 The railway embankment

In the model studies, not only the slope of a terrain, but the railway embankment also influences the impact force exerted on a railcar. Similar to a terrain's roughness, the embankment's surface roughness will influence the mudflow velocity in the same way. What is different is that during a mudflow impacting a railway embankment, the flow ascends on the embankment instead of flowing downward on the hillside. In addition to the influence of railway embankment surface roughness, the gravitational acceleration also plays a role in resisting the rise of the mudflow. Thus, under such circumstance, the smaller impact force of the mudflow generated by decelerating the flow speed by introducing rather steep embankment slopes. Moreover, the embankment height is another parameter that should be taken into account, when embankments are constructed too low, the mudflow will easily threaten rail vehicles, that's the reason that embankment height H_2 is one of the key factors to reduce or avoid the destructive force of mudflows.

5.2.3 The buffer plane

It is worth noting that the buffer distance D (shown in Figure 5.1) between the bottom of the hillslope and the railway embankment parallel to the ground surface cannot be ignored. This distance D can be constructed when establishing a railway embankment, which is another one of the key parameters that can be artificially controlled in railway engineering to decelerate mudflows, and to further reduce or avoid the destructive force of the mudflow. For that reason, regarding the amount of buffer distance, under the same roughness condition, if the distance is too short, the deceleration effect on mudflows is small so that the mudflow could easily wash up on the railway embankment and impacts the trains. On the contrary, the mudflow perhaps cannot reach the toe of embankment if buffer distance is long enough, thereby achieving the purpose of ensuring the safety of trains on top of the railway embankment.

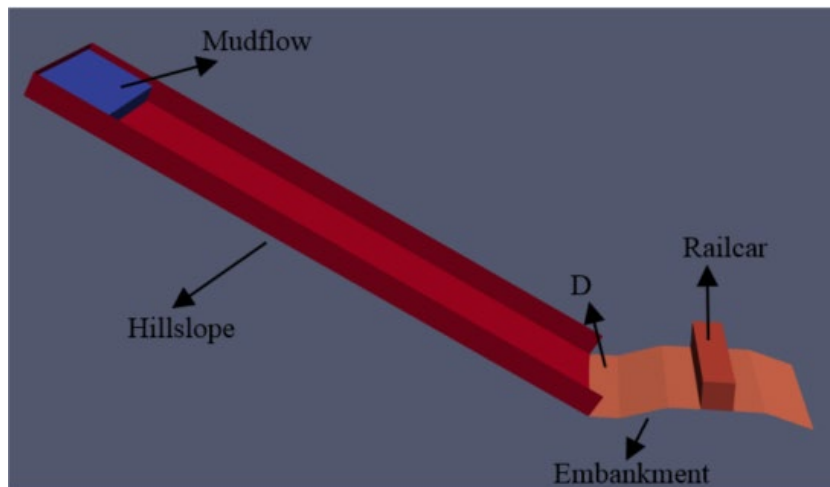


Figure 5. 2. The components of model created in DualSPHysics

5.2.4 Mudflow material properties

As seen in the calibration studies, the mudflow material properties are among the factors adopted in DualSPHysics that most affect the simulations. The impact force, which the mudflow exert on a train, apart from the effects of the terrain, as stated in key parametric studies of Chapter 3, depends on parameters such as the viscosity, density and volume of the mudflow. Moreover, the shape, the state and the uniformity of the flow could be controlled by assigning various values to these factors representing the properties of mudflow within the simulation tool.

The detailed information regarding creation of the model, the environment of each of the parametric model studies and the results of the simulations are presented and discussed in the following sections.

5.3 Model Parameters and Model Set-up

The aim of the model study is to investigate the effect of the abovementioned parameters on a mudflow's impact force and how their effect will affect the flow behavior and its destructive power. Furthermore, perhaps an insight will be gained toward the usefulness of mitigation measures to reduce the destructive power of mudflow, based on the observations obtained. To achieve this goal,

the model studies will be performed using the *Control Variable* method, meaning that the value of one of the afore considered factors needs to be separately varied and the values for the rest of parameters are taken as constant. By this way, as the variable parameter changes, its effect on the impact force could be observed, compared and analyzed. Hence, several series of tests will be performed in this study.

This section presents the input data of different test series regarding modeling the scene of a mudflow hitting a railway car to be implemented in the simulation tool DualSPHysics.

5.3.1 Parameters describing terrain geometry

The terrain created in this model study is mainly composed of three parts: hillslope, railway embankment and the buffer plane D between them, as shown in Figure 5.1. Being the factors affecting the impact force of mudflow in this model studies, as described above, the parameters describing the terrain geometry will be considered as variable, here, five variables as shown in Figure 5.1 (hillslope inclination α , terrain roughness n , railway embankment height H_2 , slope ratio of railway embankment H:V, and buffer distance D) will be separately changed in turn by following various subsets tests to observe their effect on the impact force generated by mudflow:

- In terms of hillslope inclination α , as the study area is located in the Ottawa Valley area of Canada, according to a manual regarding stability of natural slopes in the Ottawa area (Slope Stability Guidelines for Development Applications 2001), any land which is sloped or inclined more steeply than about 11 degrees from horizontal (5 horizontal to 1 vertical) has the potential for instability. This “stable slope allowance” is simplistically and generally conservatively calculated based on a projection up from the slope toe level at 5 horizontal to 1 vertical unit (11 degrees) for soils comprised of Champlain Sea clays. Therefore, considering that, in order for the terrain simulated to maximally resemble the natural one and for accuracy of the model simulation, the value of 10 degrees could be assigned to hillslope inclination. In addition, since the calibration test performed by DualSPHysics has successfully reproduced a real-world large-field experiment conducted by Bugnion et al. (2010), hence, this experimental investigation references the terrain environment settings (including terrain roughness) adopted in the simulation tool in the calibration test. Therefore, a hillslope with 41-m-long, 8-m-wide and slope inclination of 10° degree is employed in the first series test: Set I . On basis of that, in subsequent tests, with the aim of further analyzing the effect of changes in slope inclination on the impact force, different values of hillslope angle should be employed. Referring to various experiments performed by other authors which refer to lab or large-scale field mudflow flume test, showing that the most used slope inclination values for experimental investigation range around 10°~ 30°. For example, Cui et al. (2015) carried out 27 laboratory debris flow flume tests to analyze the impact force of viscous debris flow where the considered slope ranges were between 10°~ 15°; Iverson et al. (2010) performed 28 controlled large field experiments with a flume bed slopes uniformly at 31°, comparable to the angles of many debris-flow initiation sites (Iverson et al. 1997); Bugnion et al. (2010) successfully carried out large-scale field test to measure debris flow impact pressure under the condition of 30° slope. Therefore, the inclination values α from 10° to 30° in increments of 10 degrees will be separately adopted to observe the effect of hillslope inclination on the impact force. While the slope length is a constant and height H_1 would be changed by changing the slope angle.

- Concerning the terrain roughness n , the parameter related to terrain roughness in the simulation tool DualSPHysics is `ViscoBoundFactor`, which is a dimensionless coefficient and is only available for artificial viscosity. As stated in the section 4.2 of Chapter 4, the parameter of artificial viscosity represents the energy dissipation between the fluid particles in DualSPHysics, correspondingly, there is a parameter that represents the energy dissipation as the fluid particles interact with boundary particles, which is based on the artificial viscosity and introduced by a coefficient named `ViscoBoundFactor`. Since the natural hillslope terrain condition in this experimental investigation references that of the large field test conducted by Bugnion et al. (2010) and has been calibrated, hence, the parameter describing terrain roughness in the simulation tool is adopted as same as that in calibration test, with the value equal to 0.025. In the following model studies, assuming the terrain roughness of the terrain includes natural hillslope, railway embankment, and buffer distance D have the same value.

As mentioned previously, apart from hillslope inclination, terrain roughness is another key component of hillslope terrain which can affect the mudflow's destructive power. To observe the effect of terrain roughness on mudflow, the corresponding parameter adopted in the simulation tool should be varied. Regarding the terrain environment employed in Set I (`ViscoBoundFactor` equals 0.025) as a reference, values of 0.0125 (half of 0.025) and 0.05 (double of 0.025) are assigned to terrain roughness respectively as a comparison to observe their effect on the impact force.

- Like before, as the factors that can be built and controlled artificially in railway engineering, the optimal railway embankment height H_2 (as shown in Figure 5.1) and slope ratio (H:V) need to be investigated in order to achieve the goal of reducing or avoiding the destructive force of mudflows while assuring the optimize cost of construction. According to the information provided in parametric studies of Chapter 3, the slope ratio of railway embankment is normally either 2H:1V or 3H:1V (horizontal to vertical) in the North American practice. Thus, these two values are assumed as the railway embankment slope ratio, and values of 1m, 2m, 3m, and 4m for railway embankment height H_2 would be adopted separately under these two slope ratios to observe their effect on the impact force.
- The buffer distance D between the bottom of slope and railway embankment, as another factor that could be artificially constructed to serve the purpose of protecting railway infrastructure and trains, its effect on reducing the impact force produced worth considering. In accordance with the key parametric studies in Chapter 3, values of 1m, 2m, 4m, and 6m would be assigned to it to investigate its effect on impact force, and the condition under which the mudflows would not affect operations of the train on top of the railway embankment could be observed.

5.3.2 Parameters describing mudflow

Although the default values of parameters like artificial viscosity and fluid density in DualSPHysics cannot reproduce a mudflow, as it was reported in the model calibration section, the values assigned to these parameters that can represent a mudflow and flow behavior have been calibrated, which would be applied in this experimental investigation.

Theoretically, in accordance with the Manning's Equation and hydrodynamic model stated in parametric studies of Chapter 3, the flow depth has a positive correlation with the flow speed,

meaning a higher flow (a larger volume) causes a larger velocity, further leads to a greater impact force. On basis of that, considering the effect of the mudflow depth on its corresponding destructive power, as a comparison, different volumes of mudflow (50m^3 , 75m^3 and 100m^3) are adopted in the simulation tool by increasing the depth of mudflow to perform the investigation.

5.3.3 Modelling experiments of a mudflow impacting trains

In accordance with the information provided in the former sections, there would be six variable parameters with different values in this experimental investigation as summarized in Table 5.1 below, which need to be separately investigated for its effect on the impact force generated by a mudflow on a railway car:

Slope inclination α ($^\circ$)	Buffer distance D (m)	Railway embankment height H_2 (m)	Slope ratio of railway embankment (H:V)	Volume of mudflow (m^3)	Terrain roughness (ViscoBoundFactor)
10, 20, 30	1, 2, 4, 6	1, 2, 3, 4	2:1, 3:1	50, 75, 100	0.0125, 0.025, 0.05

Table 5. 1. The values of parameters in the numerical investigation

Within this numerical investigation, to serve the purpose of finding the effect of changes in the individual parameter on the result of the tests, that is, the effect of these changes, such as increases in the value of hillslope inclination α , on the destructive force exerted by the mudflow on railway cars whether the value increases or decreases can be studied and analyzed, the *Control Variable* method was applied to investigate model parameters. The abovementioned parameters describing terrain environment and properties of the mudflow would be changed individually in the simulation tool. The values assigned to density of the mudflow ($1,850 \text{ kg/m}^3$) and the parameters of artificial viscosity (6) and initial particles distance d_p (0.05m) in the simulation tool have a mudflow-like characteristic, which have been calibrated in the calibration section of Chapter 4 and are remain the same during the analysis.

Therefore, five different sets of simulations were studied with the aid of DualSPHysics software to achieve the goal of finding the effect of changes in the individual parameters aforementioned on the result of the tests and under what conditions (slope geometry, embankment geometry, mudflow volume, etc.) the train derailment occurs:

1. Set I investigated the effect of changes in buffer distance D and railway embankment height (H_2) on the impact force exerted on railway cars.
2. Considering the influence of natural hillslope environment, as a further step based on Set I, the models performed in Set II consider not only the buffer distance D and railway embankment height H_2 , but also hillslope inclination α , that is, each case simulated in Set I is investigated under different natural hillslope inclination α in Set II.
3. Apart from the steepness of hillslope α , the slope ratio of railway embankment H:V also influences the impact force exerted on trains. Since the railway embankment is constructed in the slope ratio of either 2H:1V or 3H:1V in the North American practice

as stated previously, the slope ratio of railway embankment H:V is studied on top of the Set II and forms simulations of Set III.

4. For the experimental test: Set IV, with the aim of investigating the relationship between the volume of mudflow and its corresponding destructive power, the volume of mudflow V released is regarded as the variable parameter.
5. Terrain roughness is another factor related to the natural terrain on which the mudflow is running on. Considering its deceleration effect on mudflow's movement, terrain roughness n will be considered in the Set V.

The input data of each case are presented in detail in the next section. Each set is interpreted from the following aspects: a) grouping for parametric study; b) interpretation of simulation results; c) discussion of results. It is worth noting that, within all tests, one cube-shaped object is simulated on the railway embankment's top surface which is parallel the ground surface. As stated in section 2.2.4.3 previously, selecting a range of boundary particles within model, for this research, the cube-shaped object on top of the railway embankment are selected, at the instant of this solid object is impacted by a mudflow (fluid particles), the force exerted by the fluid onto a boundary object, the corresponding impact force exerted by a mudflow on a solid object could be computed by the simulation tool DualSPHysics by solving the particle interactions with fluid neighboring particles. As stated previously in Chapter 3 of key parametric studies, considering the case of train derailment, not only the impact force, but it is also necessary to take the weight of the train into account, which generates vertical wheel-rail force. Regarding the circumstances that a train can derail, as discussed in section 2.3.5 of literature review of Chapter 2, the critical derailment coefficient Q/P (Nadal 1896) could be the judgement criteria, where Q represents the transverse force exerted on railway cars which is the impact force generated by mudflows and P is vertical wheel-rail force. Normally, the standards of the critical derailment coefficient for derailment prevention are different in various countries and the value of Q/P less than 1.0 is set in North America (Xiang and Zeng 2005). Thus, it is not difficult to infer that the train derailment occurs when the critical derailment coefficient larger than 1.0 ($Q/P \geq 1.0$). Based on the key parametric studies performed in Chapter 3, it could be assumed in this model studies that, when the impact force Q exerted by mudflows on the simulated cuboid object is more than 1293600 N ($Q \geq 1293.6$ kN), train derailment occurs. Therefore, in this investigation, comparing the impact force obtained under different cases by simulation tool to the critical value of train derailment $Q=1293.6$ kN, and then the case of train derailment and the corresponding conditions (e.g., slope geometry, embankment geometry, and mudflow volume) could be investigated.

5.4 Results and Discussions

The following sections present the results of the impact force obtained from the model studies of mudflows impacting a railway car on top of a railway embankment under different circumstances. Five sets of simulations were performed with the values assigned to the parameters representing terrains and mudflows differing from model to model, as discussed in the preceding section. The details of values assigned to each parameter in each case are presented in the following tables and the following diagrams presented are the results of five sets simulations performed in DualSPHysics.

5.4.1 The effect of buffer distance D and railway embankment height H₂ (Set I)

The tests in Set I are implemented using the variable parameter of buffer distance D and railway embankment height (H₂), respectively. The group contains four tests, each of which consists of 4 subtests with 16 cases in total, to examine how these two factors affect the impact force of mudflow. The values assigned to the mudflow and the terrain parameters in this set model cases are presented as follows:

Test	Subtests	Railway embankment height H ₂ (m)	Buffer distance D (m)	Slope ratio of railway embankment (H:V)	Slope inclination α (°)	Volume of mudflow (m ³)	Terrain roughness (ViscoBoundFactor)
1	Subtest 1	1	1	2:1	10	50	0.025
	Subtest 2		2				
	Subtest 3		4				
	Subtest 4		6				
2	Subtest 5	2	1	2:1	10	50	0.025
	Subtest 6		2				
	Subtest 7		4				
	Subtest 8		6				
3	Subtest 9	3	1	2:1	10	50	0.025
	Subtest 10		2				
	Subtest 11		4				
	Subtest 12		6				
4	Subtest 13	4	1	2:1	10	50	0.025
	Subtest 14		2				
	Subtest 15		4				
	Subtest 16		6				

Table 5. 2. Input data of Set I for the investigation of the effect of buffer distance and railway embankment height

Test 1 starts with subtest 1, a railway embankment with the height of one meter (H₂=1m) and slope ratio of 2H:1V (horizontal:vertical) is simulated at the distance of one meter from the bottom of the slope (D=1m), as shown in Figure 5.3, keeping the railway embankment height (H₂=1m) as constant and larger values (2m, 4m, and 6m) are assigned in turn to buffer distance D. In other three tests (Test 2, Test 3, and Test 4), the assignment of buffer distance D is the same as that in

Test 1 that has four values (1m, 2m, 4m, and 6m), while railway embankment height (H_2) is changed, values of 2m, 3m, and 4m are separately assigned to H_2 in Test 2, Test 3, and Test 4.

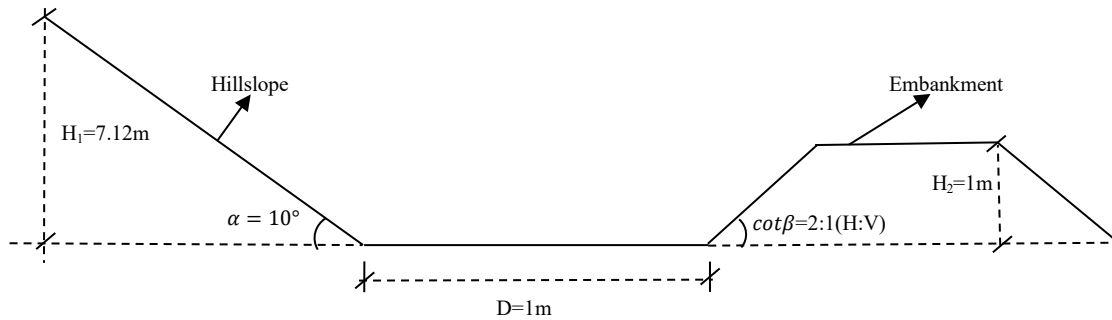


Figure 5. 3. The slope terrain and railway embankment of Subtest 1

The results obtained in Set I are presented in the following diagram:

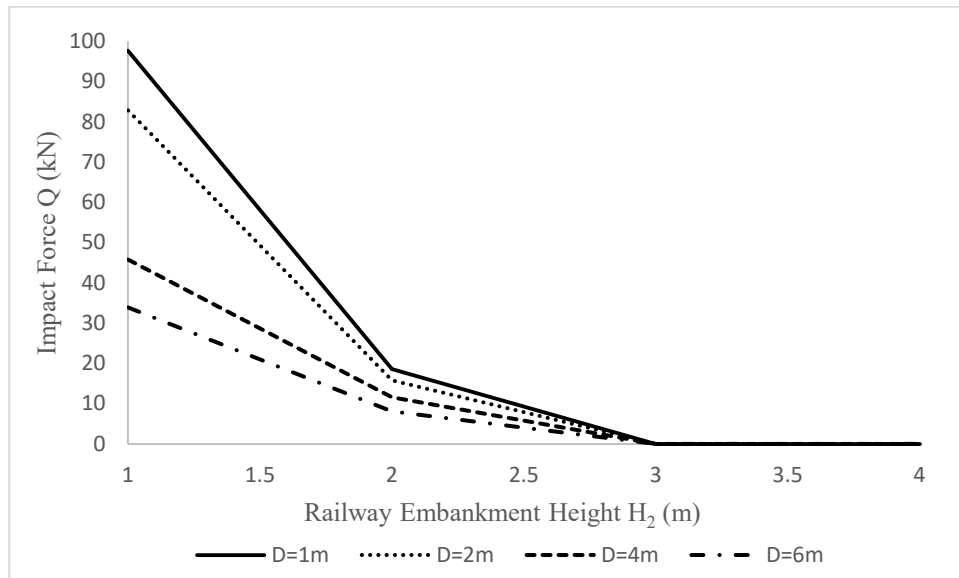


Figure 5. 4. Diagram of the impact force exerted on the railway car for Set I tests (note: the critical value of train derailment $Q=1293.6kN$)

Utilizing the rendering software mentioned in the former section 2.2.2, the following figures are the snapshots obtained in some simulations of Set I to show keyframes from the release of the mudflow up to the railway embankment and including the mudflow hitting a railway car:

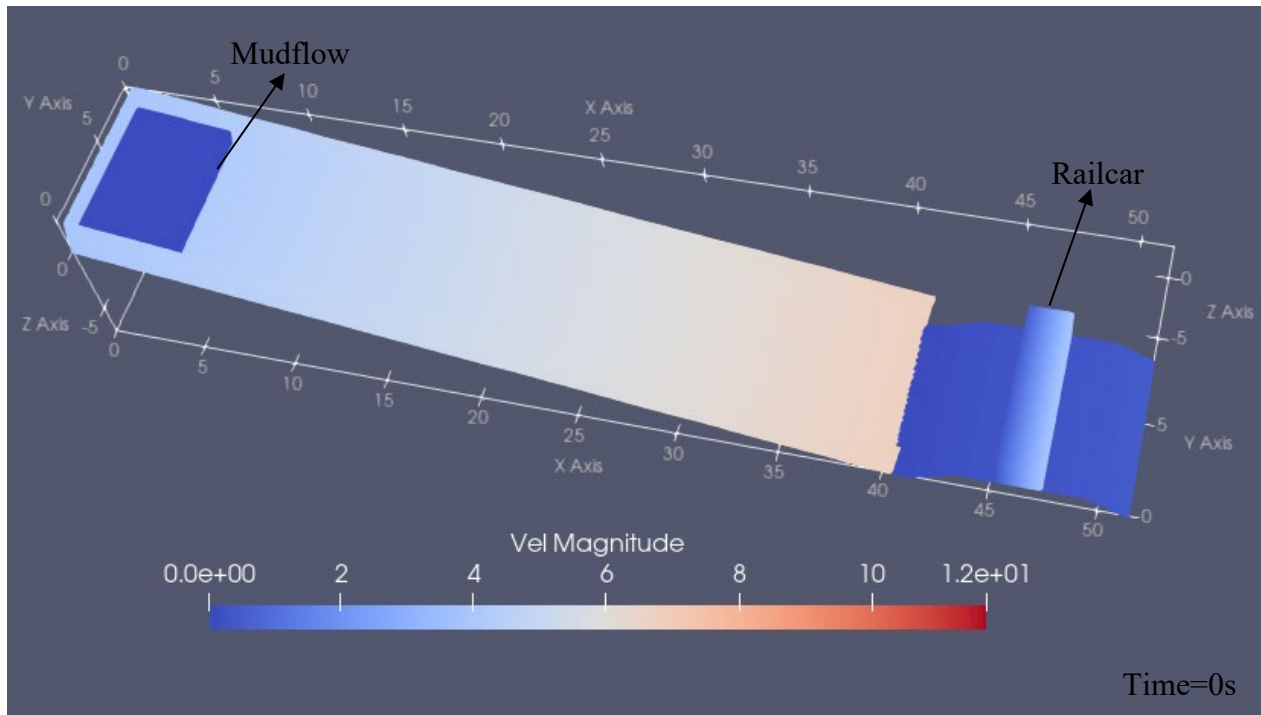


Figure 5. 5. a) Snapshot of mudflow motion at time=0s for a model with $D=1\text{m}$ and $H_2=1\text{m}$

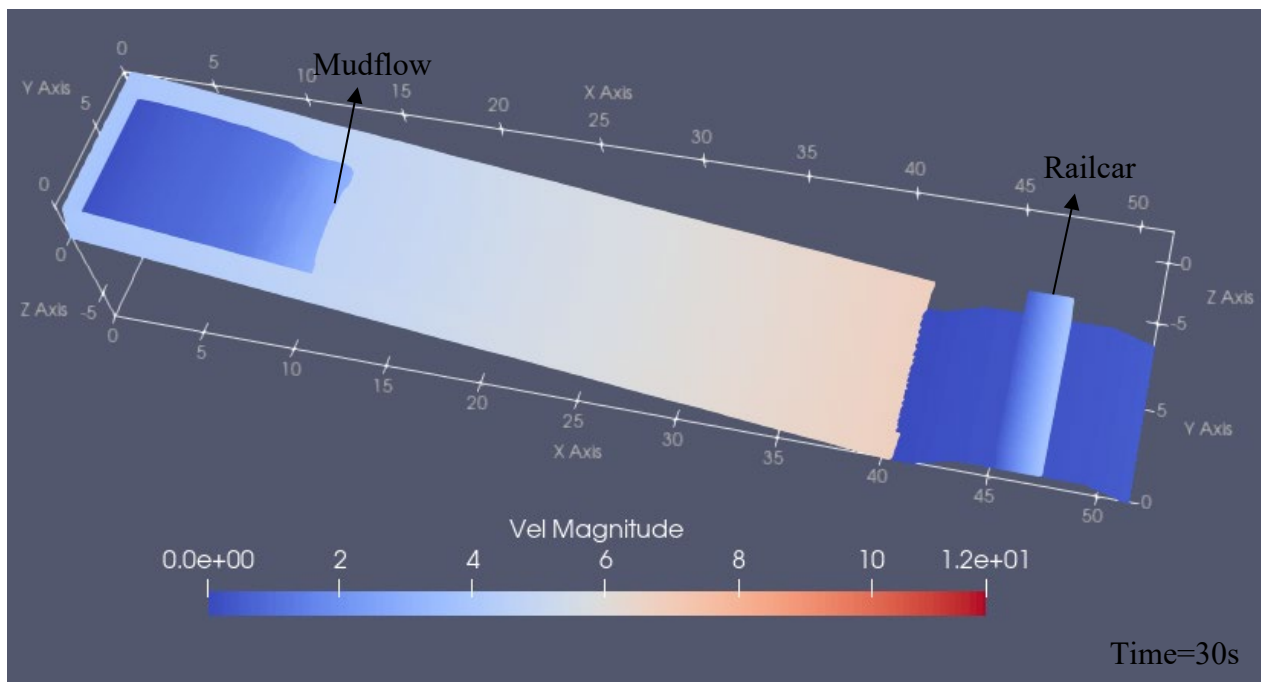
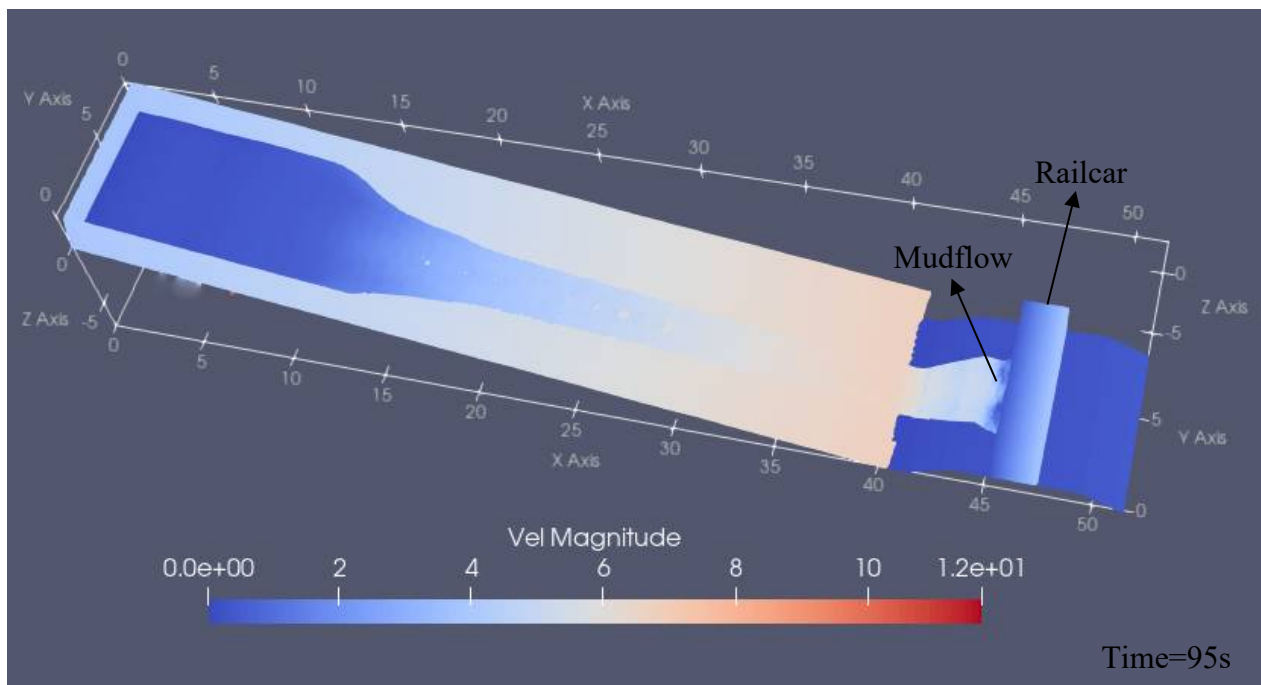
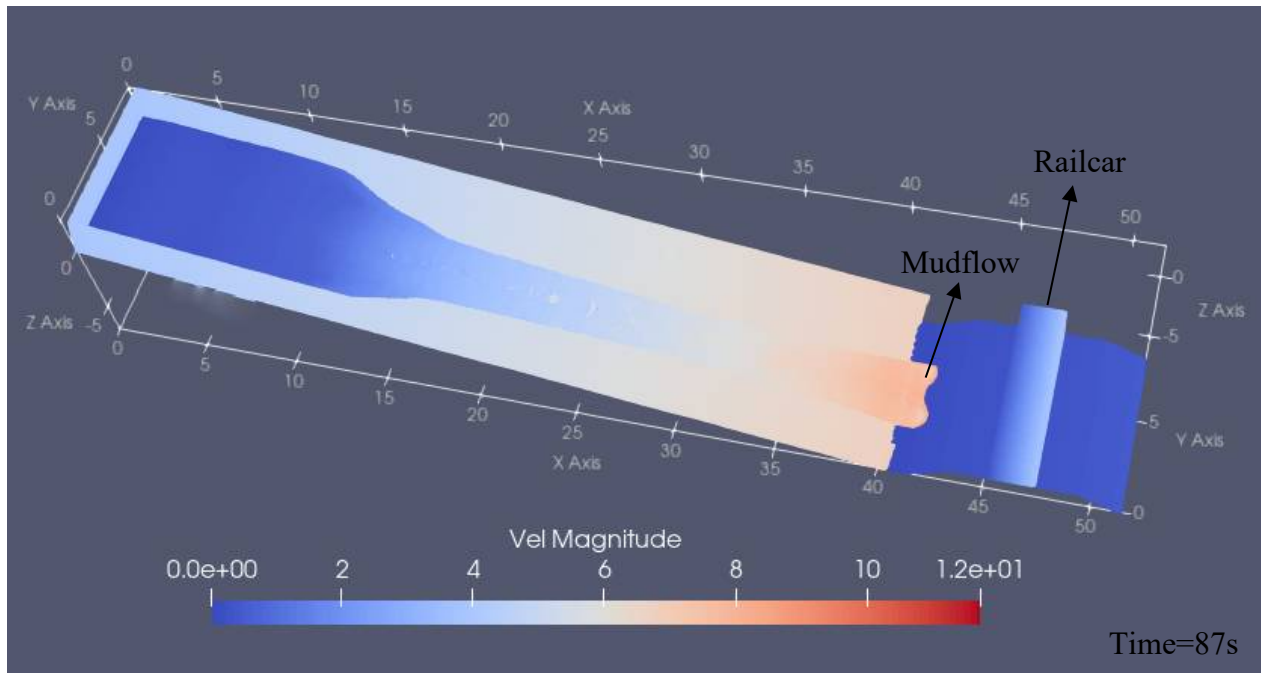


Figure 5. 5. b) Snapshot of mudflow motion at time=30s for a model with $D=1\text{m}$ and $H_2=1\text{m}$



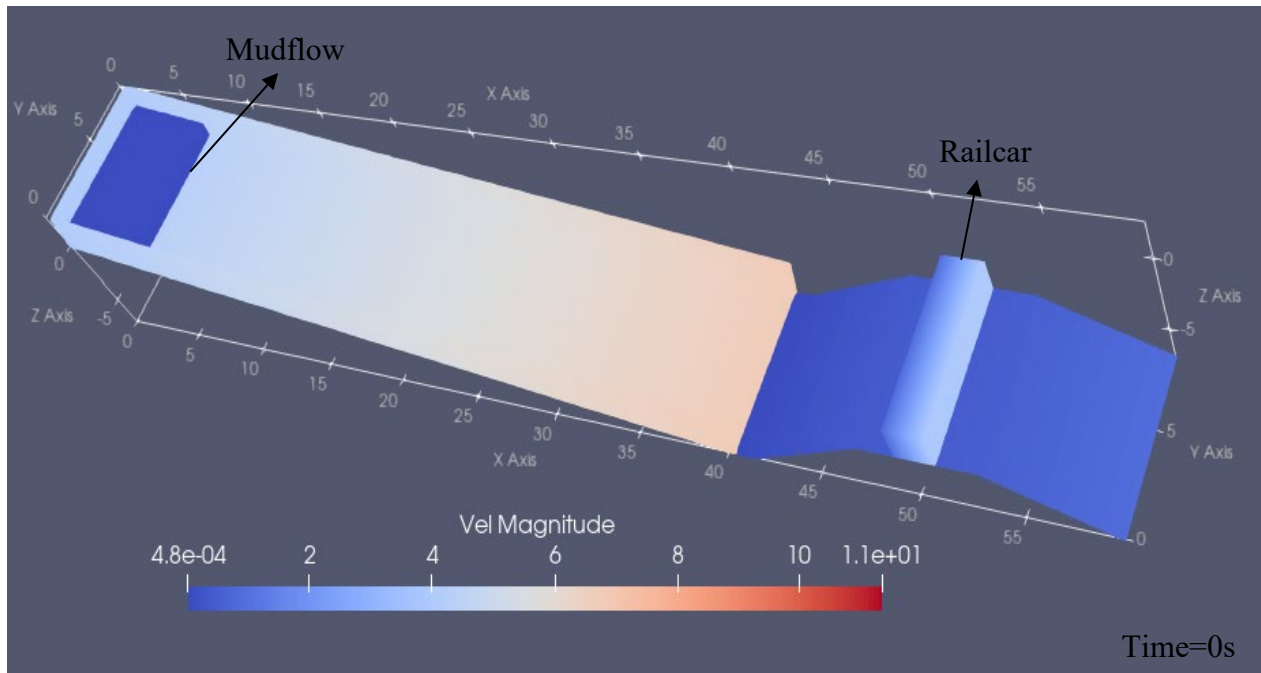


Figure 5. 6. a) Snapshot of mudflow motion at time=0s for a model with $D=1\text{m}$ and $H_2=3\text{m}$

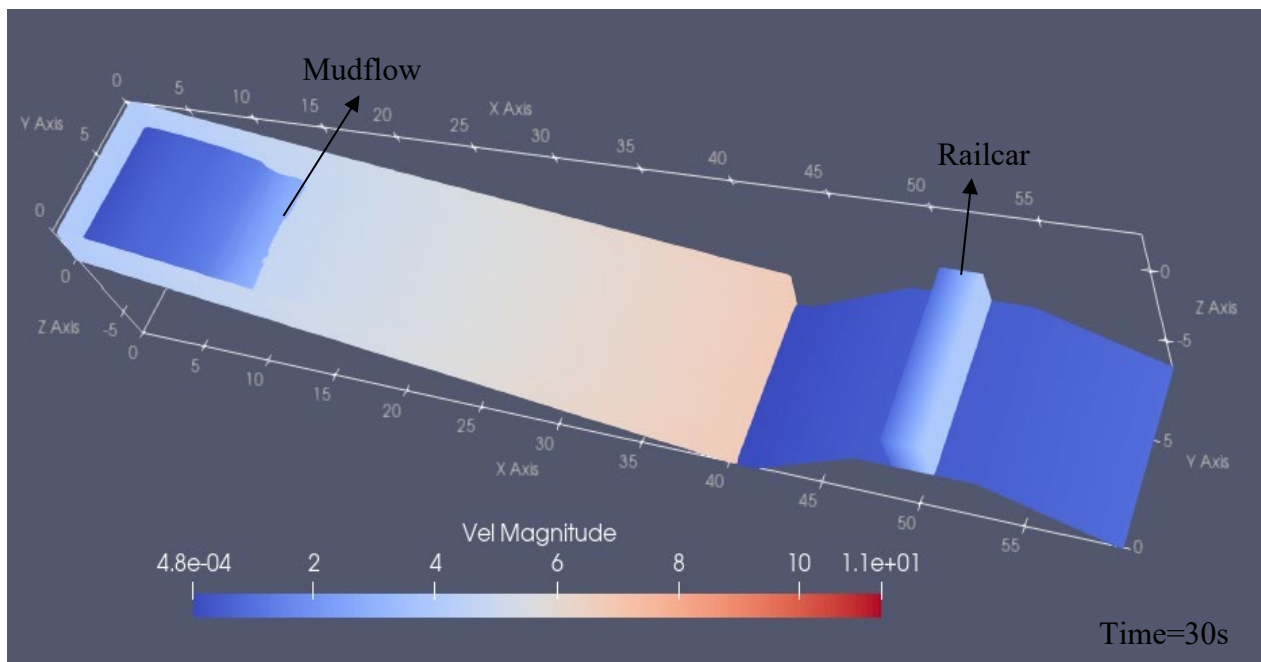


Figure 5. 6. b) Snapshot of mudflow motion at time=30s for a model with $D=1\text{m}$ and $H_2=3\text{m}$

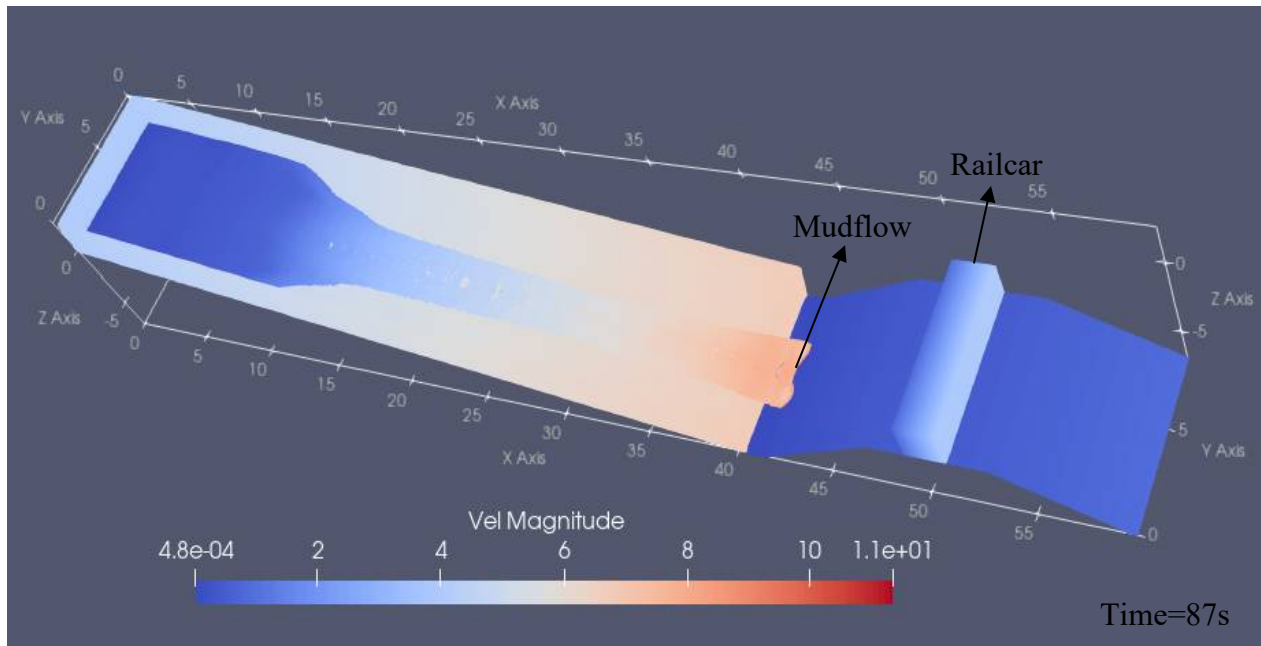


Figure 5. 6. c) Snapshot of mudflow motion at time=87s for a model with $D=1\text{m}$ and $H_2=3\text{m}$ (continued)

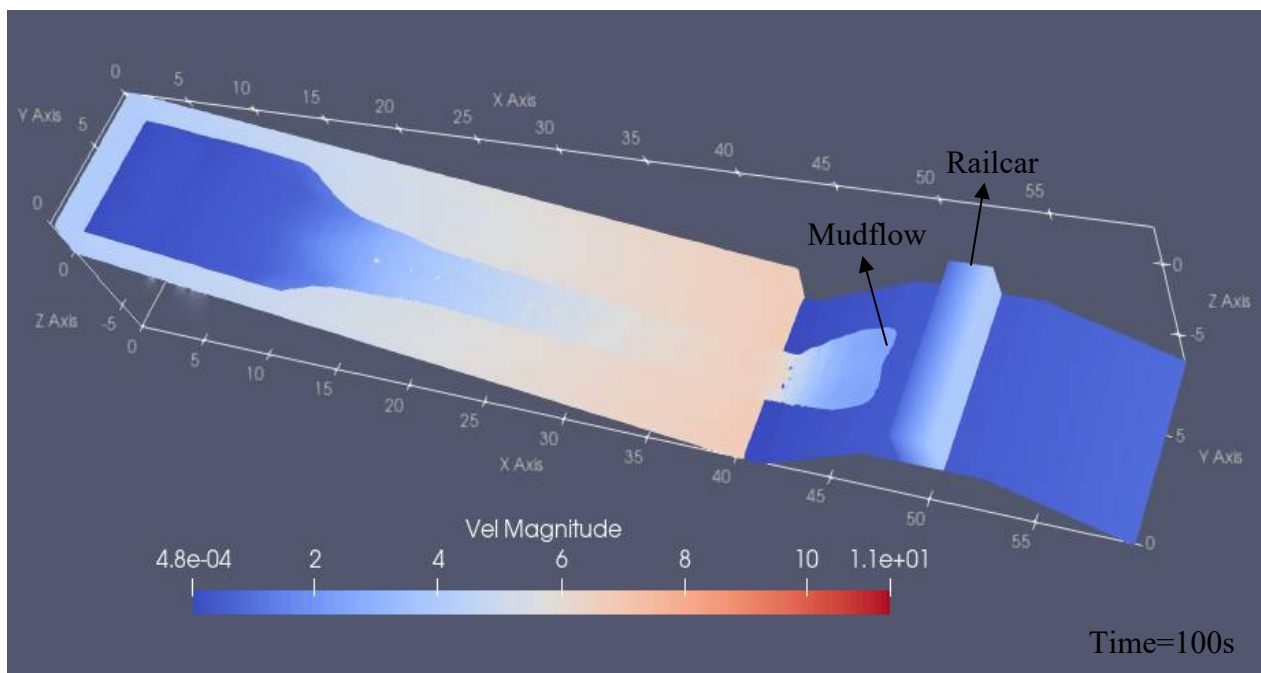


Figure 5. 6. d) Snapshot of mudflow motion at time=100s for a model with $D=1\text{m}$ and $H_2=3\text{m}$ (continued)

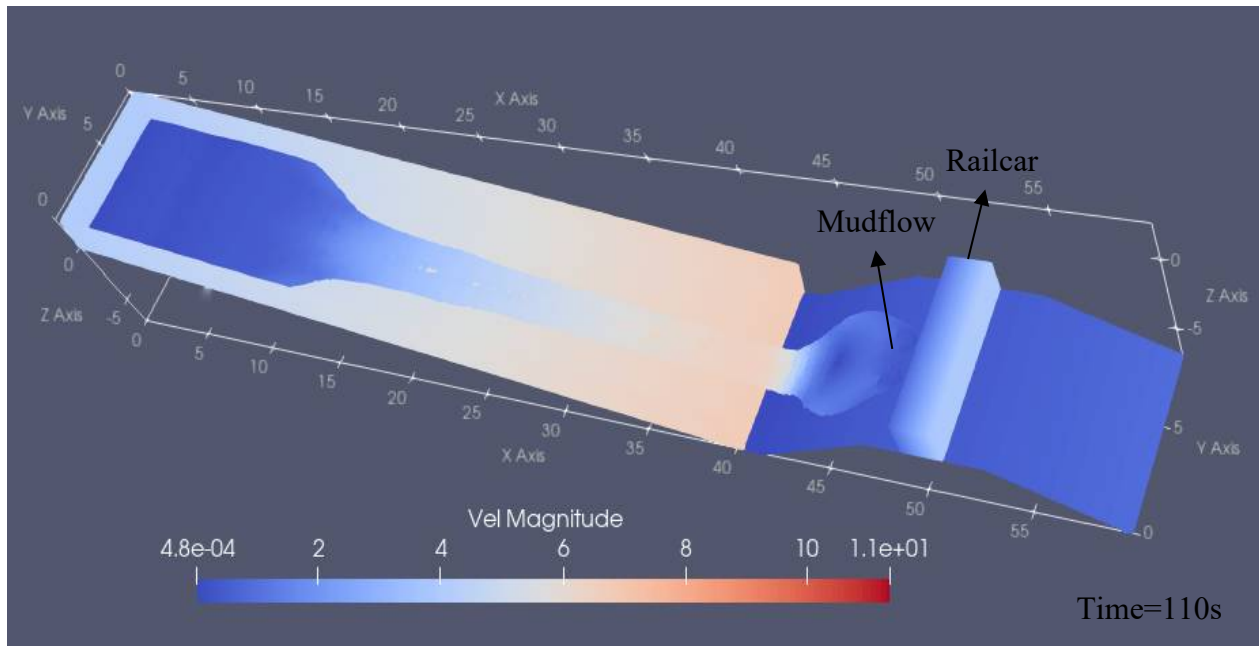


Figure 5. 6. e) Snapshot of mudflow motion at time=110s for a model with $D=1\text{m}$ and $H_2=3\text{m}$ (continued)

Among the tests performed in Set I from Test 1 to Test 4, here, the snapshots of the process of a mudflow flowing down a hillslope and impacting a railway embankment under two different terrain conditions are presented above (Figure 5.5 and Figure 5.6), representing two typical results of Set I. As shown in Figure 5.5a to Figure 5.5d, when a mudflow occurs, it could easily wash up on a railway embankment and pose a danger to trains on top of the railway embankment if a short buffer distance is built (1m) and the railway embankment is not high enough. However, by adopting a higher railway embankment (when $H_2=3\text{m}$) as shown in Figure 5.6, it could be observed that the mudflow cannot reach the surface on which the railway cars are (Figure 5.6d). Rather the flows gather on the side slope of the railway embankment and fall back due to the gravity, as shown in Figure 5.6e. The snapshots presented above (Figure 5.5) also represent the process and the outcomes of simulations performed in other set tests of this research: a mudflow released on the hillslope climbing up to railway embankment and impacting a railcar on top of the embankment. In the case of mudflow impacting trains, the train derailment depends on the impact force exerted by mudflow, which is mainly investigated and discussed in the research.

For the impact force obtained in Test 1 to Test 4, as shown in Figure 5.4, keeping the buffer distance D unchanged, trains on a lower railway embankment are impacted by greater impact force, while, regardless of the railway embankment height H_2 , the greatest destructive force generates at the case of $D=1\text{m}$. The maximum impact force computed by the simulation tool in Set I is obtained when buffer distance D is 1m and the railway embankment equals 1m. According to the diagrams shown in Figure 5.4, when the buffer distance D is a constant, the impact force generated by the mudflow experiences a significant decrease as the railway embankment height H_2 increases, even being zero which means mudflows cannot impact the railway train on top of the railway embankment as shown in Figure 5.6d & 5.6e. Since the mudflow ascends, impacting a railway embankment, during such a process, the mudflow is retarded under the combined effect of terrain roughness and gravity.

Similarly, with railway embankment height H_2 is a constant and the remaining parameters unchanged, the destructive power exerted on trains is also reduced by increasing buffer distance D as the mudflow is resisted by terrain roughness on the buffer plane. Therefore, based on these observations obtained, longer buffer distance D or higher railway embankment is useful to resist the movement and the advancement of a mudflow, further, is helpful to reduce the danger exerted by the mudflow on railway cars. On the contrary, when a mudflow occurs, a railway embankment that is not high enough (like $H_2=1\text{m}$) along with a short buffer distance ($D=1\text{m}$) result in the greatest destructive force which is the most detrimental to railway cars. Hence, for the safety of trains, the protective measures like raising railway embankment height H_2 or increasing buffer distance D are recommended. Moreover, it is necessary to note that, as the small value is assigned to the parameter of hillslope inclination and mudflow volume, the maximum impact force generated by the mudflow in Set I is around 100 kN which is much less than the critical train derailment value ($Q=1293.6$ kN). To investigate these two variables' contribution to the train derailment and the corresponding value, each of them is considered in the subsequent tests.

5.4.2 The effect of hillslope steepness α (Set II)

Besides the two parameters (buffer distance and railway embankment height) discussed in the previous tests in Set I, the simulations performed in Set II consider the hillslope steepness α , being the variable parameter to investigate its effect on the impact force exerted by the mudflow on railway cars. As stated previously, the slope angle α from 10° to 30° in increments of 10 degrees will be adopted. Therefore, a totally of 48 different cases are investigated in Set II. All these cases are summarized in Table 5.3 below with 3 tests in total including 12 subtests, 48 cases.

Test	Subtests	Slope inclination α ($^\circ$)	Railway embankment height H_2 (m)	Buffer distance D (m)	Slope ratio of railway embankment (H:V)	Volume of mudflow (m^3)	Terrain roughness (ViscoBoundFactor)
5	Subtest 17	10	1	1,2,4,6	2:1	50	0.025
	Subtest 18		2	1,2,4,6			
	Subtest 19		3	1,2,4,6			
	Subtest 20		4	1,2,4,6			
6	Subtest 21	20	1	1,2,4,6	2:1	50	0.025
	Subtest 22		2	1,2,4,6			
	Subtest 23		3	1,2,4,6			
	Subtest 24		4	1,2,4,6			
7	Subtest 25	30	1	1,2,4,6	2:1	50	0.025
	Subtest 26		2	1,2,4,6			
	Subtest 27		3	1,2,4,6			
	Subtest 28		4	1,2,4,6			

Table 5. 3. Input data of Set II for the investigation of the effect of hillslope steepness

The hillslope steepness has three conditions which are 10°, 20° and 30°. Under each hillslope condition, the railway embankment height is separately set to be 1, 2, 3, and 4 meters. While the buffer distance $D=1, 2, 4,$ and 6 meters. The impact force exerted on railway cars obtained under the condition of different hillslope steepness are presented below:

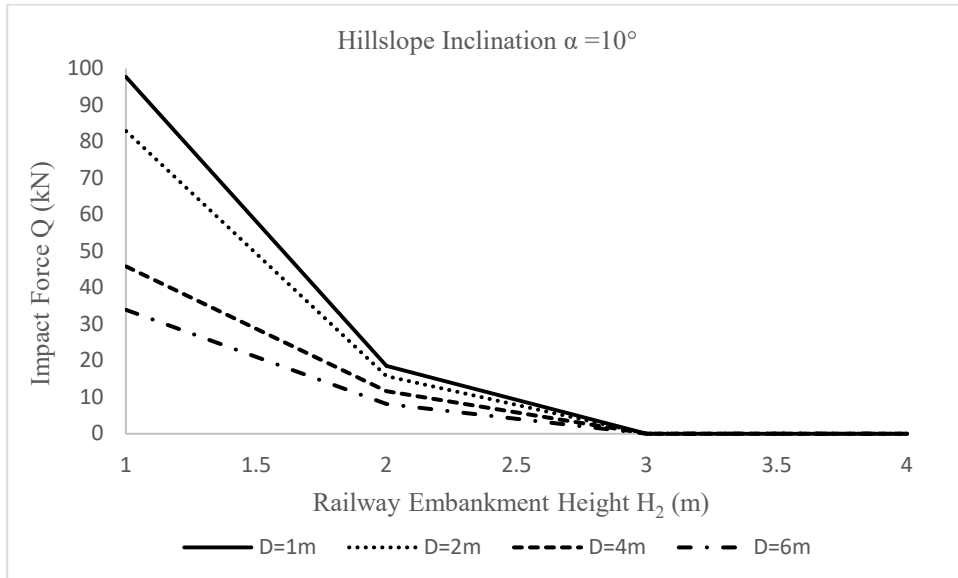


Figure 5. 7. a) Diagram of the impact force exerted on the railway car with hillslope inclination equal to 10 degrees

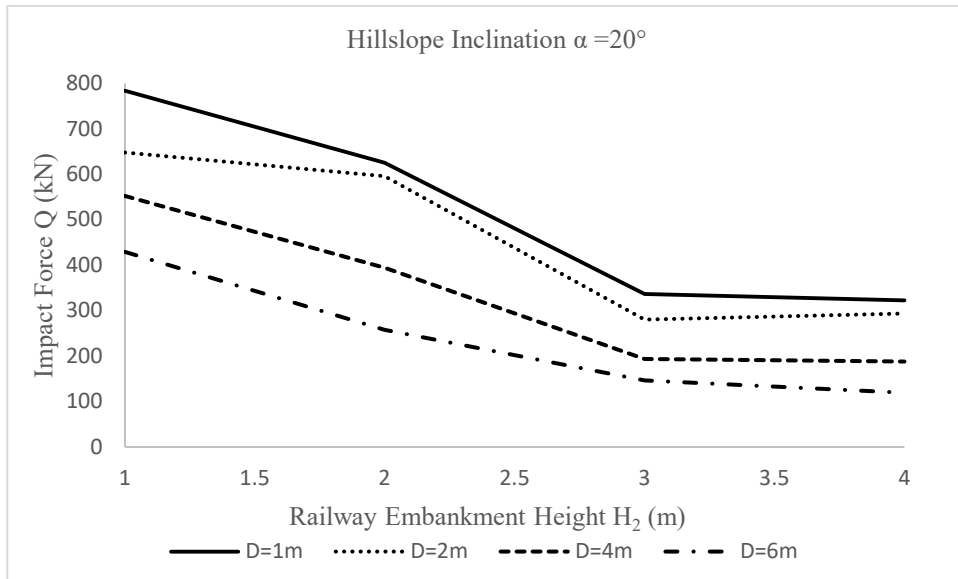


Figure 5. 7. b) Diagram of the impact force exerted on the railway car with hillslope inclination equal to 20 degrees

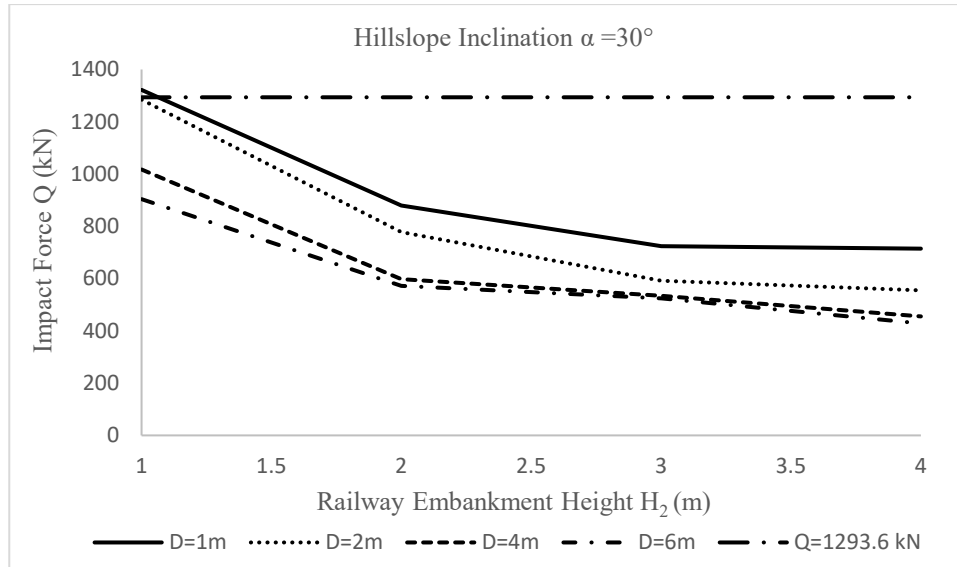


Figure 5.7. c) Diagram of the impact force exerted on the railway car with hillslope inclination equal to 30 degrees (continued)

Figure 5.7 presents three diagrams obtained from Test 5 to Test 7. The first diagram (Figure 5.7a) is the result of Test 5 which are simulated under the circumstance of the hillslope is sloped 10° , the second figure (Figure 5.7b) is the impact force obtained in Test 6 which are performed in case of hillslope steepness equals 20° , the third one (Figure 5.7c) shows the outcomes of Test 7 that are simulated at hillslope is inclined 30° . As a further investigation based on Set I (Test 1 to Test 4), it is observed that, even if different hillslope inclinations are considered in Set II, similarly, like the observation obtained in Set I, the impact force experiences a decreasing trend by increasing either buffer distance or railway embankment height. Although the hillslope steepness increases gradually, either the lower railway embankment height or the shorter buffer distance is detrimental to railway cars. The maximum impact force exerted by the mudflow on railway cars is always generated when buffer distance D is 1m and the railway embankment height H_2 equals 1m, on the contrary, the minimum one is obtained with long buffer distance ($D=6m$) and high railway embankment ($H_2=4m$). This means that regardless of the hillslope inclination, the low railway embankment ($H_2=1m$) and short buffer distance ($D=1m$) is the most detrimental and critical case for railway cars, under such case, mudflow generates the maximum impact force on trains. On basis of that, considering the effect of natural hillslope inclination α , it is observed in Figure 5.7 that the maximum impact force obtained under the circumstance of different hillslope steepness increases with a steep hillslope: a) around 100 kN at $\alpha=10^\circ$; b) about 800 kN at $\alpha=20^\circ$; c) approximately 1300 kN at $\alpha=30^\circ$. Furthermore, not only for the maximum force, but the minimum one (at the terrain condition of $D=6m$ with $H_2=4m$) computed by the simulation tool also increases as the hillslope is steeply inclined: a) 0 kN at a gentle hillslope (10 degrees); b) about 100 kN as the hillslope steepness is 20° ; c) approximately 400 kN when hillslope is inclined 30° . Therefore, it is apparent that the impact force generated on the steep hillslope is larger than that generated on the gentle one regardless of other parameters. It is worth noting that as the hillslope steepness is increased to 30 degrees, the maximum impact force exerted on trains starts to exceed the critical value of train derailment $Q=1293.6$ kN, meaning that the destructive force exerted on railway cars

causes train derailment when natural hillslope is inclined 30° . Moreover, to fully investigate the effect of hillslope steepness on the impact force exerted on railway cars, comparing the maximum impact force obtained under different hillslope steepness, the relationship of the maximum destructive force versus the inclination of hillslope can be expressed in the figure below:

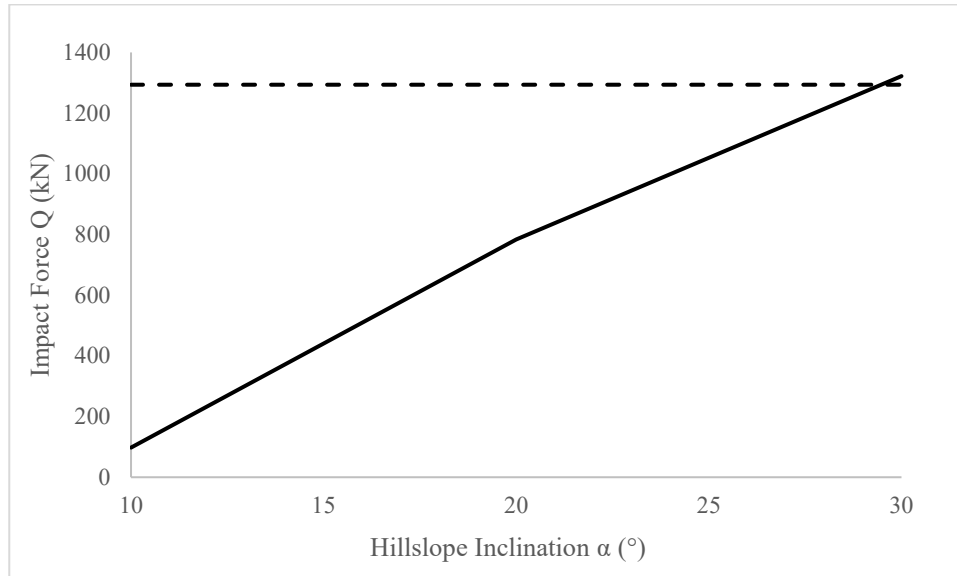


Figure 5. 8. The relationship between the maximum impact force and the hillslope inclination (note: the horizontal dashed line is $Q=1293.6$ kN)

As shown in Figure 5.8, the experimental results evidently show that there is a linear correlation between the impact force and hillslope inclination. The impact force increases significantly as the hillslope becomes steeper. When mudflows occur on a gentle hillslope ($\alpha = 10^\circ$), the maximum impact force generated by mudflows is much smaller (about 100 kN) than the critical value causing train derailment (1293.6 kN). With increasing hillslope inclination with other parameters unchanged, the destructive force exerted on railway cars dramatically increases. The maximum impact force generated by mudflows is increased to around 800 kN in the case of $\alpha = 20^\circ$ while a greater one was generated (approximately 1300 kN) with $\alpha = 30^\circ$, which exceeds the critical train derailment value (1293.6 kN), meaning the railway cars derail under such circumstance.

Therefore, based on the results investigated of all tests of Set II, it could be concluded that a positive linear correlation exists between the impact force and hillslope inclination. Although the quantity of the mudflow released is as small as 50 m^3 , as the hillslope where the mudflow occurs becomes steep, the destructive power generated by the mudflow increases dramatically as the inclination of the hillslope increases, even leading to the train derailment when natural hillslope steepness is increased to 30° . Hence, regardless of other parameters, the steeper hillslope, the greater the impact force exerted on the railway cars, resulting in a higher potential of the train derailment.

5.4.3 The effect of railway embankment slope ratio H:V (Set III)

To fully investigate the effect of changes in slope inclination on mudflows, not only the natural hillslope needs to be considered but also the railway embankment slope. As previously stated, the

slope ratio of the railway embankment is normally either 2H:1V or 3H:1V (horizontal:vertical) in North American railway engineering practice. To observe the mudflow behavior and its corresponding destructive effect on railway cars under such two different circumstances, the slope ratio of railway embankment as a variable is studied on top of the Set II (Test 5 to Test 7). The values of 2H:1V and 3H:1V were both considered to the slope ratio of the railway embankment and forms the simulations of Set III. The remaining parameters are set as the same as that of the former simulation Set II. The table below presents the input data:

Test	Subtests	Slope ratio of railway embankment (H:V)	Slope inclination α ($^{\circ}$)	Railway embankment height H_2 (m)	Buffer distance D (m)	Volume of mudflow (m^3)	Terrain roughness (ViscoBoundFactor)
8	Subtest 29	2:1	10	1	1,2,4,6	50	0.025
	Subtest 30			2	1,2,4,6	50	0.025
	Subtest 31			3	1,2,4,6	50	0.025
	Subtest 32			4	1,2,4,6	50	0.025
9	Subtest 33		20	1	1,2,4,6	50	0.025
	Subtest 34			2	1,2,4,6	50	0.025
	Subtest 35			3	1,2,4,6	50	0.025
	Subtest 36			4	1,2,4,6	50	0.025
10	Subtest 37		30	1	1,2,4,6	50	0.025
	Subtest 38			2	1,2,4,6	50	0.025
	Subtest 39			3	1,2,4,6	50	0.025
	Subtest 40			4	1,2,4,6	50	0.025
11	Subtest 41	3:1	10	1	1,2,4,6	50	0.025
	Subtest 42			2	1,2,4,6	50	0.025
	Subtest 43			3	1,2,4,6	50	0.025
	Subtest 44			4	1,2,4,6	50	0.025
12	Subtest 45		20	1	1,2,4,6	50	0.025
	Subtest 46			2	1,2,4,6	50	0.025
	Subtest 47			3	1,2,4,6	50	0.025
	Subtest 48			4	1,2,4,6	50	0.025
13	Subtest 49		30	1	1,2,4,6	50	0.025
	Subtest 50			2	1,2,4,6	50	0.025
	Subtest 51			3	1,2,4,6	50	0.025
	Subtest 52			4	1,2,4,6	50	0.025

Table 5. 4. Input data of Set III for the investigation of the effect of railway embankment slope ratio

Table 5.4 contains 6 tests, consisting of 24 subtests with 96 cases in total. The railway embankment slope ratio has two conditions which are 2H:1V (β approximately equals 27 degrees) and 3H:1V (β is about 18 degrees) respectively. Under such two conditions, the mudflow is released on hillslope inclined at 10° , 20° , and 30° respectively, flowing on the buffer distance D with 1, 2, 4, or 6 meters, impacting the railway embankment with different heights (1, 2, 3, or 4 meters).

To have a straightforward comparison of the railway embankment slope ratio with 2H:1V and 3H:1V respectively, according to the investigations observed in previous tests (Set I and Set II), the models with 1-meter buffer distance at different hillslope inclinations are taken as an example presented below. Under such condition, regardless of the railway embankment height and the

hillslope steepness, the mudflow generates the greatest impact force impacting a railway car, which is the most detrimental to trains. The corresponding results of simulations are presented in the following diagrams:

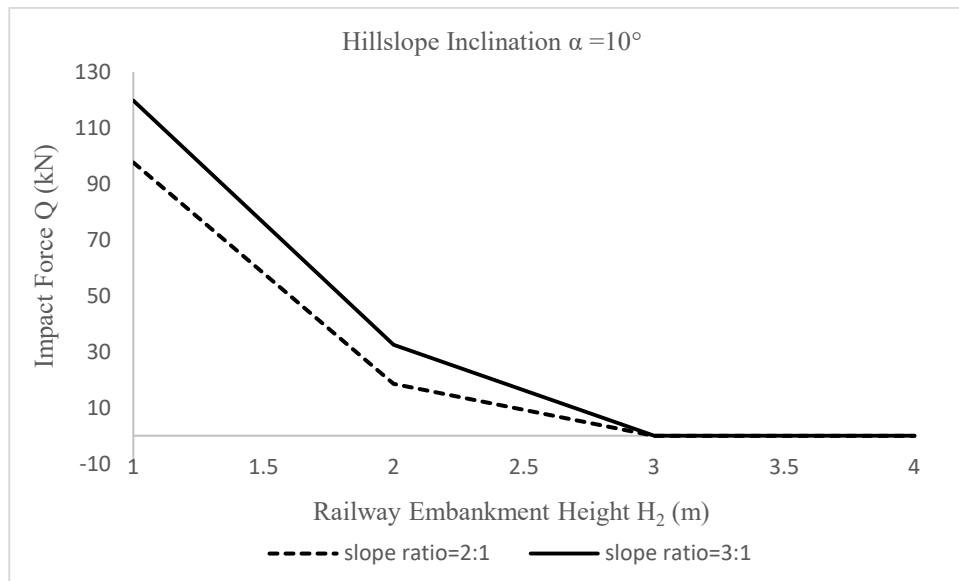


Figure 5. 9. a) Comparison diagram of the impact force exerted on a railway car with hillslope inclination equal to 10 degrees

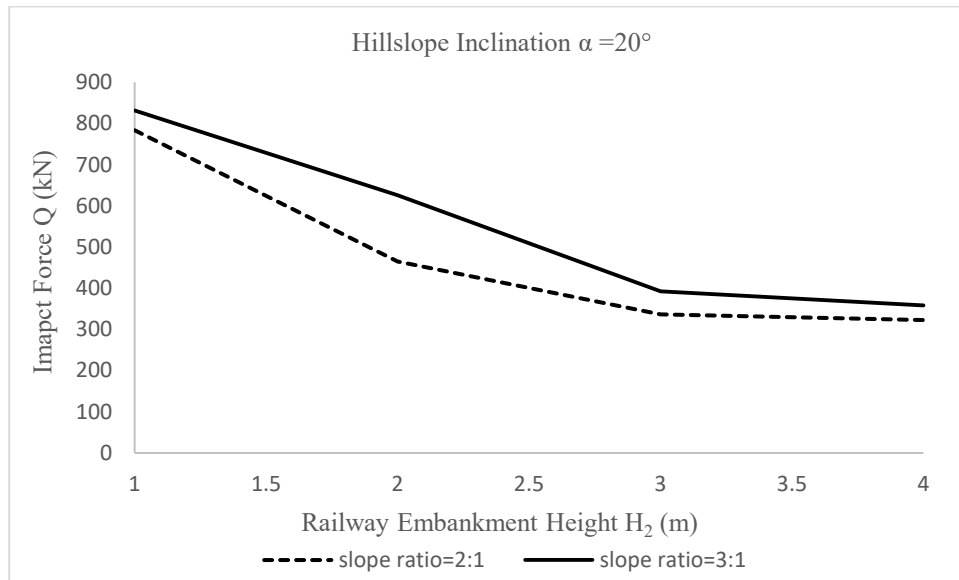


Figure 5. 9. b) Comparison diagram of the impact force exerted on a railway car with hillslope inclination equal to 20 degrees

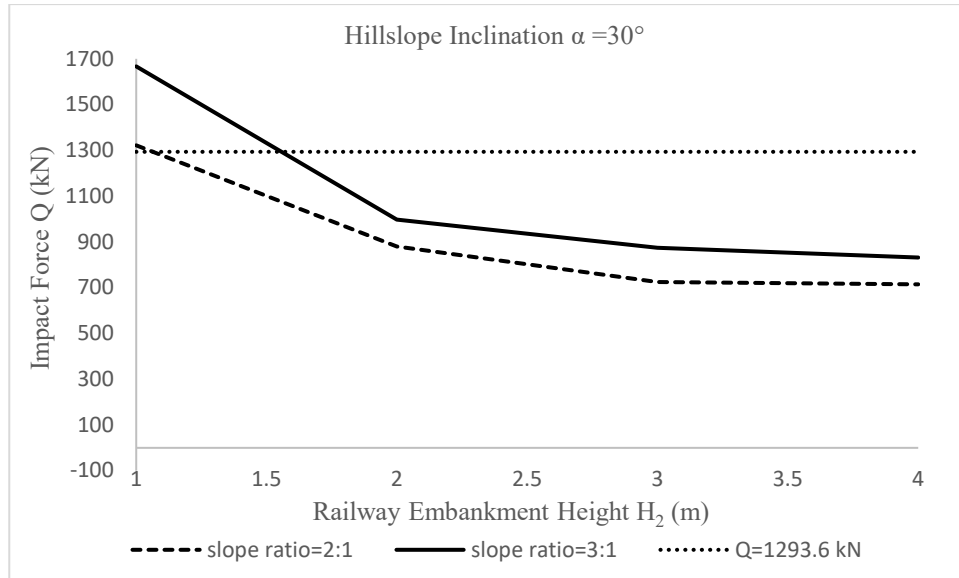


Figure 5.9. c) Comparison diagram of the impact force exerted on a railway car with hillslope inclination equal to 30 degrees (continued)

Comparing the diagrams obtained under such two different conditions where railway embankment with the slope ratio (H:V) of 2:1 (approximately 27 degrees) and 3:1 (about 18 degrees), respectively. It is observed in Figure 5.9 :

1. In Set III, with the same railway embankment height H_2 and buffer distance D , under the circumstance of the same hillslope inclination, the impact force Q exerted on railway cars at the condition of embankment slope ratio equals 3H:1V is larger than that under the case of 2H:1V one, meaning that the potential of the train derailment in case of embankment slope ratio equals 3H:1V is larger than that under the circumstance of 2H:1V one.
2. Additionally, when the natural hillslope is inclined to 30 degrees as shown in Figure 5.9c, like the investigations observed in Set II that the destructive force produced by mudflows starts to make the train derail (the critical value of hillslope inclination α), it is obvious from Figure 5.9c that adopting a steep railway embankment with the slope ratio of 2H:1V (around 27°), the destructive force exerted on cars is reduced, smaller than that at the condition of 3H:1V (about 18°) but still exceeds the critical value of the train derailment.
3. Similar to the observations obtained in the previous test (Set I and Set II), even though the slope ratio of railway embankment is changed from 2H:1V to 3H:1V, the destructive force hitting railway cars has a declining trend with the increasing height of railway embankment. And the impact force increases as the natural hillslope steepness α increases: a) about 120 kN at $\alpha=10^\circ$; b) around 800 kN at $\alpha=20^\circ$; c) approximately 1700 kN $\alpha=30^\circ$.

Based on the observations above, depending on the slope geometry, it is apparent that a steeper slope generates a larger force parallel to the slope surface due to gravity, not only for the natural hillslope also for the railway embankment. Different than a flow down on the natural hillslope, the mudflow ascends instead of flowing downward during the mudflow while impacting a railway

embankment. Thus, the force generated by gravity serves as a driving force that promotes the mudflow running down on the natural hillslope while serves as a resisting force against the mudflow's advancement onto the railway embankment. That is the reason that the steep natural hillslope causes a greater impact force, on the contrary, the steep railway embankment hillside retards the mudflow and reduces the impact force. Therefore, from the investigations obtained in Set III, the comparison clearly indicates that compared to the railway embankment with slope ratio of 2H:1V, 3H:1V one is more detrimental to railway cars, that is, a relatively steep railway embankment slope is helpful for reducing the impact force exerted on a railway car and further preventing trains from tipping over by mudflows. Moreover, the railway embankments must have a side slope of not less than 2H:1V, as specified in the Canadian railway engineering specifications (CN's Engineering Specifications 2019) and AREMA's Manual for Railway Engineering recommends a typical slope ratio of 2H:1V (AREMA 2010). Therefore, the investigation obtained from the simulations in Set III agrees well with the specifications of the literature mentioned.

However, it is worth noting that, when the natural hillslope is steeply sloped to 30 degrees, even though a steep railway embankment is adopted to reduce the impact force exerted on trains, mudflows could still derail railway cars as shown in Figure 5.9c. This indicates that as the hillslope exceeds a certain inclination (like 30 degrees), adopting a steep railway embankment cannot effectively prevent the train derailment since the steep hillslope generates the greater impact force. Hence, considering the effect of changes in slope inclination (including natural hillslope and railway embankment slope) on mudflows, the hillslope inclination plays a crucial role in the case of the train derailment. The relatively gentle hillslope helps reduce the potential of the train derailment. Additionally, as specified in "Slope Stability Guidelines for Development Applications" compiled by the City of Ottawa Planning and Environment Committee and Council (2001) that, the stable natural hillslope allowance in the study area is generally conservatively calculated based on a projection up from the slope toe level at 5 horizontal to 1 vertical (approximately 11 degrees) for Champlain Sea clay, otherwise there is the potential for slope instability. Thus, considering the natural slope instability, it is not recommended to construct the railway system where the natural hillslope in the study area is inclined steeper than about 11 degrees (5H:1V).

Therefore, based on the simulations performed in Set III (Test 8 to Test 13) and the information specified in the literature mentioned above, to reduce the potential of the train derailment in the study area, the railway embankment with the slope ratio of 2H:1V (about 27 degrees) and the relatively gentle hillslope (about 10 degrees) should be considered. In contrast, a relatively flat railway embankment (slope ratio is 3H:1V) along with a steep natural hillslope (e.g., 30 degrees) would pose the largest derailment potential to railway cars.

5.4.4 The effect of mudflow volume V (Set IV)

After careful investigations of the cases in Set I (buffer distance and railway embankment height being variable), Set II (hillslope inclination being variable) and Set III (railway embankment slope ratio being variable), the next step is to study the models considering mudflow volume V . As explained previously, according to Manning's Equation and the hydrodynamic model, the changes in flow depth affect the impact force generated by the flow. Meanwhile, the volume of mudflow was one major factor considered for designing countermeasures against the danger of the train

derailment in railway engineering. To observe the relationship of the impact force versus the volume of mudflow, simulations of Set IV were developed. As the investigation obtained in Set III that, when a mudflow occurs, the largest derailment potential is posed to railway cars under the circumstance of a relatively flat railway embankment (3H:1V) along with a steep natural slope (30°). Therefore, on basis of that, different volumes of mudflow are released to investigate their effect on the destructive force generated by mudflow. Within these models of Set IV, the following input data was used:

Test	Subtests	Volume of mudflow (m ³)	Railway embankment height H ₂ (m)	Buffer distance D (m)	Slope ratio of railway embankment (H:V)	Slope inclination α (°)	Terrain roughness (ViscoBoundFactor)
14	Subtest 53	50	1	1,2,4,6	3:1	30	0.025
	Subtest 54		2				
	Subtest 55		3				
	Subtest 56		4				
15	Subtest 57	75	1	1,2,4,6	3:1	30	0.025
	Subtest 58		2				
	Subtest 59		3				
	Subtest 60		4				
16	Subtest 61	100	1	1,2,4,6	3:1	30	0.025
	Subtest 62		2				
	Subtest 63		3				
	Subtest 64		4				

Table 5. 5. Input data of Set IV for the investigation of the effect of mudflow volume

Table 5.5 lists all combined cases of Set IV with 3 tests, consisting of 12 subtests with 48 cases in total. The experimental results of all cases are provided in the following diagrams:

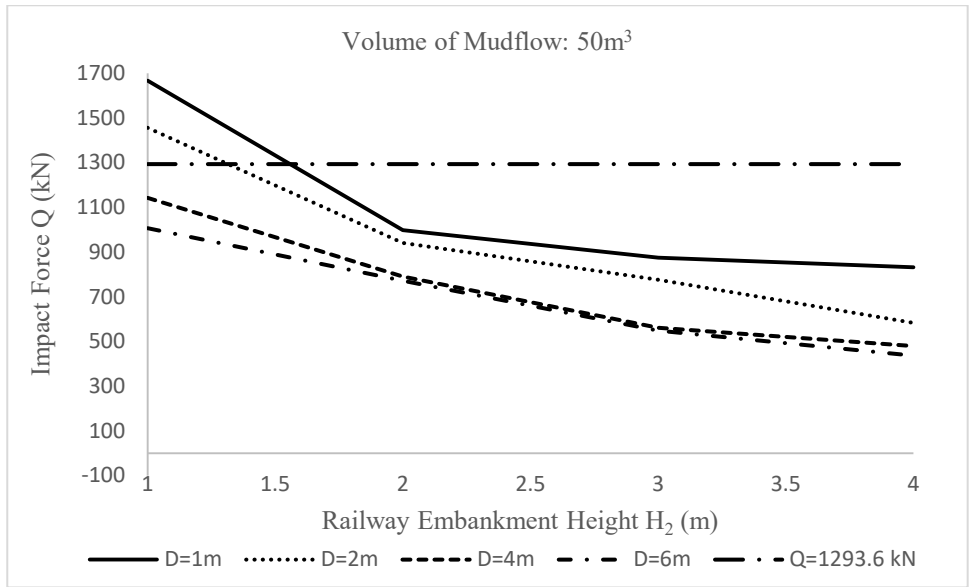


Figure 5. 10. a) Diagram of the impact force exerted on the railway car with mudflow volume $V=50\text{m}^3$

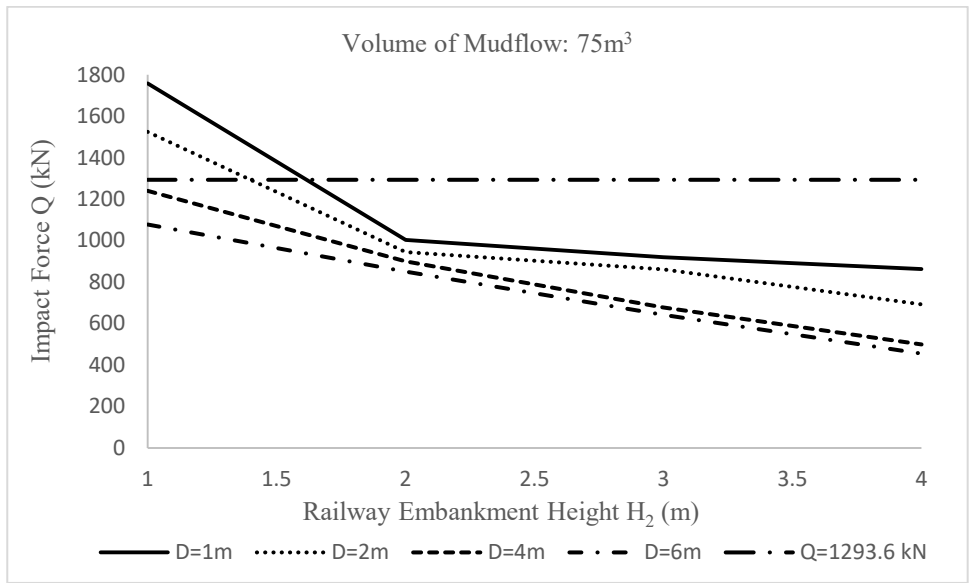


Figure 5. 10. b) Diagram of the impact force exerted on the railway car with mudflow volume $V=75\text{m}^3$

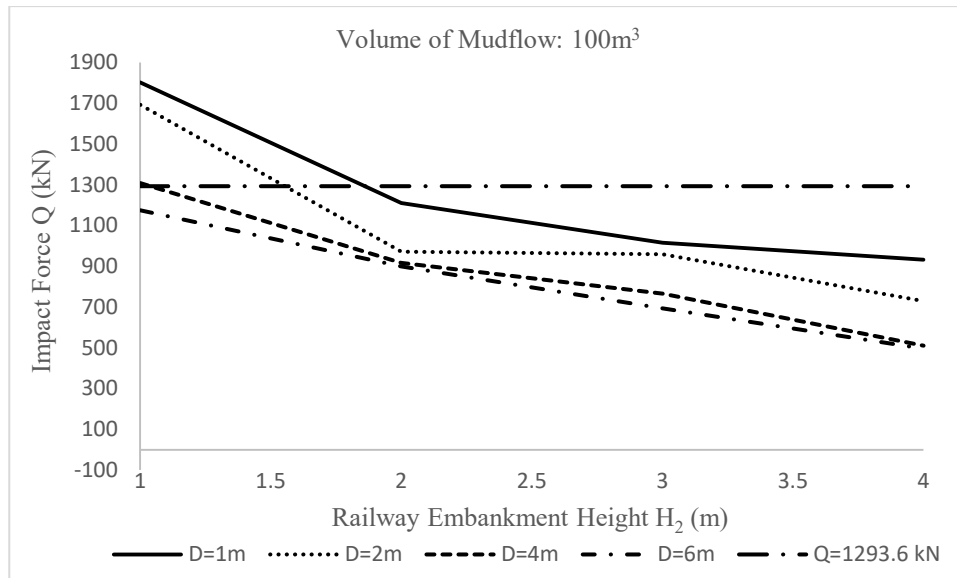


Figure 5. 10. c) Diagram of the impact force exerted on the railway car with mudflow volume $V=100\text{m}^3$ (continued)

Figure 5.10 presents the diagrams obtained from the investigations of Set IV (Test 14 to Test 16). According to the data obtained in Set IV (Test 14 to Test 16), which is simulated under the condition of hillslope is inclined 30 degrees along with a relatively flat railway embankment (3H:1V), it is observed that, as the volume of mudflow released increases, the corresponding destructive force exerted on trains increases. When a mudflow is released with a quantity of 50 m^3 , the maximum impact force exerted on trains is about 1700 kN. Increasing the volume of mudflow released to 75 m^3 , the maximum destructive force increases to approximately 1800 kN, while, the greater impact force (around 1900 kN) is generated by continuing to increase the quantity of mudflow released (100 m^3). Moreover, similar to the simulations performed previously, although different volumes of mudflow are released, the maximum impact force is computed at the case of 1-meter buffer distance D and 1-meter railway embankment height. Under such terrain condition, even as small as 50 m^3 of mudflow released could generate the impact force exceeding the critical value of the train derailment that derails trains, so do for the mudflow released with 75 m^3 and 100 m^3 . Additionally, according to the three diagrams shown in Figure 5.10, when the case of the train derailment occurs (the impact force computed exceeds the critical value $Q=1293.6\text{ kN}$), increasing the buffer distance D or raising the railway embankment is helpful to reduce the impact force to a value that smaller than the critical value of the train derailment ($Q=1293.6\text{ kN}$) to avoid trains derail.

To have a straightforward observation of the effect of increasing mudflow volume on the impact force, taking the maximum impact force generated by mudflows with different quantities as an example for comparison. The diagram of the maximum impact force exerted on trains with flow volume changes is provided below:

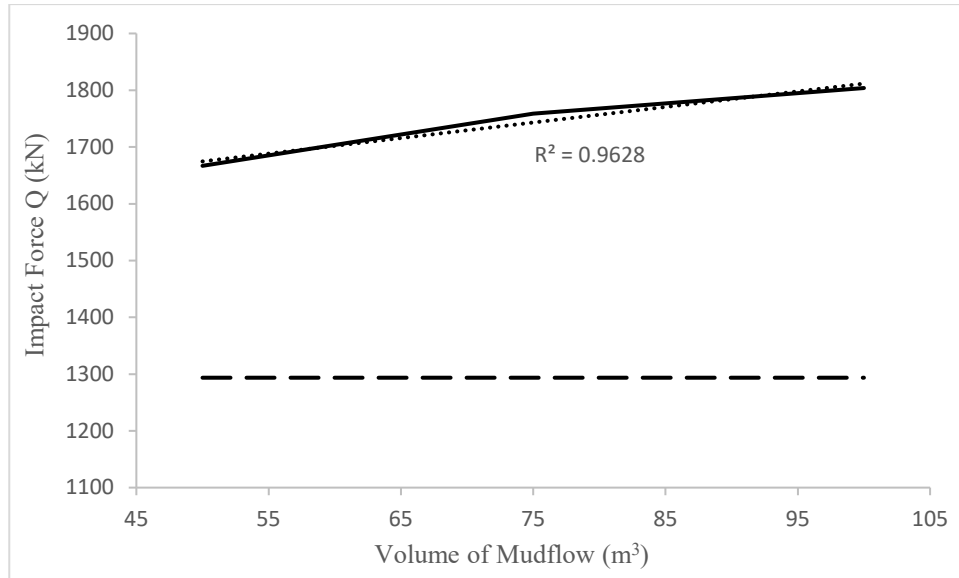


Figure 5. 11. The relationship between the maximum impact force and the volume of mudflow (note: the horizontal dashed line is the critical value of train derailment $Q=1293.6$ kN)

As shown in Figure 5.11, comparing the maximum impact force with different volumes of mudflow released (50 m^3 , 75 m^3 , and 100 m^3) under the same terrain environment, experimental data indicates that the destructive force of mudflow exerted on the railway cars has a positive correlation with the mass volume of mudflow, that is, the greater mudflow volume released, the greater impact on trains. As presented in the three diagrams of Figure 5.10, for the models simulated in Set IV, the experimental results show that although the volume of mudflow released from the hillslope increases from 50 m^3 to 75 m^3 , then to 100 m^3 , leading to derail trains, the protective measures like raising railway embankment or constructing a longer buffer distance can effectively reduce the destructive force exerted on trains and decrease the detrimental effect of mudflow on railway cars. For all cases simulated in Set IV as shown in the diagrams of Figure 5.10, the minimum impact force is obtained when a long buffer distance (6-meter) and a high railway embankment (4-meter) are constructed, which is between 400 kN to 500 kN that is much less than the critical value of train derailment ($Q=1293.6$ kN). However, unlike the experimental simulations performed, as an uncontrollable factor in the reality, the quantity of mudflow generated could be millions of cubic meters when a mudflow occurs which would produce an enormous destructive force on the railway cars. It could very well be that these protective measures cannot prevent trains from being tipped over when the volume of mudflow beyond a certain volume (the critical volume), that is, the impact force exceeds the critical value of train derailment ($Q=1293.6$ kN) even if a long buffer distance (6-meter) along with a high-enough railway embankment (4-meter) is constructed. Therefore, it is important to investigate the critical value of mudflow volume that causes the train derailment under such terrain condition. With the goal of investigating the critical value of mudflow volume, the subsequent tests with the increasing quantity of mudflow released are simulated and the input data is shown in Table 5.6 below:

Test	Subtests	Volume of mudflow (m ³)	Railway embankment height H ₂ (m)	Buffer distance D (m)	Slope ratio of railway embankment (H:V)	Slope inclination α (°)	Terrain roughness (ViscoBoundFactor)
17	Subtest 65	100	4	6	3:1	30	0.025
	Subtest 66	250	4	6	3:1	30	0.025
	Subtest 67	500	4	6	3:1	30	0.025
	Subtest 68	750	4	6	3:1	30	0.025

Table 5. 6. Input data of Test 17 for the investigation of the critical mudflow volume

The results are presented in the following figure:

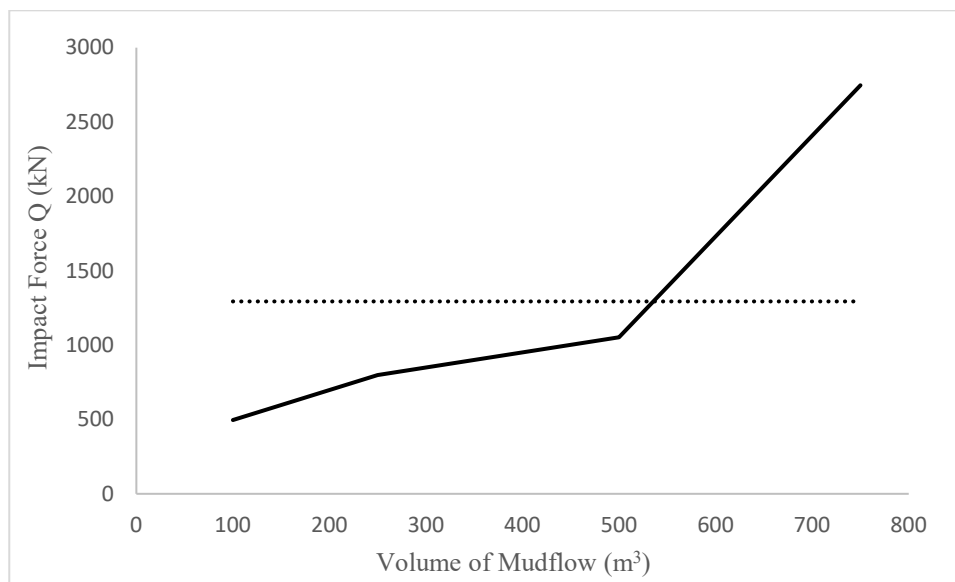


Figure 5. 12. The impact force obtained of Test 17 (note: the horizontal dashed line is the critical value of train derailment $Q=1293.6$ kN)

According to the results obtained in Test 17 as shown in Figure 5.12, it is observed that as the quantity of mudflow V released increases, from 100 m^3 to 500 m^3 , the impact force exerted on trains increases gradually, from around 500 kN to 1000 kN , which is near but less than $Q=1293.6 \text{ kN}$ (the critical value of train derailment), whereas, when the mudflow volume exceeds 500 m^3 , the destructive force increases dramatically and exceeds the critical value of train derailment, reaching at about 3000 kN as $V = 750 \text{ m}^3$. Therefore, based on the simulations performed in Test 14 to Test 17, it could be concluded that even though a small quantity of mudflow released (e.g., 50 m^3 , 75 m^3 , and 100 m^3) can derail railway cars at the worst case of the hillslope steepness equals 30 degrees along with a relatively flat railway embankment (slope ratio is $3H:1V$), the protective measures like raising embankment or constructing buffer distance D is useful to protect trains from being tipped over, whereas, when the mudflow volume is greater than 500 m^3 , no protective measures can prevent railway cars from derailing, which is the critical value of mudflow volume.

5.4.5 The effect of surface roughness n (Set V)

During the process of a mudflow flowing down a hillslope and beyond, impacting railway cars on top of the railway embankment, apart from the inclination of hillslope, terrain roughness is another factor related to the natural terrain. Since its deceleration effect on the mudflow as mentioned previously, to investigate the effect of the terrain roughness on the destructive force exerted by mudflows on the railway cars, the parameter related to terrain roughness will be variable in this fifth series test (Set V). It is worth noting that the parameter related to the terrain roughness in the simulation tool DualSPHysics called `ViscoBoundFactor` which is a dimensionless coefficient as stated previously. It is assumed that the terrain includes hillslope, buffer plane, and railway embankment has the same value of roughness.

Regarding the critical case (Subtest 68) investigated previously in Test 17 (in which `ViscoBoundFactor`=0.025) as the reference experiment, that is, no man-made controllable protective measures can protect trains, on basis of that, terrain roughness is studied. As a comparison, the values of 0.0125 and 0.05 are separately assigned to `ViscoBoundFactor` to represent different surface roughnesses. The input data of the subsequent simulations is provided below:

Test	Subtests	Terrain roughness (<code>ViscoBoundFactor</code>)	Railway embankment height H_2 (m)	Buffer distance D (m)	Slope ratio of railway embankment (H:V)	Slope inclination α ($^\circ$)	Volume of mudflow (m^3)
18	Subtest 69	0.0125	4	6	3:1	30	750
	Subtest 70	0.025	4	6	3:1	30	750
	Subtest 71	0.05	4	6	3:1	30	750

Table 5. 7. Input data of Set V for the investigation of the effect of surface roughness

The results are presented in Figure 5.13 below. Figure 5.13 shows the results of the effect of changes in the terrain roughness on the impact force exerted by mudflows on the railway cars. According to the diagram, it is apparent that a negative correlation exists between the impact force and the terrain roughness, that is, as the terrain surface becomes rougher, the destructive force posed on the railway cars can be reduced. However, as the case of mudflow occurs on hillslope with great quantity, although the surface of terrain becomes rough on which mudflow is running, it is obvious in Figure 5.13 that, with a large quantity mudflow occurring, the roughness surface terrain could reduce the danger posed on trains to some extents but still cannot effectively avoid a train derailing. Additionally, it needs to be noted that, unlike constructing a buffer plane with a certain length or building a railway embankment with the precise height and corresponding slope ratio, the natural terrain roughness is a constant which is normal and cannot be easily controlled or changed by human activities in the reality since a solid surface has a complex structure and complex properties depending on the nature of the solids and the interaction between the surface and the environment (Bhushan 2001).

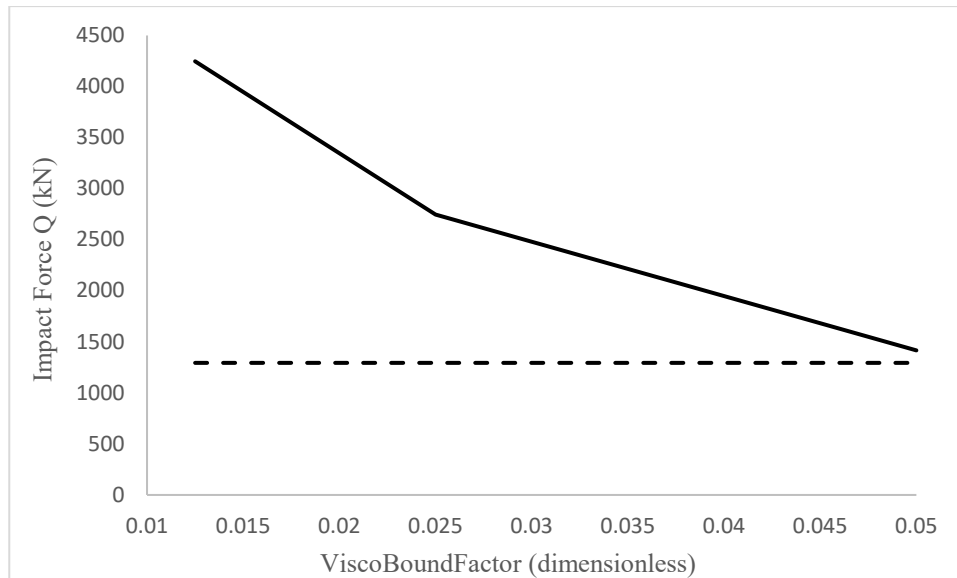


Figure 5. 13. The relationship between the impact force and the terrain roughness (note: the horizontal dashed line is the critical value of train derailment $Q=1293.6$ kN)

5.4.6 Discussion and summary

Based on the observations obtained from five experimental tests (Set I to Set V) performed with the aid of DualSPHysics, it could be concluded that:

1. Combining the investigations in Set I (Test 1 to Test 4) and Set IV (Test 14 to Test 17), protective countermeasures like constructing buffer plane and raising the railway embankment can reduce the destructive force exerted by mudflows on the railway cars to some extent, that is, a small-scale mudflow occurs. Since the impact force increases dramatically with greater quantity of mudflow released. When a large-scale mudflow occurs, like the case of Subtest 68 in Set IV, these two mitigation measures cannot prevent trains from derailing.
2. The investigation of the terrain environment where the railway systems is constructed is crucial. Owing to the slope's geometry, the natural hillslope steepness has a linear positive correlation with the impact force of mudflow, which can dramatically increase the potential of the train derailment. According to the outcomes of the experimental simulations performed in Set II (Test 5 to Test 7), it is not recommended to build railway lines in the place where the hillslope is steeply inclined, especially exceeding 30 degrees which is the most detrimental to railway cars. Moreover, the manual of the stability of natural slopes in Ottawa area compiled by City of Ottawa Planning and Environment Committee and Council (2001) indicates that any natural hillslope is inclined more steeply than about 11 degrees (5 horizontal to 1 vertical) has the potential for instability wherever there is Champlain Sea clay. Thus, it is strongly recommended to conduct investigation of the terrain environment before constructing railway systems in the study area, choosing the gentle hillslope (like 10 degrees).
3. In accordance with the results obtained in the Set III (Test 8 to Test 13), as a mudflow ascends instead of flowing downward during a mudflow impacting a railway embankment,

considering the slope's geometry, the steep slope is useful to retard the mudflow's upward climb, hence, a relatively steep railway embankment slope (2H:1V, about 27°) is helpful for train safety as compared to a flatter one (3H:1V, about 18°). In addition, the information is specified in the literature of Canadian engineering specifications for industrial tracks (CN 2019) that the embankment must have a side slope of not less than 2H:1V and AREMA's Manual for Railway Engineering recommends a typical slope ratio of 2H:1V (AREMA 2010). Therefore, the railway embankment with slope ratio of 2:1 (horizontal:vertical) is recommended in study area.

4. Experimental data investigated in Set IV (Test 14 to Test 17) illustrates that the impact force of mudflow has a positive correlation with the volume of mudflow, which could be increased significantly by greater quantity mudflow. As investigated in Test 17, it is observed that when mudflow volume is increased to more than 500 m^3 , protective measures as stated previously cannot avoid the train derailment. While, unlike the experimental simulations, as an uncontrollable factor in the reality, the quantity of mudflow generated could be millions of cubic meters which is much greater than 500 m^3 , that would produce an enormous destructive force on the railway system. Thus, the mitigation countermeasures with the aim of diverting or reducing the potential flow is essential to reduce the hazard of mudflow.
5. Additionally, as investigated in Set V (Test 18), there is a linear negative correlation between the terrain roughness and the impact force of mudflow exerted on trains as the terrain roughness always serves as a resisting force to retard the mudflow's advancement, indicating that, the preventive measure of taking a rough terrain surface into account could be necessary. Whereas, with a large-scale mudflow, the mitigation effect of terrain roughness on mudflows cannot effectively avoid the train derailment.

Moreover, it is necessary to mention that different case studies' environment in the parametric studies (e.g., different mudflow volumes, different buffer distances, different railway embankment heights) created the different amounts of fluid and boundary particles in the simulation. More particles created can result in a higher number of particle interactions to be calculated. Therefore, it is normal for DualSPHysics program to take more time to process the simulation. Among the parametric studies performed previously, the least particles (425,851 fluid particles and 577,741 boundary particles) were created in the case of subtest 1, requiring around 1 hour for an NVIDIA Tesla-P6 GPU to compute simulation. The largest number of particles (6,127,341 fluid particles and 651,785 boundary particles) generated in the case of subtest 71, the computational runtime required for an NVIDIA Tesla-P6 GPU is about three days (63 hours). Among the investigations performed above in Set I to Set V, six parameters are investigated above could be divided into two groups: a) controllable factor in reality; b) uncontrollable one. The parameters of buffer distance D , railway embankment height H_2 and railway embankment slope ratio β could be man-made controllable. By contrast, the factors of natural hillslope steepness α , natural surface roughness n and mudflow volume V are uncontrollable in real-life. The investigations concluded above indicate that, although the mitigation measures (e.g., constructing long buffer plane, raising the embankment, and adopting a relatively steep embankment) are helpful to reduce the detrimental effect of mudflow posed on railway cars, these protective measures cannot protect trains from derailing with a large-scale mudflow occurs on the steep natural hillslope. Being the factor that is uncontrollable in real-life, great mudflow volume plays the most important role in derailing trains,

second is the steep natural hillslope where mudflows occur, making great contributions to derail railway cars, in contrast, rough surface is helpful to resist the mudflow's movement. To serve the purpose of reducing the detrimental effect of potential flow on public properties and human lives, the corresponding protective countermeasures to divert or reduce the discharge of potential mudflow should be considered. According to the practice performed in China that, a diversion dike was constructed in Jiangjia Gully and Daqiao stream and has successfully diverted viscous debris flow and protected the hillside of the canyon (Bi 1985; Xu 1985), hence, the mitigation measures like constructing a diversion dike could be recommended. As the natural terrain condition, including natural hillslope steepness and surface roughness, could be investigated in advance, hence, the proper choice of natural terrain where the railway systems are constructed is indispensable. Based on the numerical simulations studied above, it is strongly recommended to construct railway lines considering the gentle natural hillslope (less than 11 degrees) for Champlain Sea clay with the rough surface.

Furthermore, in accordance with the previous practice applied in preventing mudflows, the importance of the prediction and warning system for debris flow must be highly appraised. For example, the prediction and warning device for debris flow has been successfully developed and experimented at the Jiangjia Gully Observation and Research Station in China (Zhang 1993); A precipitation telemetering apparatus was developed in 1981 and successfully forecasted 20 debris flows during 1982-1984 (Zhang 1993). Moreover, the ultrasonic mud-level warning device was successfully used in the Jiangjia Gully during three debris flows in 1985 (Zhang et al., 1990). Therefore, such equipment is highly recommended to be introduced to be installed near the railway lines. By this way, the hazards of mudflow can be forecasted and prevented in advance.

In conclusion, the prevention of debris flow includes an overall controlling plan using both hard (engineering, e.g., increasing buffer plane) and soft ways (prediction and warning, etc.).

Chapter Six: Conclusion and Recommendations

6.1 Introduction

This chapter summarizes the investigation and contribution of this research, limitations of this study and recommendations related to possible future direction of this project. Section 6.2 reviews the objective of this research, the methodology opted and the conclusions obtained after the analysis and discussion of the numerical studies results. The limitations of this research and recommendations for future work are addressed in Section 6.3.

6.2 Conclusion

These model studies focused on the impact force of mudflow impacting railway cars and the parameters influencing destructive force exerted by mudflows on railway cars, in order to assess the potential of train derailment and provide insight into the corresponding mitigation measures. Different from the conventional ways to conduct research like using field tests or laboratory experiments, this research was implemented by the fluid flow model in a simulation tool. Performing the mudflow model utilizing Smoothed Particle Hydrodynamics (SPH) method is the basis of this study, to determine the impact force exerted by flow on trains and the condition under which the mudflow causes the train derailment.

To quantify the effect of six major parameters on the impact force exerted by mudflows on trains, the *Control Variable* method was adopted to perform numerical model studies. Before performing the model studies, several simulations based on the larger-field test performed by Bugnion et al. (2010) were performed to calibrate the simulation tool based on mudflows. Modeling Bugnion et al. (2010) mudflow flume experiments by DualSPHysics reveals that the capacity of DualSPHysics to reproduce a real-world event. Additionally, utilizing the simulation tool, although the values assigned to a number of the parameters in the simulation tool defining the characteristics of the mudflow, some parameters applied are still not representative of their corresponding physical values, which is a common problem. For example, there is no setting for presenting fluid viscosity and the roughness of terrain on which the mudflow flow in DualSPHysics. Therefore, a calibration of such kind can be a means to adjust the values by using the data provided in the physical experiments, in addition, maximizing the authenticity of the models.

Having calibrated the simulation tool, numerical model cases with different geographic terrain conditions are simulated using DualSPHysics to estimate the potential of the derailment of the railway cars. The results of the tests demonstrate the simulation tool's ability to simulate the scenario of a mudflow impacting railway cars. In accordance with the numerical model studies investigated in Chapter 5, several dimensional parameters should be carefully considered in railway engineering:

- The quantities of mudflow occurring; in the investigation, as the major parameter contributing to train derailment, greater quantities of mudflow ($V > 500 \text{ m}^3$) generating an enormous destructive force, under which no mitigation measures could prevent trains from being tipped over.

- Gentle natural hillslope ($\alpha \leq 10^\circ$); in the research, the hillslope inclination has a positive correlation with the impact force. The steeper natural hillslope, the greater impact force exerted by mudflows on trains. The hillslope inclination exceeds 30° results in the train derailment.
- Steep railway embankment hillside with slope ratio of 2H:1V; in the model studies, 2H:1V slope ratio could theoretically, practically and effectively retard the ascent of mudflows on railway embankment and protect trains, which also agrees well with the specification specified in the Canadian railway engineering (CN's Engineering Specifications 2019).
- Longer buffer plane and higher railway embankment; in this study, 6-meter buffer distance with 4-meter railway embankment height proved the better mitigation effect on mudflows. In addition, according to the key parametric studies in Chapter 3, considering current railway construction practice, the slope stability and the optimal cost, 4-meter-high railway embankment is the better choice.
- Relatively rough terrain surface; in this project, a relatively rough terrain surface demonstrated a way to retard the movement and advancement of mudflows.

Therefore, based on the findings above, to better reduce the detrimental effect of mudflows on railway cars, different mitigation measures are concluded for two different categories of railway lines, the existing railways and the new railways to be constructed:

- 1) For the existing railways that have been constructed and operated decades ago; under the certain terrain condition, the volume of mudflow plays a critical role in the train derailment, which indicates the mitigation measures should mainly focus on the ways to divert or reduce the discharge of mudflow to reduce the quantities of mudflow ($V < 500 \text{ m}^3$) exerted on trains.
- 2) For the new railways to be built in the future; apart from the protective measures mentioned above, in the study area of this research, according to the numerical experimental outcome and existing literature applied in the stability of natural slopes in the Ottawa area, railway construction in areas with natural slopes greater than 10 degrees is not recommended. It is recommended to apply a relatively steep railway embankment with a slope ratio of 2H:1V in Canadian railway engineering. Constructing a long buffer plane (6m) and high railway embankment (4m) with a relatively rough surface to retard the movement of mudflows.

It is worth mentioning that owing to the uncontrollable parameters in real-life, such as the mudflow volume and hillslope inclination, making a great contribution to the train derailment, although the parameters of buffer distance and optimum railway embankment height could retard the movement of mudflows and reduce their destructive power, the mitigation measures as constructing long buffer plane or building high railway embankment are only useful to a certain extent. Therefore, from the research performed, it could be concluded that, in terms of the prevention of the detrimental effect of mudflows, the quantities of mudflow released, that is, the capability of predicting debris flow and the factors of geographic location are the most important. Thus, the prevention of mudflow hazards to the railway system is an overall controlling plan that includes both preliminary topographic investigation and continuous prediction and early warning at a later stage.

The results of these model studies reveal that the idea of modeling mudflows in case of the train derailment by means of the mentioned simulation tool (where sufficient data is provided) has the potential to be performed. Moreover, as stated previously, the advantages of investigating fluid flow utilizing the simulation tool instead of field tests or laboratory experiments are apparent. It can save test costs, shorten test cycles and provide the critical parameters' data and the important guarantees for solving practical engineering problems. Therefore, this method could be used to predict the impact force exerted by mudflows on railway cars in order to take necessary actions and mitigation precautions to prevent or reduce the potential damages and losses. Modeling mudflows could also be considered in the preliminary phase of the railway line construction, and based on the results, the location of the railway embankment and the suitable terrain environment and the methods to prevent the train derailment can be determined.

In conclusion, this research was performed to provide a new perspective in modeling trains derailment owing to mudflows by introducing the application of a simulation tool, thus generating a basis and providing a method for the prevention of future disasters on railway systems caused by mudflows.

6.3 Recommendations

On basis of the conclusions stated above, for the railway engineering in the Ottawa Valley, it is recommended to construct railways in areas with natural slopes less than 10 degrees and build a relatively steep railway embankment (slope ratio equals to 2H:1V) with the height of 4-meter. The buffer plane between natural slope and railway embankment should be no less than 6 meters.

However, in this model study, although the general characteristics of fluid and the shape of terrain covered resembled the physical natural conditions to a great extent, the shortcoming still exists with regards to the absence of no real terrain maps are adopted in the simulation tool. With regards to the enhancement of modeling the case that a mudflow impacts the railway cars, further leads to the train derailment. There are a number of recommendations that could be considered in further research:

- Lack of corresponding data concerning the physical derailment of the railway cars in the Ottawa Valley, such as the data regarding the characteristics of mudflow and terrain, the volume of mudflow generated on the hillslope, and the viscosity of the mudflow, which requires further research on the railway car derailment incidents for a comprehensive set of data to be provided for the desired simulation.
- With the availability of data collected from the physical incident occurring in a certain area, steps to modeling possible future train derailment or estimating the potential train derailment on existing railway lines in the study area can be taken in order to prevent possible damages and losses.
- The use of the high quality Digital Elevation Models (DEMs) with accurate terrain characteristics, including the data of vegetation, in the simulation tool to perfectly restore the local topography is recommended. As the data of the terrain on which the mudflow traveling is still not sufficient to create the real physical incidents' scene due to no DEMs (when focusing on a specific area) are used in the simulations. Moreover, the absence of

structures and vegetation of the terrain in the model also plays an important role in the events in the physical incidents.

- In the case of predicting and further preventing the train derailment caused by a possible mudflow generated on rainy days, studies can be performed on the possibility of making changes in the topography of the area or in a way to reduce the flow length in order to control the flow. Alternatively, constructing a diversion dike, the obstacle or the drainage channels between the hillslope and the railway embankment to change the flow direction of mudflow to avoid their harmful impact on the railway system.
- The research results of the previously model studies computed by utilizing DualSPHysics as the meshless simulating tool can be compared to the results produced by other tools such as Fluent, one mesh-based simulation tool, in order to determine the most accurate simulation tool.

References

1. Altomare, C., Crespo, A. J. C., Domínguez, J. M., Gómez-Gesteira, M., Suzuki, T., and Verwaest, T. (2015). “Applicability of Smoothed Particle Hydrodynamics for estimation of sea wave impact on coastal structures.” *Coastal Engineering*, 96, 1-12.
2. Altomare, C., Domínguez, J., Crespo, A., Gonzalez-Cao, J., Suzuki, T., Gomez-Gesteira, M., and Troch, P. (2017). “Long-crested wave generation and absorption for SPH-based DualSPHysics model.” *Coast Eng. J.*, 127, 37e54.
3. Armanini, A. (1997). “On the dynamic impact of debris flows.” *Recent developments on debris flows*, Armanini, A., and Masanori, M., ed., Chap. 3, pp. 208-226, Springer, Berlin.
4. AGICO GROUP (2020). “Ballasted Track and Non-Ballasted Track Introduction.” Accessed August 01, 2020. <http://www.rail-fastener.com/ballasted-and-non-ballasted-rail-track.html>.
5. American Railway Engineering and Maintenance-of-Way Association (AREMA) (2010). *AREMA manual for railway engineering*, Landover, MD.
6. Bagnold, R. A. (1966). “The shearing and dilatation of dry sand and ‘singing’ mechanism.” *Proc. R. Soc. London. Series A, (Mathematical, Physical and Engineering Sciences)*. <https://doi.org/10.1098/rspa.1966.0236>.
7. Batchelor, G. K. (1974). *Introduction to fluid dynamics*. Cambridge University Press.
8. Bonnett, C. F. (1996). *Practical Railway Engineering*. London: Imperial College Press.
9. Bentley, D. (2014). “Lost in time: The long-gone trains and stations of Birmingham’s Age of Steam.” Accessed August 08, 2020. <https://www.birminghammail.co.uk/news/nostalgia/gallery/7244755>.
10. Barreiro, A., Crespo, A., Domínguez, J., and Gomez-Gesteira, M. (2013). “Smoothed particle hydrodynamics applied in fluid structure interactions.” *Fluid Structure Interaction VII*, vol. 129, pp. 75.
11. Bugnion, L., McArdell, W. B., Bartelt, P., and Wendeler, C. (2010). “Measurements of hillslope debris flow impact pressure on obstacles.” *Landslide (2012)*, 9:179-187. DOI: 10.1007/s10346-011-0294-4.
12. Bhushan, B. (2001). *Surface Roughness Analysis and Measurement Techniques*. CRC Press LLC 2001.
13. Bi, C. (1985) “The diversion dam for debris flow at Jiangjia Gully of Dongchuan in Yunnan.” *Memoirs of the Lanzhou Institute of Glaciology and Gryopedology of the Chinese Academy of Sciences (No. 4)*, Yuan, Y. ed. Science Press, Beijing, pp. 134-139 (In Chinese).
14. Coussot, P., and Meunier, M. (1996). “Recognition, classification and mechanical description of debris flows.” *Earth-Science Reviews*, vol. 40, pp. 209-227.
15. Chigira, M. (2001). “Large scale landslide.” *Handbook of disaster reduction science (DPRI*

- ed.*), Asakura Shoten, Tokyo: 190–191 (In Japanese).
16. Campbell, C. S. (1990). “Rapid granular flows.” *Annu. Rev. Fluid Mech.*, 22: 57-92. <https://doi.org/10.1146/annurev.fl.22.010190.000421>.
 17. Chung, T. J. (2002). *Computational Fluid Dynamics*. Cambridge University Press 2002.
 18. Crespo, A. C., Dominguez, J. M., Rogers, B. D., Gomez-Gesteira, M., Longshaw, S., Canelas, R., Vacondio, R., Barreiro, A., and Feal, G. O. (2015). “DualSPHysics: Open-source parallel CFD solver based on Smoothed Particle Hydrodynamics (SPH).” *Computer Physics Communications*, 187 (2015) 204-216.
 19. Crespo, A. C., Dominguez, J. M., Barreiro, A., Gomez-Gesteira, M., and Rogers, B. D. (2011). “GPUs, a New Tool of Acceleration in CFD: Efficiency and Reliability on Smoothed Particle Hydrodynamics Methods.” *PLoS ONE*, 6 (6) e20685. DOI: 10.1371/journal.pone.0020685.
 20. Ciotlaus, M., Kollo, G., Moldovan, D., and Muntean, L. (2016). “Slope Stability of Railway Embankments.” *10th International Conference Interdisciplinarity in Engineering (INTER-ENG 2016)*. DOI: 10.1016/j.proeng.2017.02.362
 21. Crespo, A. C. (2020). “GUIDE-DualSPHysics_v5.0.” Accessed April 06, 2020. <https://github.com/DualSPHysics/DualSPHysics/wiki>.
 22. City of Ottawa Planning and Environment Committee and Council (2001-2020). “Slope Stability Guidelines for Development Applications.” Accessed April 15, 2020. <https://documents.ottawa.ca/sites/documents/files/documents/cap137604.pdf>.
 23. Cui, P., Zeng, CH., and Yu, L. (2015). “Experimental analysis on the impact force of viscous debris flow.” *Earth Surf. Process. Landforms (EARTH SURFACE PROCESSES AND LANDFORMS)*, 40, 1644-1655 (2015). DOI: 10.1002/esp.3744.
 24. Dalrymple, R. A., and Rogers, B. D. (2006). “Numerical modeling of water waves with the SPH method.” *Coastal Engineering*, 53, 141-147.
 25. DualSPHysics (2018). “POST-PROCESSING CALCULATIONS.” Accessed April 15, 2020. <https://dual.sphysics.org/index.php/downloads>.
 26. Deveau, S. (2011). “How long can trains go?” Accessed March 03, 2020. <http://www.nationalpost.com/long+trains/4348592/story.html>.
 27. Egli, T. (2005). “Wegleitung Objektschutz gegen gravitative Naturgefahren.” *Egli Engineering, Vereinigung Kantonaler Feuerversicherungen (VKF)*, Bundesgasse 20 CH-3001 Bern.
 28. Furuya, T. (1980). “Landslides and landforms.” *Landslides, slope failures and debris flows*, Takei, A. ed., Kajima Shuppan, Tokyo: 192-230 (In Japanese).
 29. Ferdous, W., Manalo, A., Erp, G. V., Aravinthan, T., Kaewunruen, S., and Remennikov, A. (2015). “Composite railway sleepers - Recent developments, challenges and future prospects.” *Composite Structure*, 134 (2015) 158-168.

30. Fransham, P. B., and Gadd, N. R. (1977). "Geological and geomorphological controls of landslides in Ottawa Valley, Ontario." *The 29th Canadian Geotechnical Conference*, Vancouver, B.C.
31. Gotoh, H., Shao, S., and Memita, T. (2001). "SPH-LES model for numerical investigation of wave interaction with partially immersed breakwater." *Coastal Engineering Journal*, 46(1), 39-63.
32. Getzner, W.G. (2020). "Brochure Heavy Freight Solutions for Heavily Loaded Rail Tracks." Accessed March 02, 2020. <https://www.scribd.com/document/361689541/Heavy-Freight-Solutions-for-Heavily-Loaded-Rail-Tracks>.
33. Gauckler, P. H. (1867). "Etudes Théoriques et Pratiques sur l'Ecoulement et le Mouvement des Eaux." *Comptes Rendues de l'Académie des Sciences, Tome 64*, Paris, France, pp. 818-822.
34. Gómez-Gesteira, M., and Dalrymple, R. A. (2004). "Using a Three-Dimensional Smoothed Particle Hydrodynamics Method for Wave Impact on a Tall Structure." *JOURNAL OF WATERWAY, PORT, COASTAL AND OCEAN ENGINEERING*. DOI: 10.1061/(ASCE)0733-950X(2004)130:2(63).
35. Hsü, K.J. (1975). "Catastrophic debris streams (Sturzströms) generated by rockfalls." *Geol. Soc. Am. Bull. (Geological Society of America Bulletin)*, 86 (1): 129-140. DOI: 10.1130/0016-7606(1975)86<129:CDSSGB>2.0.CO;2.
36. Hu, K., Wei, F., and Li, Y. (2011). "Real-time measurement and preliminary analysis of debris-flow impact force at Jiangjia Ravine, China." *Earth Surf. Process. Landf. (EARTH SURFACE PROCESSES AND LANDFORMS)*, 36:1268-1278. DOI:10.1002/esp.2155.
37. Hübl, J., and Holzinger, G. (2003). "Entwicklung von Grundlagen zur Dimensionierung kronenoffener Bauwerke für die Geschiebemanagement in Wildbächen." *Institut of Mountain Risk Engineering*, WLS Report 50 Band 3.
38. He, S. M., Liu, W., and Li, X. P. (2016). "Prediction of impact force of debris flows based on distribution and size of particles." *Environmental Earth Sciences*. DOI: 10.1007/S12665-015-5180-2.
39. Hungr, O., Morgan, G. C., and Kellerhals, R. (1984). "Quantitative analysis of debris torrent hazards for design of remedial measures." *Canadian Geotechnical Journal*, 21(4): 663-677.
40. Henninig, S. (2006) "The early history of public transit in Detroit 1863-1890." Accessed January 08, 2020. <http://www.detroittransithistory.info/TheEarlyYears.html>.
41. Iverson, R. M., Reid, M. E., and LaHusen, R. G. (1997). "Debris flow mobilization from landslide." *Annu. Rev. Earth Planet. Sci.*, 25: 85-138. DOI: 10.1146/annurev.earth.25.1.85.
42. Iverson, R. M., Logan, M., LaHusen, R. G., and Berti, M. (2010). "The perfect debris flow? Aggregated results from 28 large-scale experiments." *Journal of Geophysical Research*, vol. 115, F03005. DOI: 10.1029/2009JF001514, 2010.
43. International Federation for Structure Concrete. (2006). "Precast concrete railway track

systems.” *State-of-art report*. DOI: doi.org/10.35789/fib.BULL.0037.

44. Kaneko, T., and Kamata, K. (1992). “Discussion of the arrival distances of pyroclastic flows at Unzen in 1991.” *By energy line/cone concept: Kazan*, 37(1): 35-46 (In Japanese).
45. Kan, Z. (1996). *Debris flow hazards and their control in China*. pp.1-118, Science Press (Chinese with English translation).
46. Leidenfrost, W. (2012). “Photos: Metro Vancouver rainstorm triggers two Langley mudslides.” Accessed September 08, 2019.
<http://www.vancouver.sun.com/news/metro/photos+metro+vancouver+rainstorm+triggers+langley+mudslides/7477582/story.html>.
47. Liu, G. R. (2003). *Mesh Free methods: Moving beyond the finite element method*. CRC Press, London.
48. Leimkuhler, B. J., Reich, S., and Skeel, R. D. (1996). “Integration Methods for Molecular dynamics.” *Mathematical Approaches to Biomolecular Structure and Dynamics*, Mesirov, P. J., Schulten, K., and Sumners, D. W. ed. pp. 161-185, Springer, USA.
49. Lo, E. Y. M., and Shao, S. (2002). “Simulation of near-shore solitary wave mechanics by an incompressible SPH method.” *Applied Ocean Research*, 24, 275-286.
50. LooiNL, I. (2007). “Wood and concrete railroad ties, next to each other, Beugen (Netherlands).” Accessed March 04, 2020.
https://commons.wikimedia.org/wiki/File:Railroad_tieswoodconcrete.jpg.
51. Li, D., Hyslip, J., Sussmann, T., and Chrismer, S. (2016). *Railway Geotechnics*. CRC Press, Taylor & Francis Group, LLC.
52. Lichtenhahn, C. (1973). “Die Berechnung von Sperren in Beton und Eisenbeton.” *Kolloquium u`ber Wildbachsperren, Mitteilungen der Forstlichen Bundesanstalt Wien*, vol. 102: 91-127.
53. Lo, K. Y., and Lee, C. F. (1973). “An evaluation of the stability of natural slopes in plastic Champlain clays.” *26th Canadian Geotechnical Conference*, Toronto, Ont., pp. 100-111.
54. Minatti, L., and Pasculli, A. (2011). “SPH numerical approach in modelling 2D muddy debris flow.” *Italian Journal of Engineering Geology and Environment*. DOI: 10.4408/IJEGE. 2011-03. B-052.
55. Monaghan, J. J. (1992). “Smoothed particle hydrodynamics.” *Annual Review of Astronomy and Astrophysics*, 30, 543-574.
56. Monaghan, J. J., and Lattanzio, J. C. (1985). “A refined method for astrophysical problems.” *Astron. Astrophys*, 149, 135-143.
57. Monaghan, J. J. (1994). “Simulating free surface flows with SPH.” *Journal of Computational Physics*, 110, 399-406.
58. Monaghan, J. J., Cas, R. A. F., Kos, A. M., and Hallworth, M. (1999). “Gravity currents descending a ramp in a stratified tank.” *Journal of Fluid Mechanics*, 379, 39-70.

59. Molteni, D., and Colagrossi, A. (2009). "A simple procedure to improve the pressure evaluation in hydrodynamic context using the SPH." *Computer Physics Communications*, 180 (6), 861-872.
60. Mitchell, J., and Markell, R. (1973). "Flow sliding in sensitive clay soils." *26th Canadian Geotechnical Conference*, Toronto, Ont., pp. 112-123.
61. Manning, R. (1891). "On the flow of water in open channels and pipes." *Transactions of the Institution of Civil Engineers of Ireland*, 20: 161-207.
62. Mizuyama, T. (1979). "Computational method and some considerations on impulsive force of debris flow acting on sabo dams." *Journal of the Japan Society of Erosion Control Engineering*, 11(2): 40-43.
63. Ministry of Railways of the People's Republic of China, The Third Railway Survey and Design Institute Group Co., Ltd. and China Academy of Railway Science. (2009). *Code for Design of High-speed Railway (Trial)*. TB 10621-2009.
64. Nadal, M. J. (1896). "Theorie de la stabilite des locomotives." *Movement de Lacet, Annales des Mines*, Part 2, 10, 232.
65. Ohyagi, N. (1985). "Definition and classification of sediment hazards: in Prediction and countermeasures of sediment hazards." *Japanese Soc. Soil Mech. Foundation Eng.*, pp. 5-15, Tokyo.
66. Okuda, S., Suwa, H., Okunishi, K., Nakano, K., and Yokoyama, K. (1977). "Synthetic observation on debris flow." *Annuals, DPRI ed.*, 21B-1, pp. 277-296 (In Japanese).
67. O'Brien, S. J., and Julien, Y. P. (1988). "Laboratory Analysis of Mudflow Properties." *J. Hydraul. Eng.* 114(8): 877-887. [https://doi.org/10.1061/\(ASCE\)07339429\(1988\)114:8\(877\)](https://doi.org/10.1061/(ASCE)07339429(1988)114:8(877)).
68. Office of Chief Engineer Structures, Design and Construction, CN. (2019). *CN Engineering Specifications for Industrial Tracks*. Accessed April 05, 2020. <https://www.cn.ca/-/media/Files/Customer-Centre/TrackSpecifications/CN-Industry-Track-Standards.pdf>.
69. Pierson, T. C., and Costa, J. E. (1987). "A rheologic classification of subaerial sediment-water flows." *Debris flows/avalanches: process, recognition, and mitigation*, Costa, J. E., and Wiczorek, G. F. ed., Rev. Eng. Geol., 7, Geolo. Soc. Am: 1-12.
70. Pastor, A., Blanc, T., Haddad, B., Petrone, S., Morles, M. S., Dremptic, V., Issler, D., Crosta, G. B., Cascini, L., Sorbino, G., and Cuomo, S. (2014). "Application of a SPH depth-integrated model to landslide run-out analysis." *Landslides (2014)*, 11:793-812. DOI: 10.1007/s10346-014-0484-y.
71. Padova, D., Dalrymple, R. A., and Mossa, M. (2014). "Analysis of the artificial viscosity in the smoothed particle hydrodynamics modelling of regular waves." *J. Hydraul. Res.*, 52 (6), 836e848.
72. Quorum Corporation (2005). "Railway Capacity Background & Overview." Accessed April 15, 2020. <http://www.grainmonitor.ca/Downloads/Papers/RailwayCapacityOverview.pdf>.

73. ReadyBurbank. org (2019). “Debris flow (Mud Slide) & Mudflow.” Accessed November 11, 2019. <http://www.readyburbank.org/debris-flow-mud-slide>.
74. Roanes-Lozano, E. (2013). “The Geometry of Railway Geometric Overthrow Revisited Using Computer Algebra Methods.” *Math. Comput. Sci.*, 7:473-485. DOI: 10.1007/s11786-013-0164-7.
75. Remennikov, A., and Kaewunruen, S. (2006). “Experimental Investigation on Dynamic Railway Sleeper/Ballast Interaction.” *Experimental Mechanics*, 46:57-66. DOI: 10.1007/s11340-006-5868-z.
76. RTA (Railway Tie Association). (1919). Accessed February 14, 2020. <https://www.rta.org/faqs-main>.
77. Rogers, B. D., Dalrymple, R. A., and Stansby, P. K. (2010). “Simulation of caisson breakwater movement using 2-D SPH.” *J. Hydraul. Res.*, 48 (S1), 135e141.
78. Roselli, R. A. R., Vernengo, G., Altomare, C., Brizzolara, S., Bonfiglio, L., and Guercio, R. (2018). “Ensuring numerical stability of wave propagation by tuning model parameters using genetic algorithms and response surface methods.” *Environmental Modelling & Software*, 103 (2018) 62-73.
79. Sujay (2017). “Railway Track Bed Formations-Basics.” Accessed January 08, 2020. <http://railengdigest.com/technical-articles/track/railway-track-formation-basics/>.
80. Selig, E. T., and Waters, J. M. (1994). *Track technology and substructure management*. Thomas Telford, London.
81. Scotton, P., and Deganutti, A. (1997). “Phreatic line and dynamic impact in laboratory debris flow experiments.” *Proceedings of the 1st International conference on debris-flow hazards mitigation: mechanics, prediction and assessment, American Society of Civil Engineers*, pp. 777-786, New York.
82. Scheidl, C., Chiari, M., Kaitna, R., Mullegger, M., Krawtschuk, A., Zimmermann, T., and Proske, D. (2012). “Analyzing debris-flow impact models, based on a small-scale modelling approach.” *Surv. Geophys.*, 34:121-140. DOI: 10.1007/s10712-012-9199-6.
83. Sangrey, A., and Paul, J. (1971). “A regional study of landslides near Ottawa.” *Canadian Geotechnical Journal*, pp. 315-335.
84. St-Germain, P., Nistor, I., Townsend, R., and Shibayama, T. (2013). “Smoothed-particle hydrodynamics numerical modeling of structures impacted by tsunami bores.” *Coast. Ocean Eng.*, 140 (1), 66e81.
85. Takahashi, T. (2014). *Debris Flow, Mechanics, Prediction and Countermeasures, 2nd edition*. CRC Press Taylor & Francis Group, LLC.
86. Takahashi, T. (2001). “Mechanics and simulation of snow avalanches, pyroclastic flows and debris flows.” *Spec. Publs., Int. Ass. Sediment*, 31: 11-43.
87. Takahashi, T. (2006). *Mechanisms of sediment runoff and countermeasures for sediment*

hazards. Kinmirai-sha, Japan, pp.420 (In Japanese).

88. VanDine, D., and Bovis, M. (2002). "History and Goals of Canadian Debris Flow Research, A Review." *Natural Hazards*, 26(1):67-80.
89. Varnes, D. J. (1978). "Slope movement types and processes." *Landslides analysis and control*, Scguster, R. L., and Krizek, R. J. ed., NAS. Sp. Rep. 176: 11-33.
90. Verlet, L. (1967). "Computer "Experiments" on Classical Fluids. I. Thermodynamical Properties of Lennard-Jones Molecules." *Physical Review*, 159, 98-103. <https://journals.aps.org/pr/pdf/10.1103/PhysRev.159.98>.
91. Wang, Z., Chen, R., Wang, H., Liao, Q., Zhu, X., and Li, S. Z. (2016). "An overview of smoothed particle hydrodynamics for simulating multiphase flow." *Journal of Applied Mathematical Modelling*. DOI: 10.1016/j.apm.2016.06.030.
92. Wendland, H. (1995). "Pieciwise polynomial, positive definite and compactly supported radial functions of minimal degree." *Advances in Computational Mathematics*, 4, 389-396.
93. Wendeler, C. (2007). "Murgangsrückhalt in wildba"chen. grundlage zur planung und berechnung von flexiblen barrieren." *PhD thesis, Swiss Federal Institute of Technology Zurich, Zürich*. DOI:10.3929/ ethz-a-005699588.
94. Watanabe, M., and Ike (1981). "Investigation and analysis of volcanic mud flows on mount sakurajima." *Erosion sediment transport measurement, International Association on Hydrology*, vol. 133, 245-256, Florence, Science Publication.
95. Widjaja, B., Setiabudi, D. W., and Ivan Arista, I. (2014). "Recommendation of Viscosity Values for Mudflow." *The International Conference on Environmentally Friendly Civil Engineering Construction and Materials*, Manado, Indonesia, 13-14 (2014).
96. Widjaja, B., and Lee, S. H. H. (2013). "Flow box test for viscosity of soil in plastic and viscous liquid states." *Soils and Foundations*, 2013,53(1):35-46.
97. Xu, R., Stansby, P., and Laurence, D. (2009). "Accuracy and stability in incompressible SPH (ISPH) based on the projection method and a new approach." *Journal of Computational Physics*, 228(18), 6703-6725.
98. Xiang, J., and Zeng, Q. Y. (2005). "A study on mechanical mechanism of train derailment and preventive measures for derailment." *International Journal of Vehicle Mechanics and Mobility*. DOI: 10.1080/004231104123313220.
99. Xu, D. (1985). "Debris flow and its prevention along Daqiao stream of Dongchuan in Yunan." *Memoirs of the Lanzhou Institute of Glaciology and Gryopedology of the Chinese Academy of Sciences (No. 4)*, Yuan, Y. ed. Science Press, Beijing, pp. 130-138 (In Chinese).
100. Zhang, S. C. (1993). "A comprehensive approach to the observation and prevention of debris flows in China." *Natural Hazards*, 7:1-23, 1993.

101. Zhang, S., Chen, J., and Ye, M. (1990). "Measurement and research of physical parameters of debris flow in Jiangjia Ravine." *Debris Flow Observation and Research in Jiangjia Ravine, Yunnan*, J. Wu et al. ed., pp. 141-164, 213-217, Science Press, Beijing (In Chinese).